LBL-30605

Center for Advanced Materials

CAM

Improving Fatigue Life in Near-Eutectic Sn Pb Solders

T.S.E. Summers
(Ph.D. Thesis)

May 1991

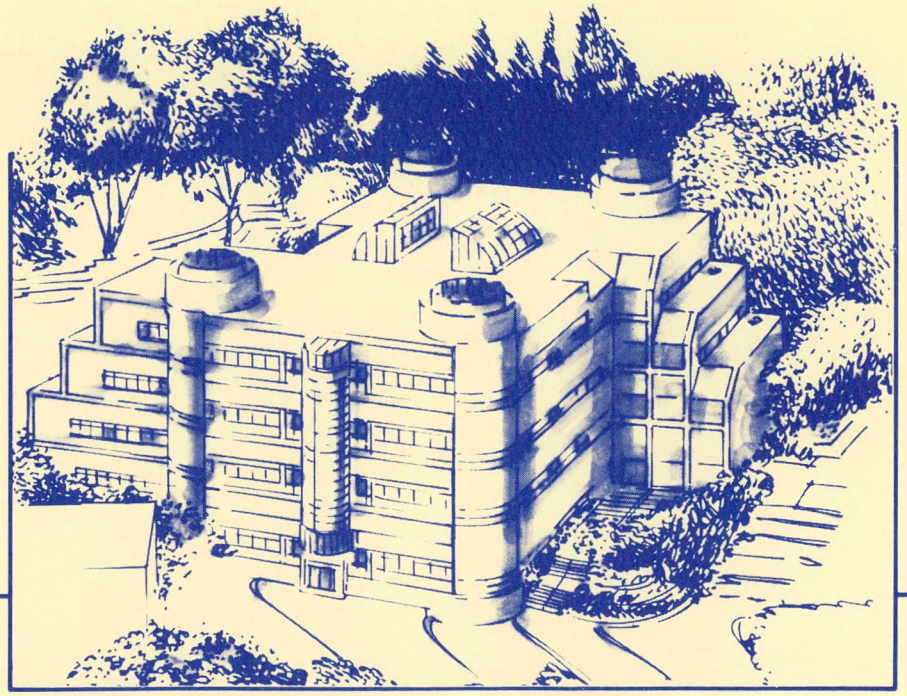

Materials and Chemical Sciences Division

Lawrence Berkeley Laboratory • University of California

ONE CYCLOTRON ROAD, BERKELEY, CA 94720 • (415) 486-4755

Prepared for the U.S. Department of Energy under Contract DE-AC03-76SF00098

DISCLAIMER

LBL--30605

DE91 013844

Improving Fatigue Life in Near-Eutectic Sn Pb Solders

T.S.E. Summers

Ph.D. Dissertation

Department of Materials Science and Mineral Engineering
University of California

and

Center for Advanced Materials
Materials Sciences Division
Lawrence Berkeley Laboratory
University of California
Berkeley, CA 94720

May 1991

This work was supported by the Director, Office of Energy Research, Office of Basic Energy Science, Materials Sciences Division of the U. S. Department of Energy under Contract No. *DE-AC03-76SF00098.*

Improving Fatigue Life in Near-Eutectic Sn-Pb Solders

by

Tammy Suzanne Edgecumbe Summers

Abstract

Due to technical advances in packaging technology, solder joint thermal shear fatigue failures pose reliability concerns and limit current packaging designs in the electronics industry. Past work has shown that thermal fatigue failures, as well as isothermal fatigue and creep failures, in the commonly used near-eutectic Sn-Pb solders are preceded by the formation of a band of coarsened material. Examination of crept and fatigued eutectic solder joints shows that shear deformation concentrates along relatively soft heterogeneities, the eutectic grain and colony boundaries, in the as-cast microstructure which happen to line up into long straight bands parallel to the applied shear strain. Improvement of the fatigue properties requires an elimination or, at least, a reduction in the length of these long straight boundaries. Several methods of doing that are proposed. These methods basically fall into two groups: one involving homogenization of the as-cast microstructure aimed at eliminating these heterogeneities and the other involved with breaking up the as-cast microstructure in such a way that long straight boundaries do not form parallel to the direction of shear.

To study the effect of homogenization of the microstructure, room temperature aging of solder joints was studied. Softening was found to occur over a period of about 40-50 weeks levelling off at about 70-75% of the initial strength (31 MPa). Microstructural changes noticeable after about 40 weeks increase the elongation to failure during shear testing and improve resistance to fatigue.

The effect of breaking up the as-cast microstructure was studied by comparing various off-eutectic alloys. The alloys studied consisted of Pb with 40 and 50 wt.% Sn in addition to the near-eutectic 63Sn-37Pb alloy. The proeutectic particles in these off-eutectic alloys were shown to spread out the deformation sufficiently to prevent the formation of

long straight shear bands. As expected, the fatigue life of these off-eutectic alloys was significantly greater than the eutectic even though all three failed by formation of a coarsened band when tested at 75°C with strain ranges between about 5 and 10%.

The 40Sn-60Pb alloy, which is further off eutectic and therefore has more of the beneficial proeutectic particles than the 50Sn-50Pb alloy, was less resistant to fatigue failure. It was concluded that the interdendritic, eutectic regions in the 40Sn-60Pb alloy had a structure, for reasons which are proposed, promoting heterogeneous deformation than those in the 50Sn-50Pb alloy.

In addition, the Pb-rich 20Sn-80Pb and 5Sn-95Pb alloys were studied in fatigue at 75°C. Both alloys showed evidence of locallized recrystallization ahead of the fatigue crack and failed intergranularly at all strain ranges tested between about 5 and 10%.

ACKNOWLEDGEMENTS

Throughout my childhood, my parents were a continuing source of encouragement and support. They set excellent examples and raised me to believe that there was nothing I could not do if I wanted to. Without them, I would not be where I am today, and their efforts are appreciated. I must also thank my husband, Lenny Summers, whose support, understanding and patience all these years have been a great help to me.

I'd like to thank my research advisor, Professor J.W. Morris, Jr., for continued academic guidance. He could not have been more knowledgeable, supportive or understanding and was a major influence throughout my graduate career. Completion of this project would not have possible without him. I would also like to thank my other thesis committee members, Professors R.O. Ritchie and D.A. Dornfeld, for their time taken reading my thesis and their helpful comments.

Finally, I would like to thank all my fellow Morris Group students for their support and encouragement. In particular, I'd like to thank D. Tribula, Z. Mei and J. Glazer for helpful technical discussions, J. Chan for moral support and experimental assistance in addition to many technical discussions, and Jane Fortado for her bright smile as well as her administrative assistance.

This work is supported by the Director, Office of Energy Research, Office of Basic Energy Science, Material Sciences Division of the U.S. Department of Energy under Contract No. DE-AC03-76SF00098.

TABLE OF CONTENTS

1. INTRODUCTION

1.1. Background

Interest in tin(Sn) - lead(Pb) solder fatigue has come mainly from the electronics industry where current trends place increasing demands on solder joints. In the past, the plated-through-hole (PTH) technology, where leaded components are soldered through holes in the printed wiring board (PWB), was almost exclusively used. In PTH-soldered joints, compliant leads absorb any strains present so that the solder is mainly required for electrical contact rather than for mechanical support. Also, with PTH components, the lead size and spacing is determined by how small and how closely spaced the holes in the PWB can be made while still allowing insertion of the component leads without damaging them. As a result, PTH solder joints tend to be rather large and mechanical failure of them is relatively rare. Fatigue failures have been seen, however, in plated-through-hole joints due to, for example, thermal expansion mismatches through the thickness of the PWB [1,2] and from a stiff encapsulating material pushing the lead through the PWB hole with thermal cycling [3,4].

Although introduced in the 1960's, surface mount technology (SMT), where components with or without external leads are mounted to the surface of the PWB, has become widely used only within the past 10-15 years. With surface mounted components, the leads, when present, are not subject to the same restrictions as PTH components and, therefore, can be made much smaller. As a result, the advantages of SMT include: greater input/output density due to smaller components and smaller solder joint sizes, cheaper and easier manufacture of PWBs without plated through holes, greater suitability for automated processes and better electrical properties. The main disadvantage of SMT, then, is that smaller solder joint sizes and more severe loading geometries require that solder joints provide mechanical support as well as electrical continuity.

Strains in the solder joint come from many sources. For example, temperature gradients present when chips are powered on can cause a variety of tensile and/or shear strains in nearby joints [5]. Distortion of components and PWBs due to in-plane thermal gradients can cause tensile strains in the solder joints, while through-thickness temperature gradients and the presence of materials with differing thermal expansion coefficients across the solder contacts can cause shearing of the solder joint. Failures, although aggravated by the presence of tensile stresses [6-8], are generally observed to initiate in regions where the shear strains are highest in the joint [7-11]. Power cycling and cyclic temperature changes cause cyclic straining so that the limiting problem with current solders is their lack of adequate resistance to thermal fatigue in shear. Thermal shear straining due to thermal expansion coefficient mismatches across a surface-mounted solder joint is schematically illustrated in Figure 1.1.

Thermal fatigue of solder alloys is one of the most complicated subjects to study. By definition, soldering occurs below about 400°C, but alloys with much lower melting points are generally used. Room temperature, then, is greater than half the melting point of most solder alloys. Because of high service homologous temperatures, recovery and creep mechanisms almost certainly operate during fatigue. As a result, microstructural changes such as coarsening and recrystallization can be expected to occur in some cases with thermal cycling. These changes in addition to the imposed cyclic temperature changes cause the mechanical properties of the solder to change with cycling as well as during any given cycle. For these reasons, all aspects of solder fatigue are not likely to be well understood any time soon. In the meantime, the electronics industry must design around the problem of solder fatigue.

Quite often the thermal expansion coefficients of the PWBs are tailored to match that of the chip carrier [12-14]. This approach, however, only works if all the components on the board are made of the same material. And even if they are, temperature gradients between hot components and the cool boards can cause relative displacements across the solder

joint. Also, some designers resist changing the material their boards are made of because of fears that the electrical properties of the assembly will be adversely affected [15]. In some cases, tailoring the in-plane expansion of polymer boards increases the thermal expansion coefficient in the through thickness direction to a great enough extent that the performance of plated-through-hole joints on the board is adversely affected [16,17]. In any case, it has been shown [18] that matching the thermal expansion coefficients of the bounding materials only postpones failure due to the mismatch between the solder and the substrates.

In Figure 1.2, a schematic illustration of a leadless surface-mounted solder joint is shown. Cracking usually starts at the corner of these components initially propagating under the component where the shear strain is greatest and finally propagating through the fillet region [7-11]. Some solutions to the problem of thermal fatigue of these components have involved increasing the fillet size of the joint [7,10] in order to increase the crack propagation path length. Chilton et al. [8], on the other hand, suggest that removal of the fillet region improves fatigue properties by eliminating the stress concentration at the corner of the device thus postponing crack initiation in addition to decreasing tensile stresses in the joint. Others attempt to decrease the solder joint shear strain by increasing the solder joint thickness [19,20]. In any case, chip carriers are usually kept relatively small so that strains in the outermost joints do not reach high levels, and in extreme cases, compliant leads which take up any strains present are added [15,21]. Thus, only relatively small strains are present in the solder joints. Solder joint reliability in these cases requires the ability to predict life at small strain amplitudes. As will be discussed in a subsequent section, published data are somewhat biased toward solving this aspect of the reliability issue.

In minimizing device sizes, designers attempt to maximize the functions performed per unit area of printed circuit board or function density. This density can be increased by increasing the chip size or at least the number of input/output contacts within a single package. If the chip size or function density increases, however, then the surrounding

package (or chip carrier) must also increase resulting in larger strains on the outer solder joints connecting the chip carrier to the printed circuit board. To optimize the advantages of SMT, then, leadless chip carriers of rather large size would be used. Assuming the solder is completely compliant, an assumption which generally results in an overestimate of the strain, and assuming linear thermal expansion, the strain in a solder joint at the corner of a leadless chip carrier is given by:

$$\Delta\gamma = \frac{(\Delta\alpha\Delta T)L}{(\sqrt{2}\,h)} \tag{1.1}$$

where $\Delta\alpha$ is the difference in thermal expansion coefficient of the materials across the joint, ΔT is the temperature cycle seen at the joint, L is the length of a side of the chip carrier and h is the solder joint height. The dimensions in the above equation are illustrated schematically in Figure 1.3. For a ceramic chip carrier typically made of Al_2O_3, the thermal expansion coefficient is 6 ppm/°C, and for a typical polyimide/glass board, it is 15 ppm/°C. Neglecting temperature gradients due to power cycling, joule heating during a power on/off cycle is about 50-75°C. For a 3-cm square chip carrier and .2-mm thick solder joints under the above conditions, the strain range in the corner joints is about 10%. Current solder alloys do not have sufficient fatigue resistance at these strain levels, and it has been suggested [7,22] that only minor, if any, improvements can be made by substituting other low-melting solders. Another aspect of solder joint reliability, then, is the need to improve the fatigue properties of existing solders at relatively high strains so that more aggressive SMT designs can be used. It is this approach that is emphasized in this work.

1.2. Solder Fatigue Data

The review here is by no means complete and is only meant as a summary to illustrate a few points which are relevant to this work. For more extensive reviews see Lau and Rice [23] and Fine and Jeannotte [24].

1.2.1. Fatigue Life Prediction

As stated above, most surface mount components used today are leaded. Because the leads are very compliant, the solder joints see relatively small strains. Consequently, published data have focused more on fatigue life prediction at low strain levels than on improving fatigue life at the higher strain levels that would be seen by leadless components. Many of these studies have involved thermal cycling [25-30], but most involve isothermal fatigue [10,13,14,31-44]. At present, no prediction method has been universally accepted [45,46] although many have been proposed [10,12-14,25-44]. It is likely that more attention will have to be focused on the initial solder microstructures seen in various soldering procedures and on the microstructural changes occurring as a result of deformation under various loading conditions before any universal prediction technique can be developed.

1.2.2. Near-Eutectic Sn-Pb Solder Fatigue Data

As shown in Figure 1.4, Sn and Pb make up a simple eutectic system. The most commonly used solders in the electronics industry are the 60 and 63 wt.% Sn-Pb alloys which are near the 61.9 wt.% Sn eutectic composition. The 63Sn-37Pb alloy is commonly called the eutectic composition even though, in bulk at least, it is not. After using it to form a joint on say copper, however, intermetallic formation at the interface depletes enough of the Sn that the remaining joint composition is at least very close to the 61.9Sn eutectic composition. This would explain the absence of the primary Sn-rich phase in 63Sn-37Pb joints. In this study, no distinction is made between the 63Sn-37Pb and the eutectic alloy

since most microstructural analyses and all the data taken for the 63Sn-37Pb alloy are done for solder joints on copper rather than in bulk. Much data has been published for these two alloys both in bulk and as joints.

Because the strength of solder is low and the plastic strains are high, solder fatigue data are generally represented by the Coffin-Manson [47-50] low-cycle fatigue relation:

$$\Delta\varepsilon_p N_f^z = M \tag{1.2}$$

where $\Delta\varepsilon_p$ is the plastic strain range, N_f is the number cycles to failure, M is a constant related to the ductility of the material and z is a constant approximately equal to .5 for many materials. When testing in shear, as is typical for solder joints, $\Delta\gamma$ is simply substituted for $\Delta\varepsilon$ in equation (1.2). Of course, a different value for the constant M is expected when testing in shear.

1.2.2.1. Coffin-Manson Data

Values for the Coffin-Manson constants vary depending on the condition of the solder tested as well as on the actual testing procedure. In general, when testing solder joints in shear under total strain or stroke control at a constant temperature, the Coffin-Manson exponent is approximately .35 [2,51,52], but values as low as .18 [53-55] and as high .85 [32] have been reported. Solomon [37,56] showed that testing under plastic strain control results in an exponent near .5 at least at lower temperatures. At a testing temperature of 150°C, he reported a value of .37. Taylor and Peddar [57] fit thermal cycling lifetime data to a modified Coffin-Manson equation and obtained an exponent of .6. In bulk isothermal tension-tension fatigue tests, Cutiongco et al. [58] determined z to be approximately .75.

There is considerably more scatter in the values reported for the Coffin-Manson coefficient, M. Since M is related to the ductility of the material tested (a fact easily verified by setting N_f in equation (1.2) equal to 1/4 [47-50]) and since ductility is a strong function

of the microstructure, this scatter may be an indication that the microstructures of the solders tested by different investigators varies considerably. Of course, these values also depend on the testing conditions such as temperature and strain rate used. Reported solder joint values vary from about .14 to 2.4 [2,32,37,51,56].

1.2.2.2. Effect of Testing Parameters

When attempting to design an accelerated fatigue test, the effect of various testing parameters such as strain rate, strain amplitude, temperature and temperature cycles, hold time intervals, and cycle shape must be known. Many investigators have looked into these effects [2,7,33,36,38,58-64]. In general, it is found that decreasing the frequency (i.e. strain rate) below a certain value decreases the fatigue life when testing under isothermal conditions whether testing bulk solder in tension [58] or solder joints in shear [2,36,60]. The same trend is seen with increasing hold time [38,58-60,62]. The effect of strain rate, hold time and other testing parameters on the thermal fatigue life of near-eutectic solder joints is less well understood. The data of Shine, Fox and Sofia [33,60] suggest that the overall life behavior as a function of frequency in thermal fatigue is the same, but the effect may be stronger than in isothermal fatigue. The work of Wild [7] and Frear and Jones [63,64] suggest that an opposite trend may be seen for thermal fatigue (i.e. an increasing life with decreasing testing strain rate). Although these results are preliminary, they are not unreasonable at least for the case of rather severe temperature extremes. As will be discussed later, shear fatigue failures of near-eutectic solder joints involve recrystallization at least under certain loading conditions. When a specimen is cycled between very low and very high temperatures (eg., the military specification of -55 to 125°C), part of the time spent during cycling occurs below the recrystallization temperature. Therefore, a slower strain rate allows more recovery to take place during deformation below the recrystallization temperature. This recovery may reasonably be expected to decrease the driving force for recrystallization and thus increase the recrystallization temperature so that damage

accumulated during one cycle is decreased. During isothermal fatigue at temperatures above about room temperature, however, deformation occurs above the recrystallization temperature throughout any given cycle and a slower strain rate would be expected to produce greater damage per cycle. The quantitative as well as mechanistic aspects of these differences must be worked out before accelerated tests designed to predict fatigue life can be produced.

1.2.3. Fatigue Data for the Pb-Rich Sn-Pb Alloys

In addition to the near-eutectic alloys discussed above, the 5Sn-95Pb and other Pb-rich alloys are also used, for example, when a higher melting temperature is needed. A higher melting point may be necessary in relatively high-temperature applications such as in automobile engines or when a hierarchy of melting points is needed for multistep soldering processes.

1.2.3.1. Coffin-Manson Data

There are less high-lead solder joint fatigue data published than exist for the near-eutectic Sn-Pb alloys. Solomon [65,66] measured Coffin-Manson type fatigue data for Pb-rich solder joints containing 2.5 wt.% silver (Ag) as well as 5 wt.% Sn and found that the Coffin-Manson exponent was higher than it had been for the 60Sn-40Pb alloy. This result suggests that the Pb-rich solders have better fatigue properties than the near-eutectic Sn-Pb solders at high strains, but that the reverse is true at low strains. The effect of the Ag intermetallics present in this solder is unknown, however, the same trend was seen in bulk 5Sn-95Pb and 60Sn-40Pb samples tested in torsion fatigue by Kitano et al. [67]. At higher strains (20 to 35%) and a lower frequency than that used by Solomon [65,66], McCormack et al. [53-55] could not fit their data to an equation of the form of equation 1.2.

In testing bulk 5Sn-95Pb at temperatures between 25 and 80°C, Rathore et al. [68] found that the Coffin-Manson exponent, z, was approximately 0.5. Between 5 and 100°C,

Vaynman et al. [69-73] found a break in the slope of the Coffin-Manson curve. While z varied from 0.45 to 0.62 depending on temperature at low strain amplitudes (< ~0.3%), it was lower (0.25 to 0.45) at higher strains. They attributed this shift in value to a change in the fracture mode from purely intergranular at low strains to mixed intergranular-transgranular at higher strains.

A break in the Coffin-Manson curve is not entirely unexpected. Using a simple argument first proposed by Shine et al. [33-35], when anelastic deformation during fatigue is pure creep, the number of cycles to failure can be approximated by

$$N_f = \varepsilon_f/\Delta\varepsilon_p \tag{1.3}$$

where ε_f is the creep rupture strain and $\Delta\varepsilon_p$ is the applied plastic strain amplitude. Comparison of equations (1.3) and (1.2) shows that the Coffin-Manson exponent in this simple case is 1 rather than 0.5 which is seen for fatigue by conventional dislocation glide mechanisms.

Stone [74] also proposed a mechanism by which there would be a shift in the strain-life behavior. At higher strain amplitudes, deformation occurs by slip resulting in typical Coffin-Manson behavior and an exponent, z, of about 0.5. At lower strain amplitudes or strain rates, grain boundary sliding increases the amount of creep deformation resulting in a value of z closer to 1. His model involves nucleation of cracks at the specimen surface due to grain boundary sliding and oxidation of the newly exposed grain boundaries. Once oxidized, these boundaries cannot reweld upon reverse straining and eventually cracking occurs.

Both of the above arguments are consistent with the observed effects of environment on fatigue life [75-78]. In the case of the model of Stone [74], oxidation of the boundaries in air would be greater than it would be in vacuum so that the fatigue life, as is observed

[75-78], decreases. The model of Shine et al. [33-35] differs only in that the amount of strain and not the fraction of creep is assumed to change with frequency and hold time.

As can be seen in the phase diagram of Figure 1.4, the tin precipitates present at room temperature in a 5Sn-95Pb alloy dissolve at about 100°C. This fact presents an added complication when comparing fatigue data. Stone and Raman [79] found that grain boundary migration decreased in the presence of cellular Sn precipitates so that the different values of z reported may be due to the presence or absence of these precipitates as well. In fact, Rathore et al. [68] found that z approached 1 at strains greater than 1% for temperatures greater than 120°C and attributed this shift to the dissolution of Sn precipitates. Kitano et al. [67] found that the effect of temperature on the fatigue life of 5Sn-95Pb solder was stronger than it was for 60Sn-40Pb and suggested that the difference was due to dissolution of Sn precipitates at the higher temperatures.

1.2.3.2. Effect of Testing Parameters

The effect of frequency on fatigue life appears to be the same as for the near-eutectic alloys (i.e. life decreasing with frequency below a certain value of the frequency). This conclusion is drawn mostly from bulk data [31,67-73,80] but also from the torsion fatigue of solder joints [60].

Applying a hold time [69-73] as well as increasing the testing temperature [65-67,70,73] has been found to decrease the fatigue life. At relatively large strains, however, temperature seems to have relatively little effect [54,55,67,68] and at higher temperatures, the fatigue life becomes relatively insensitive to temperature [68-73]. Rathore et al. [68] suggested that at high temperatures, the effect of temperature decreases because the Sn precipitates are completely dissolved. Vaynman et al. [69-73] later drew the same conclusion from their data. At lower temperatures, life, then, probably decreases as temperature increases due to the decreasing volume fraction of the beneficial Sn precipitates present.

The presence of Sn precipitates in Pb-rich solder adds a complication to thermal fatigue where the specimen is often cycled between two temperatures one of which is above 100°C and the other below. Under these conditions, it is quite possible that Sn precipitates may repeatedly dissolve and reprecipitate during thermal cycling. When tested in thermal fatigue, 5Sn-95Pb solder joints yield Coffin-Manson exponents from 0.3 [81] to 0.5 [82] when fit to modified Coffin-Manson equations. Water-cooled joints were reported [81] to have shorter thermal fatigue lives than the normally air-cooled joints and an exponent of 0.19. Other thermal fatigue studies of 5Sn-95Pb solder joints include those of Levine and Ordonez [83], D. Frear et al. [18,84], Goldman et al. [85], and Kang et al. [86].

1.2.3.3. Failure Mechanism

As stated above, loading conditions which tend to shift creep processes from bulk to grain boundary mechanisms also appear to shift fatigue failures in the Pb-rich alloys from within the grains to the grain boundaries. This change in mechanism resulted in a switch from mixed mode intergranular/transgranular fracture to purely intergranular fracture as the applied strain amplitude and frequency were decreased or the tensile hold time was increased [69-73] and also as the temperature was increased [67,68]. Grain boundary cavitation and migration failures have also been reported [75,87-92], but these observations were made on specimens fatigued in tension. The deformation behavior in shear may actually be different. In some cases, grain boundary migration was reported to lead to the formation of a diamond configuration or a mosaic cracking pattern [87,88,93]. This mosaic pattern was later observed after thermal fatigue by Frear et al. [18,84] and after isothermal fatigue in shear by McCormack et al. [53-55]. One study [90] reported recrystallization of a high-Pb alloy during fatigue.

1.3. Emphasis for this Study

Reliability, especially in more aggressive leadless SMT designs, will require an improvement of the solder fatigue properties. Alloy development, in turn, requires an understanding of microstructural changes and failure mechanisms occurring during service. Even for fatigue life prediction, an understanding of the failure mechanism is necessary to insure that the accelerated testing procedures employed reproduce the failure mechanism seen in service.

Failure in actual joints made of the near-eutectic alloys by thermal cycling are generally observed to be accompanied by the formation of a band of coarsened material along the directions of shear straining [11,26,94-96]. Heterogeneous coarsening has also been seen in fatigue of experimental solder joints [2, 9, 61]. Once this coarsened band forms, further deformation presumably concentrates within it, and failure ultimately occurs there. It is upon this failure mechanism as well as methods of fatigue life improvement inferred from it that this study is focused.

2. FATIGUE FAILURE MECHANISM

Before presenting the fatigue failure mechanism, it is first necessary to discuss the specimens used for testing under thermal fatigue and other conditions and how they are made. Then, because fatigue failure involves microstructure-induced heterogeneous deformation and microstructural changes, the eutectic microstructure must be examined. First a review of general eutectic microstructures will be given. Then an examination of the microstructures seen in our cast joints will be made.

2.1 Experimental Specimens

2.1.1. Thermal Fatigue Specimen

The specimen used and developed here at LBL [18,53] to reproduce thermal fatigue conditions is shown schematically in Figure 2.1. Because aluminum (Al) and Copper (Cu) have greatly differing thermal expansion coefficients, as shown, the two solder joints are fatigued in shear when the specimen is cycled between two temperature baths. In the past, these specimens were made under an argon (Ar) atmosphere. As described elsewhere [18,97], two 3.2-mm (1/8-inch) Cu plates and one 6.4-mm (1/4-inch) Al plate were polished down to 6μm using standard metallographic procedures. The Al plate was then electroplated with a Ni diffusion barrier and Cu so that the interfaces exposed to the solder had the same composition on both sides of the joint. The plates were then etched in diluted nitric acid, coated with flux, and assembled with wire spacers of appropriate diameter. The assembled block was heated in the upper portion of an Ar-filled two-stage furnace while the solder, which was contained within a graphite crucible which in turn was held within a quartz crucible used to seal the vacuum chamber, was simultaneously melted in the lower half. When both reached a temperature of about 50°C above the melting point of the solder used, the Cu-Al block was lowered into the molten solder. The entire Cu-Al block/solder/graphite crucible/quartz crucible assembly was then quenched in ice water while the furnace was still filled with Ar. Because the semi-evacuated space between the graphite and quartz crucibles is relatively insulating, the cooling rate seen by these specimens was relatively slow. Once cool, the block was removed from the furnace, the excess solder was removed by machining, and the block was sliced. Typical solder joint microstructures will be discussed in a subsequent section.

The strain in this specimen is zero at the center and increases in moving toward the edges. To calculate the strain, an equation similar to equation 1.1 is used:

$$\Delta\gamma = \frac{(\Delta\alpha\Delta T)L}{(2\,h)} \tag{2.1}$$

where, here, L is the specimen length. For a 100-mm specimen, the strain range at the edge of a .5-mm joint for a temperature excursion from -55 to 125°C, which is the military specification, is about 16%. Equation 2.1, of course, assumes that no stress builds up in the solder and that there is no constraint on the expansion of the Cu and Al. It is therefore an overestimate of the strain. Because the stress in the solder and therefore the constraint on the expansion of the Cu and Al is nonlinear along the length of the specimen, the strain in the solder does not increase linearly from the center of the specimen to the outside. It does, however, increase monotonically. Isolated solder joints at varying amounts of strain can thus be made by drilling holes along the specimen as shown.

2.1.2. Double Shear Specimen

For testing under conditions which require mechanical application of the shear strain, the double shear specimen, which was also designed at LBL [18,97], is used. This specimen, which is drawn in Figure 2.2, has a unique design which minimizes the amount of tensile strains due to bending seen, for example, in the more common lap joint. The method by which the double shear specimen is made produces relatively defect-free solder joints. These specimens were made in a manner similar to that discussed above for the thermal fatigue specimens. Instead of Cu-plated Al, however, a 6.4-mm (1/4-inch) Cu plate was used, and as described elsewhere [97], there were more machining steps following quenching of the block. After removing the excess solder from the Cu block, a 3.2-mm (1/8-inch) hole was drilled through the center of the center 6.4-mm (1/4-inch) Cu plate. Notches were also machined using a ball-nosed end mill across the outer Cu plates. This hole and these notches were separated by 9.5mm (.375 inch) from center to center, and the two were centered along the length of the specimen. After slicing the block to

produce specimens of about 1.5 to 1.7mm thickness, the holes in the center Cu plate were expanded to produce the slot shown in Figure 2.2.

For this work, some modifications to the casting procedure were made. First, since the intermetallic layer had been determined to have no effect on the shear properties of solder [18], it was decided that a mechanical polish down to 6μm diamond paste was unnecessary. Instead, the Cu plates were polished only to 600 grit SiC paper. No trace of these scratches was found after etching. It was also found that heating the assembled Cu block to remove the flux led to irreproducible results and wetting problems. It is possible that degradation of the furnace after several years of use allowed oxygen to leak into the chamber causing oxidation of the Cu while both the block and solder were heating. Rather than rebuild the vacuum furnace, it was decided that since solder joints in industry are made in air with success, that casting in air would be an easier solution. Following etching, the Cu blocks were dipped in Johnsons Stainless Flux and then in solder of the desired composition prior to assembly. It was found that this "pretinning layer" could be made very cleanly by scraping the oxide layer off of the top of the molten solder prior to dipping and then removing the Cu plate quickly to prevent any oxide present from depositing on the surface of the pretin layer. These pretinned plates were then assembled in the usual way, but were dipped in molten solder in air without heating the block prior to insertion. To prevent the solder from freezing when the cool Cu block was inserted, a casting temperature of 100°C rather 50°C above the melting point of the alloy was used. Final machining of the resultant block was performed in the usual way discussed above. This modified procedure is illustrated in Figure 2.3.

The shear stress on the two isolated central solder joints when the double shear specimen is loaded uniaxially in tension to load P is given by:

$$\tau = P/lt \tag{2.2}$$

where l is the joint length and t is the specimen thickness. The shear strain is given by:

$$\gamma = \Delta l/h \tag{2.3}$$

where Δl is the shear displacement of the joint and h is the joint thickness.

The double shear specimen is used whenever a shear strain is mechanically applied to the solder joint. Examples include creep, isothermal fatigue and shear strain to failure experiments. All of these methods were used in this study. Isothermal fatigue is used rather than thermal fatigue for the following reasons. First, isothermal fatigue tests are easier and more quantitative. As discussed above, the actual strain on the thermal fatigue solder joint is unknown. Also, the temperature and strain rate and therefore the mechanical properties of the solder are continuously changing during a thermal fatigue cycle. Additionally, the strain, strain rate and temperature are, to some extent, mutually dependent. The stresses on the joint of a thermal fatigue specimen discussed above cannot be determined. All of these factors combine to make analysis of thermal fatigue results difficult. Second, as will be discussed below, the failure mechanisms seen in thermal and isothermal fatigue specimens are at least similar. This similarity is expected especially for thermal fatigue cycling between two high homologous temperatures which is a more realistic thermal cycle for many electronics industry applications than the rather severe military specification of -55 to 125°C. Third, isothermal fatigue testing is often used to predict the life of solder joints used under thermal fatigue conditions. An isothermal fatigue failure mechanism is therefore in and of itself important. If there are differences from the thermal fatigue failure mechanism, it will be important to know what those differences are and under what conditions they occur before accurate predictive models can be developed. Finally, the goal of this work is to determine methods by which improvements in the fatigue properties of near-eutectic solders can be made. As already mentioned, the failure mechanisms seen in isothermal fatigue are at least similar to those seen in thermal fatigue.

Therefore, any method developed to improve the isothermal fatigue properties of solder are also likely to improve the thermal fatigue properties at least under some service conditions.

2.2. Near-Eutectic Microstructures

Before a failure mechanism can be identified, the microstructure must be discussed. Because the eutectic or near-eutectic microstructure consists of two phases which arrange themselves in many different ways especially under normal casting conditions, it is somewhat complex. Most theoretical and microstructural studies of eutectic alloys have involved unidirectional solidification under very controlled conditions. Initially, this work will be reviewed. Then it will be extended to the more complicated case seen in our cast solder joints.

2.2.1. Eutectic Microstructures -- General

Eutectic solidification is reviewed extensively elsewhere [98-100]. The resulting microstructures range from the normal lamellar microstructure to the irregular, acicular microstructure. Generally, eutectic microstructures are broken up into groups based on whether the phases are faceting or not. The simplest systems are those in which both phases are nonfaceting. Since most metals are nonfaceting, it is these systems which are emphasized here. See Elliot [100] or Hunt and Jackson [101] for a discussion of anomalous eutectic microstructures in which one of the two phases is faceting.

Among nonfaceting metals, the most common distribution of the two phases is a regular lamellar morphology resulting from anisotropic surface energies. Even though the surface to volume ratio of a plate is relatively high compared to more equiaxed shapes or even to a rod, if the lamellae lie on low-energy planes, then the overall surface energy can be reduced. Therefore, rods are sometimes seen in alloys where the surface energy is relatively isotropic [102]. Rods are also seen in alloys where the volume fraction of the two phases differ greatly [103,104]. More globular microstructures are also seen, but

these require repeated nucleation and do not result from cooperative growth of the two phases and are, thus, referred to as degenerate microstructures. Degenerate morphologies will be discussed later.

2.2.1.1. Regular Lamellar Eutectics

Regular lamellar eutectics, of which Sn-Pb eutectic is one, result from the cooperative growth of two phases arranged as adjacent plates. As one phase, α, rejects B atoms, the other phase, β, takes in the B atoms while simultaneously rejecting A atoms. It is generally believed [100,105-109] that one of the two phases nucleates at heterogeneous sites such as impurities or at the mold wall and the other nucleates heterogeneously on the first. In the case of Sn-Pb, Sn has been reported [100,105,106] to nucleate Pb. This fact is evident in off-eutectic alloys, as pointed out by Davies [106] and Mondolfo [107]. Figure 2.4 shows the microstructure a Pb-rich and of a Sn-rich, bulk, off-eutectic alloy. On the Pb-rich side, the primary Pb has not nucleated the eutectic material. Instead, "halos" of Sn form around the proeutectic particles before a normal eutectic reaction begins. These Sn-rich "halos" have been attributed [106,107] to the continued growth of the primary Pb particles near the eutectic temperature until there is sufficient undercooling to nucleate Sn. When such undercooling exists, the liquid surrounding the Pb islands is rich in Sn so that Sn nucleates and grows depleting Sn before the eutectic reaction can take place. On the Sn-rich side, eutectic lamellae grow out perpendicular to the Sn proeutectic suggesting that Sn does nucleate the eutectic while Pb does not.

It is also generally accepted that lamellae in a normal eutectic material lie on characteristic planes [110-114]. This makes sense if the anisotropic surface energy argument for the existence of lamellae holds. In Sn-Pb eutectic, however, there is some controversy over what the orientation relationship between Sn and Pb lamellae actually is [112-114]. The different values obtained are most likely due to different specimen

preparation procedures and to experimental error in attempting to obtain crystal structure data from the small lamellar regions [114].

During lamellar growth there exists, for each solidification condition, a preferred lamellar spacing. This spacing is determined by a balance between creating the shortest diffusion path and decreasing the surface energy while increasing the concentration gradient between lamellae [98,100]. Many theories exist [99,103,104,106,115-117] which quantitatively specify the lamellar spacing in terms of growth rate or undercooling. Generally, the spacing is found to be proportional to the undercooling or to the square root of the growth rate.

Even when grown under fairly ideal conditions, lamellar eutectic grains have a faulted structure due to extra or missing lamellae [118]. The presence of these faults has been attributed to local changes in the solidification conditions [118,119] and also to imperfect lattice matching on lamellar planes [103]. It has been suggested that the two phases within a lamellar eutectic grain make up two interpenetrating single crystals in that the lamellae of each phase within a grain differ in orientation by only a few degrees [116]. Verhoeven et al. [114] subsequently reported that the lamellae within a single grain were within ±5° of each other. This regularity is expected to decrease with an increase in the fault density and under less ideal solidification conditions.

2.2.1.2. Degenerate Eutectic Microstructures

The term degenerate has been used to describe divorced eutectic [107], where one phase grows prior to nucleation of the other, and wavy lamellar [114,120] as well as to globular morphologies. Here, degenerate is used to describe any nonlamellar morphology which forms in a normally lamellar eutectic. Most eutectic microstructural studies were done using unidirectional solidification so that the microstructure that forms is usually given in terms of the growth rate, R, and the temperature gradient, G.

Degenerate microstructures are seen at very slow growth rates [103,104]. Cooksey et al. [103] suggested that at the slower growth rates temperature fluctuations become more significant. Also, as the lamellar spacing increases, the surface energy decreases to the point that the surface energy differences between a lamellar and a rod-like or globular morphology become insignificant and ease of diffusion (i.e. kinetics) controls which morphology forms. At very fast growth rates, the microstructure also becomes degenerate due to independent nucleation of the two phases ahead of a solid-liquid interface which is concave towards the liquid and, when the temperature gradient is high, due to anisotropic heat conduction in the Sn [114]. It has also been proposed that degenerate structures result at fast growth rates from insufficient time to develop a preferred growth direction [121,122] and to forcing the lamellae to grow in unfavorable directions [103,112].

When impurities are present, degenerate material is sometimes seen in regions throughout the microstructure. Weart and Mack [123] first described this microstructure, called it a colony microstructure and suggested that it formed due to the cellular break down of the interface during solidification. Subsequent work [103,104,116,124] verified that a colony structure results from simultaneous rejection of an impurity from both eutectic solid phases during solidification. A schematic illustration of the formation of a colony structure is shown in Figure 2.5. During solidification, impurities are either rejected to the liquid or preferentially absorbed in the solid. Eventually, this process can result in a cellular breakdown of the interface due to constitutional supercooling [98,125]. As the solid-liquid interface curves, the lamellae are forced to curve as well. Because a curved lamella will have a higher surface energy than a straight one and because lamellae form in preference to degenerate structures only because the α-β interface lies on a low surface energy plane, the microstructure will often become degenerate in the intercellular or colony boundaries. Following Weart and Mack [123], then, there exists a hierarchy of microstructural features in an impure eutectic alloy. The largest unit is the eutectic grain which is defined as a region of the microstructure which grew from the same two-phased nucleus. A colony is a

subset of the eutectic grain which resulted from the cellular breakdown of the solid-liquid interface during growth of that grain. Within the colony are the two phase regions, and within the phase regions, there can exist single phase grains which are present in faulted lamellar microstructures as well as in most degenerate microstructures.

A similar type of breakdown, although not as dramatic, is seen in the eutectic grain boundaries. Kraft and Albright [126] attributed this effect to impurity rejection at slow growth rates (which inhibit constitutional supercooling). As the eutectic grain boundaries approach each other, they proposed that the solubility limit is reached so that the impurity precipitates and nucleates grains ahead of the interface. It is also possible that impurities perturb the interfaces as it builds up in the last liquid to solidify or that increased heat of fusion from the approaching interfaces locally perturbs the solidification conditions causing lamellae to broaden and break down into degenerate structures.

2.2.2. Solder Joint Microstructures

Solder joints are not prepared using well-controlled, unidirectional solidification techniques. Instead, temperature gradients vary throughout the joint both spatially and with time during solidification. As pointed out by Tribula [127,128], the faster cooling rates and the likelihood of there not being a seed crystal of preferred orientation present leads to microstructures containing both lamellar and degenerate structures. These more complicated cast microstructures are discussed below.

2.2.2.1. Eutectic Solder

As shown in Figure 2.6., the eutectic solder joint microstructure in specimens used in this study consist of a typical colony microstructure. This microstructure is similar for the older vacuum-casting procedure as well as the newer air-casting procedure. As shown, the microstructure consists of many globular degenerate regions as well as the more lamellar colony regions. These are not rods shown end on. As stated above, rods are not seen in

near-eutectic Sn-Pb alloys. Also, if rods were present, the chance that random sectioning always cut the rods either axially or perpendicular to the axis is negligible. In the case of rods, random sectioning should generally produce elongated phase shapes. Since elongated phase regions are never seen and only lamellar or more-or-less equiaxed morphologies are seen, it is concluded that the microstructural features may be described as lamellar or globular.

In looking optically at a solidified cross section, it is sometimes difficult to distinguish between colonies and eutectic grains. Both have relatively regular arrangements of phases within and are surrounded by somewhat irregular boundary regions. Because the mechanical properties as well as the appearance of colonies and eutectic grains are generally the same, no distinction is made here between them. Also, because a colony is a subset of a grain, all regions of the microstructure where the Pb and Sn phase morphology is the same are referred to as colonies. The boundary regions surrounding these regions are referred to as colony boundaries.

A typical colony boundary region is shown in Figure 2.7. As discussed above, it is not a planar feature as grain boundaries are in single-phase alloys but has a finite thickness. The Sn and Pb phases within the colony boundary are fairly uniformly distributed and made up of equiaxed grains. These equiaxed grains are expected to be much more deformable than the lamellar material where deformation must occur by a cooperative mechanism [129-131]. Uniformly distributed, equiaxed grains can deform much more independently and, as illustrated by the case of recrystallized and quenched eutectic microstructures, both of which consist of equiaxed grains, are much softer [132]. This was also illustrated by Tribula et al. [127,128] who performed microhardness measurements on lamellar regions of the microstructure and showed that they were about 50% harder than the more degenerate diffuse boundaries in 60/40 solder with ternary additions.

2.2.2.2. Near-Eutectic Pb-Rich Solders

Some of the earlier fatigue failure mechanism studies [6,18,53-55, 84,127,128,133-139] used the near-eutectic 60Sn-40Pb solder. A typical microstructure in those cases is shown in Figure 2.8. As shown, the amount of proeutectic is relatively small and, therefore, has little effect on the surrounding eutectic microstructure. Very near the primary Pb, however, the eutectic microstructure is somewhat degenerate. This is most likely due to lead's inability to nucleate the eutectic material [106,107]. As discussed above, the primary Pb will continue to grow enriching the neighboring liquid in Sn. Once Sn nucleation is possible, Sn then grows from the Sn-rich liquid surrounding the Pb particles until the eutectic concentration is again obtained. Only then can eutectic material be nucleated, and unless a preferred Sn seed is present, it will be degenerate until a preferred orientation develops.

2.2.2.3. Intermetallics

Cu-Sn intermetallics are present both at the interface and throughout the bulk of the solder. Examination of the interface shows that the intermetallic layer consists of a layer of Cu_3Sn adjacent to the Cu and a layer of Cu_6Sn_5 whiskers adjacent to the solder consistent with previous studies [18,97,140,141]. These whiskers are believed to grow along a screw dislocation in the intermetallic [18,142] and sometimes break off into the solder melt during casting. Examples of Cu_6Sn_5 whiskers in the bulk solder can be seen in Figure 2.6(a). A previous study [18] has shown that these intermetallics have no effect on the mechanical properties of the solder joint under normal testing conditions.

2.2.2.4. Microstructures in Actual Near-Eutectic Solder Joints

Here, what is meant by an actual solder joint is a joint made by standard industrial processes. As discussed by Tribula et al.[127,128], the microstructures seen in thermal fatigue and double shear specimens are similar to those seen in industry for at least some

processing conditions. Tribula et al.[127,128] showed the microstructure of a solder joint made by a wave soldering process in industry. That microstructure was very similar to those seen above.

2.2.3. Eutectic Microstructural Stability

It has been shown that the lamellar microstructure is very stable even with relatively high-temperature aging treatments [114,143-147]. Coarsening and spheroidization begin discontinuously at lamellar faults, at the somewhat globular eutectic grain and colony boundaries and in degenerate regions of the microstructure. Therefore, the more faulted and irregular the as-cast microstructure, the less stable it will be.

2.3. Near-Eutectic Solder Fatigue Failure Mechanism

2.3.1. Background

As discussed above, heterogeneous coarsening during fatigue of near-eutectic solders had been widely reported [2,9,11,26,61,94-96]. Frear et al. [6,18,133], however, were the first to clearly illustrate this phenomenon and to describe several conditions under which it occurs. Frear et al. [6,18] suggested that this heterogeneous coarsening was due to localized deformation along microstructural heterogeneities which resulted in localized recrystallization and strain-assisted coarsening. Tribula et al. [127,128,134-137] further showed that deformation in these alloys is heterogeneous by polishing a double shear specimen prior to creep and looking at the deformed surface following creep. An in depth microstructural study [127,128] showed that the deformation was concentrating along colony or eutectic grain boundaries which, due to their structure, were expected to be softer than the surrounding material within the eutectic colony/grains. Tribula et al. also illustrated that once the coarsened band (as the band of heterogeneously coarsened material came to be called) formed, deformation concentrated within that band.

Further microstructural studies [135,136], showed that the coarsened band cut through colonies under some testing conditions and was not confined to the colony boundaries. This result could not be explained using the simple model proposed by Frear et al. [18,133] which was then modified. It was proposed [127,128,134,135] that nonuniform deformation caused a localized region of the microstructure to deform near the largest stress concentration in the joint. Because this recrystallized material is confined to the narrow boundary region and because it is softer than the surrounding as-cast material, it would then act as a virtual mode II crack propagating along the joint in the direction of shear. At high strain rates, the coarsened band was seen to propagate straight across the joint, and at slower strain rates, it followed a more tortuous path along colony boundaries [135]. This phenomenon was explained in terms of the greater strain rate sensitivity of the more equiaxed grains within the boundary regions. In this work many relatively straight coarsened bands were seen to follow colony boundaries. It was the intention here, then, to reproduce the loading conditions giving colony-cutting coarsened bands and stop testing before a coarsened band forms to show whether deformation is localized in long straight bands before the coarsened band forms or only once it has formed.

2.3.2. Experimental

Some of the micrographs presented in the following will be of isothermally fatigued 63Sn-37Pb specimens. These specimens were fatigued by mechanically applying a shear strain between 5 and 10% to the joints of double shear specimens. The details of the fatigue testing will be described later when the fatigue data are presented.

The rest of the micrographs are from interrupted creep tests. Following Tribula et al. [127,128,134-137], 63Sn-37Pb double shear specimens were polished using standard polishing techniques down to 0.05 μm. These specimens were then examined optically and tested in creep using loads between 20 and 30 kg. From previous work [135,137], it was known that the stresses generated from these load levels produced relatively straight

coarsened bands. After creep, the surface of the deformed joints were examined to determine the deformation pattern. Then, they were lightly repolished to examine the surface directly beneath the deformation pattern and repolished again to verify that the microstructure revealed by the light repolish was not a surface effect. All creep and isothermal fatigue tests were done at 75°C.

2.3.3. Results and Discussion

The microstructure resulting from interrupting a creep test in the secondary, steady-state creep range is shown in Figure 2.9. In the as-deformed specimen, a long, straight shear band can be seen running along the joint parallel to the direction of the applied shear strain. Repolishing, however, shows that no coarsened band has yet formed suggesting that the deformation concentrates into shear bands before the coarsened band initiates. Just how much deformation concentrates within these bands and in the colony boundaries can be seen in Figure 2.10. These shear bands, however, do not run entirely along the length of the joint. In some regions, an example of which can be seen in Figure 2.11, the deformation is more obviously along colony boundaries which are at various angles to the applied shear strain and do not line up into long straight easy-deformation paths.

It is interesting to note that in regions where the long straight shear bands exist (Figures 2.9 and 2.10), the deformation throughout the rest of the joint in that region does not concentrate significantly into bands parallel to the direction of shear. While in other regions of the joint where no boundaries line up parallel to the applied shear strain (Figure 2.11), deformation occurs along many more boundaries at various angles to the joint. This observation can be explained by assuming that when long straight paths of deformable material (i.e. colony boundaries which line up to form long straight bands) exist, then most of the deformation in that region can concentrate within that band. In those regions, then, all that is needed is the shear deformation along planes perpendicular to the applied shear strain resulting from the constraint which keeps the sample from rotating. In many of the

micrographs presented by Tribula et al. [135,137], this same pattern is shown for specimens containing a coarsened band. This fact is further evidence that the shear banding occurs before the coarsened band initiates. If deformation had been concentrated along random colony boundaries prior to the formation of the coarsened band which propagated across these boundaries in a straight path, then that earlier deformation pattern would still be present in the as-deformed specimens. The fact that it is not and that the pattern seen simply consisted of the one band parallel and several bands perpendicular to the direction of shear suggests that that deformation pattern was present to a great extent before the coarsened band formed.

Once these shear bands develop, what likely happens is that localized recrystallization occurs within the shear band near the largest stress concentration in the joint as suggested by Tribula et al. [127,128,134,135]. This softer recrystallized material will further concentrate the deformation ahead of it in the direction of the applied shear strain as would a mode II crack. But the fact that a sharp mode II crack, anyway, has a very narrow plastic zone elongated in the direction of shear is no longer necessary to explain the coarsened band's propagation along the shear band. Because the shear band already concentrates the strain, the deformation ahead of the coarsened band will be concentrated into a narrow region of about the same thickness as the coarsened band itself.

The conclusion that the coarsened band consists of recrystallized rather than coarsened boundary material is drawn from two observations as first proposed by Tribula et al. [136]. First, the distribution of Pb- and Sn-rich phases within the coarsened band is similar in appearance to a recrystallized microstructure. Second, the coarsened band has clearly been observed [136] to cut through colonies. Since the evolution of the coarsened band microstructure from a lamellar colony microstructure by a simple coarsening process is virtually impossible to imagine, it is assumed that the microstructure of the coarsened band, at least where it cuts through colonies, is a recrystallized microstructure. Because the

microstructure of the coarsened band is everywhere similar, it is assumed that it is everywhere recrystallized.

Given the above description, how is it possible that coarsened bands cut through colonies? As discussed above and shown in Figure 2.11, some regions of the solder joint microstructure do not have colony boundaries which line up to form long straight bands. For simplicity, these regions are referred to as "obstacles" since they are obstacles to the concentration of the deformation into long straight shear bands. In these obstacle regions, it is likely that the coarsened band must propagate through the colonies. It can do that by one of the two mechanisms shown in Figure 2.12.

For the case where two shear bands are approximately parallel but are separated by an obstacle region, the strain would localize through that region simply by the geometry of the deformation. This geometric strain localization would probably eventually cut the obstacle region shown in Figure 2.11. In Figure 2.13, a coarsened band, which formed during isothermal fatigue of a eutectic solder joint, has propagated around one of these obstacle regions. If fatigue had been continued, the deformation would have concentrated into a band across this obstacle because of the bands on either side of it. Recrystallization would eventually take place and the coarsened band would cut through the colonies of the obstacle region.

In cases where another shear band does not exist, the coarsened band can still propagate across the obstacle by the mechanism suggested by Tribula et al. [127,128,134,135]. In this case, the plastic zone shape ahead of the coarsened band becomes important. For a sharp mode II crack, the plastic zone is elongated in the direction of shear [135,148]. The coarsened band, though, is more directly analogous to a blunt mode II crack for which the plastic zone shape has not been calculated. Assuming the region receiving enough deformation to cause recrystallization ahead of the coarsened band is approximately as wide as the coarsened band, then the coarsened band can propagate across the obstacle regions as would a crack. Figure 2.14 suggests that this assumption is

valid. The crack shown formed in a shear strain to failure test which was stopped just past the ultimate load. As shown, the crack which forms is very blunt. Ahead of this mode II crack, Sn-Sn grain boundaries can be seen. Experience has shown that these grain boundaries are only seen after polishing in highly degenerate or recrystallized material (eg. in the coarsened band). Grain boundaries are seldom seen following polishing in the as-cast condition. Given that deformation concentrates ahead of the crack, the area where these boundaries can be seen likely represents a recrystallized zone. As shown, this recrystallized zone is of a thickness on the order of the blunt crack thickness suggesting that propagation of the coarsened band by a mode II crack-like propagation mechanism is at least possible.

The more tortuous path taken by coarsened bands in near-eutectic solder joints tested in creep at slow strain rates [135] may have been due to propagation of the coarsened band along the boundaries in the "obstacle" regions that are at an angle to the applied shear strain. Because the boundaries consist of more-or-less equiaxed Sn and Pb grains, they are much softer at slower strain rates than at higher rates [132]. The intracolony regions, on the other hand, are not as sensitive to strain rate and remain relatively hard as the strain rate decreases. The decrease in shear loading on off-angle boundaries, then, can be offset by the decrease in strength of these boundaries at slow strain rates.

One question which comes out of this work is why the colony boundaries tend to line up in the as-cast microstructure along the joint. The answer becomes clear when the solidification conditions are considered. During solidification, at least some of the colonies are nucleated heterogeneously at the surface of the Cu (actually intermetallic) plates. These nucleated colonies will grow out into the solder and stop when they impinge on other colonies nucleated within the bulk on some other heterogeneous site. As shown in Figure 2.15, this heterogeneous nucleation can result in boundaries that more or less run in a band along the length of the joint. These boundaries generally result in the shear bands discussed above and most likely explain why the coarsened band is often seen near the

Cu/solder interface. The stress concentration at either end of the double shear solder joint, as discussed by Tribula et al. [127,128,134,135], likely determines at which Cu interface it forms.

A coarsened band forming during isothermal fatigue of a eutectic double shear solder joint is shown in Figure 2.16. This particular sample was fatigued with a 10% strain amplitude at 75°C. This coarsened band is similar in appearance to those seen in creep [127,128,134-137] and in previous isothermal fatigue studies [18,,135,136] of near-eutectic alloys. As first pointed out by Frear [18], however, it is much narrower than those typically shown after thermal cycling. The thermal fatigue studies mentioned above have generally involved the rather severe military specification of cycling between -55 and 125°C. Broadening of the coarsened band under these thermal fatigue conditions probably occurs due to work hardening of the solder and a resultant spreading of the deformation at the lower temperatures with recrystallization occurring at the higher temperatures. Failures under the two testing conditions are expected to be much more similar when the temperature extremes in thermal fatigue are closer to the temperature used in isothermal fatigue. In fact, the microstructure resulting from thermal fatigue between 35 and 125°C [18] is much more similar to that shown in Figure 2.16, at least in the early stages of cycling, than those of the more severely cycled thermal fatigue specimens. This suggests, as expected, that isothermal fatigue may be appropriate for modelling thermal fatigue behavior provided the service temperature extremes are similar to the temperature at which isothermal fatigue testing is done.

In any case, both thermal fatigue and isothermal fatigue failures in near-eutectic solder joints involve strain localization and localized recrystallization. Methods by which the isothermal fatigue resistance is improved are, then, also likely to improve the thermal fatigue resistance. Since this study is concerned with fatigue life improvement rather than fatigue life prediction and because isothermal fatigue, as discussed above, is easier to

perform and is more quantitative than thermal fatigue, isothermal fatigue testing is used throughout this work.

2.4. Summary

In the near-eutectic Sn-Pb alloys, the eutectic solder joint microstructure is heterogeneous with relatively hard two-phase colonies surrounded by relatively soft boundary regions. Plastic shear deformation is seen to concentrate within these boundaries as much as possible parallel to the direction of shear. The weak link in near-eutectic solder shear deformation is the presence of boundaries which line up and form relatively long straight paths parallel to the direction of shear. The longer and straighter the shear band which results along these boundaries, the more strain which will be able to concentrate there. Recrystallization occurs within this band beginning near the largest stress concentration of the joint and propagating along it.

Once recrystallization occurs within the shear band, it softens and even more deformation can concentrate within it. Further strain concentration allows the coarsened band to propagate through regions where straight shear bands parallel to the direction of shear were unable to form (obstacle regions) either by geometric strain localization or by mode II crack-like propagation. In exact analogy to the mode II crack, the longer the original shear band, the longer the coarsened band initiated, and the easier these obstacle regions can be bypassed. When enough deformation concentrates within the coarsened band to induce cracking, failure begins.

2.5. Expected Effect of Testing Parameters

All published data for near-eutectic solder joints, reviewed above, are consistent with this failure mechanism. Most of the effects of strain, strain rate, temperature and hold times have been studied using isothermal fatigue where as strain and temperature increase, the isothermal fatigue life decreases. From the above mechanism, this effect is expected in

that higher strains and temperatures promote recrystallization which accelerates failure. As strain rate decreases below a critical value, life decreases. Again, this is expected since recrystallization takes time and the more time per cycle, the more damage that can occur. At very fast strain rates, there is insufficient time for recrystallization and other creep processes so that further increases in strain rate have no effect on life. The same effect on life is seen with hold time in isothermal fatigue and can therefore be explained the same way in terms of the above mechanism. Published data, then, are consistent with the failure mechanism discussed above. That does not mean, however, that the specimens in those fatigue studies failed by the failure mechanism presented here. The exact details of failure are expected to vary depending on initial joint microstructure as well as testing conditions, and it would not be surprising if other creep-related failure mechanisms were seen.

There are less data published showing the effect of testing parameters on thermal fatigue life. The work of Wild [7] and Frear et al. [63,64] suggests that they may be quite different. As discussed in the previous section, however, even these preliminary results are consistent with the mechanism proposed above.

3. IMPROVING FATIGUE LIFE IN NEAR-EUTECTIC Sn-Pb ALLOYS

3.1. General Approaches

Given the above failure mechanism, there are three main approaches possible for improving the fatigue life of near-eutectic Sn-Pb alloys. The most obvious approaches involve prevention of the formation of the long straight shear bands which form. The other two approaches involve removal of any stress concentrations in the joint and inhibition of recrystallization and coarsening.

As discussed in the previous section, the stress concentrations in the joint determine which colony boundaries make up the principal shear band. Once this shear band develops, the stress concentration also initiates recrystallization within it and allows it to

start earlier than would otherwise be possible. Removal of these stress concentrations, however, may not always be practical and may only postpone failure by a similar mechanism. It is likely that removal of the stress concentrations in a joint will only change the colony boundaries which make up the principal shear band rather than prevent it from developing. And, within the shear band, it is likely that in the absence of any stress concentration it will only require more time to accumulate enough deformation to trigger recrystallization in the entire shear band rather than starting at one end and propagating along it. Removal of the stress concentrations in a joint should improve fatigue resistance of these alloys, but the potential exists for even greater improvements as discussed below.

Because failure is preceded by formation of a coarsened band and because the coarsened band develops through recrystallization and strain-assisted coarsening, anything which inhibits recrystallization and coarsening should improve the fatigue resistance of these alloys. Inhibition of recrystallization is most often accomplished by the additions of second-phase particles which pin grain boundaries. In the two-phase near-eutectic Sn-Pb microstructures, dispersoids would have to be added to both the Sn- and the Pb-rich phases. This approach, although not impossible, would be relatively difficult and may even be relatively ineffective. Because deformation is concentrated within a narrow band, the strains within that band are very high. In addition, even room temperature is 0.6 of the melting temperature of eutectic Sn-Pb solder. It therefore, may not be possible to inhibit recrystallization within these bands under normal operating conditions.

The best approaches involve preventing the long straight shear bands from forming in the first place. There are two main ways of doing that. The first is to change the microstructure in such a way that it can deform more uniformly. In cases where that is not possible, obstacles can be added to break up the microstructure and shorten the length of the shear bands that can form. Both of these approaches were investigated here.

3.2. Producing More Uniform Eutectic Microstructures

There are many ways in which as-cast near-eutectic Sn-Pb solder can be manipulated to produce a more uniformly deformable microstructure. One way of doing that is to work and recrystallize the material. As pointed out recently by Tribula et al. [127,128,135], the recrystallized microstructure consists of a uniform dispersion of equiaxed Pb and Sn grains. Because the microstructure is uniform, it can be expected to deform much more uniformly than normal as-cast eutectic structures. In fact, under certain conditions, it is even superplastic [132]. This uniform microstructure should have better fatigue resistance than as-cast microstructures which fail by formation of a coarsened band. No fatigue data exists for recrystallized solder joints. Preliminary bulk fatigue results [132], however, suggest that the recrystallized microstructure provides better fatigue resistance than the as-cast microstructure. The fatigue failure mechanism in bulk near-eutectic solder may differ from that seen above in solder joints. Also, it may be difficult to produce solder joints with a uniformly recrystallized microstructure.

An easier way to create a uniform dispersion of equiaxed Pb and Sn grains is to quench the alloy after casting. A typical quenched microstructure is shown in Figure 3.1. Again, this relatively uniform microstructure is expected to deform more homogeneously than more slowly cooled alloys, and preliminary results [132] suggest that quenched solder joints do have better fatigue resistance than air-cooled solder joints. Quenching as a solution has been proposed before [7], but it is often not possible. Steep temperature gradients caused by quenching can result in failures due to thermal shock elsewhere in the system.

To create a uniform dispersion of Pb and Sn grains without quenching, grain nucleants could be added. This approach would be difficult, however, in that both Sn and Pb nucleants would have to be added and that may involve the precipitation of two phases simultaneously in the melt. In addition, the volume fraction of these dispersoids may be

high enough to adversely affect other soldering parameters such as viscosity and wettability.

More recently, the effect of small additions of third elements on the microstructure and fatigue properties of 60Sn-40Pb solder were studied [127,128,137-139]. Due to segregation of a third element during solidification and subsequent cellular breakdown of the solidifying interface, a much more degenerate microstructure can result in ternary alloys depending on the third element. According to the work of Tribula et al. [127,128,137,138], the improvement in fatigue life scaled with the degree to which the third element broke up the as-cast microstructure. In that study, In and Cd had the greatest effect while Sb and Bi had relatively little effect.

All of the above existing data are consistent with the proposed failure mechanism. Here, the effect of homogenizing the microstructure was studied by aging 63Sn-37Pb double shear specimens.

3.2.1. Past Aging Studies

One area of interest to the electronics industry has been the effect of long time, room temperature storage on the mechanical properties of solder joints. In addition, the effect of aging on the results obtained by testing the specimens used here at different times following casting was of interest. For these reasons, the effects of aging at room temperature were investigated.

One of the first Sn-Pb aging studies was done in 1939 by Baker [149]. He found that at room temperature, Sn-Pb alloys soften to a value which stabilized after 100 to 150 days. Because the original strength could be restored by annealing and the actual magnitude of the strength after annealing depended on the annealing temperature, Baker concluded that the amount of Sn retained in solid solution in the Pb-rich regions determined the hardness of Sn-Pb alloys. Aging, he reasoned, causes Sn to precipitate thus softening the alloy while annealing forces the Sn back into solid solution. Of course, an annealed specimen would

begin softening again upon returning it to room temperature. More recently, others [150-152] have attributed this softening to the precipitation of Sn in the Pb-rich phase regions as well. None of these studies, however, were carried out for periods longer than about 5-6 months. Also, the initial microstructures were much more degenerate than our microstructures so that coarsening could be expected to occur much more rapidly than in our specimens.

Lampe [151] showed the shear strength of 63Sn-37Pb solder joints to level off after about 30 days. Because he saw no Sn precipitates in the Pb-rich regions of the eutectic microstructure and because coarsening of the microstructure stabilized at about the same time as softening levelled off, he attributed softening to a plating of the Sn in supersaturated solid solution in the Pb-rich phase onto adjacent Sn-rich grains in the 63Sn-37Pb alloy. He, however, showed quite a bit of coarsening in that time due to the relatively degenerate structures in his alloys. In the off-eutectic, 50Sn-50Pb alloy where he did see Sn precipitates in the Pb-rich proeutectic particles, Lampe attributed softening to Sn precipitation, and annealing at a temperature near the eutectic temperature restored the strength of this alloy. It would have been interesting to see how much of the strength of the aged 63Sn-37Pb specimens could have been restored by a similar anneal.

Aging is expected to cause the as-cast microstructure to become more uniformly deformable through softening. In fact, short-time (10-30 days) aging at room temperature was shown [8] to improve fatigue strength.

3.2.2. Experimental

Double shear specimens were made as described above. From each block, three specimens were used to measure the shear strength one week after the block was cast. This initial strength was later compared to the strength of aged specimens from the same block. Most of the aging was done at room temperature, but one block was aged at 110°C.

Double shear specimens used for the aged and unaged fatigue tests came from different blocks.

One batch of specimens, identified in the following as block 4, were cast directly into a quartz crucible. The cooling rate for these specimens was higher than those cast in both graphite and quartz crucibles, and the microstructure was thus more degenerate. The shear strength of these solder joints was measured 9 days after casting and after 48 and 73 weeks at room temperature to compare effects of aging on solders with differing initial microstructures.

3.2.2.1. Shear Strength Measurements

Initially, older grips described elsewhere [18] and shown in Figure 3.2 were used to measure shear strength. The space between the screws of these grips, however, was too small for the specimens used here. This required that the edges of the specimens be milled before testing. To eliminate this problem, the friction grips shown in Figure 3.3 were designed and made. A plate the width of the grips with a notch the width of the specimen machined down its center was used to center the specimen within the grips as shown. Thus, these newer grips also provided more centered loading and less bending of the specimen during testing.

Both sets of grips were pin loaded on a screw-driven Instron load frame. Testing was done at room temperature with a displacement rate of 0.05 mm/min. Neglecting machine compliance, the strain rate on the specimen is given by:

$$\dot{\gamma} = (0.05\ \text{mm/min})(1/0.51\text{mm})(1\text{min}/60\text{s}) = 1.6 \times 10^{-3}\text{s}^{-1}$$

since the joint thickness is 0.51mm (.02 inch). Unfortunately, the machine compliance does not turn out to be negligible. Because any displacement in the machine is attributed to a 0.51-mm (.02-inch) joint when the load frame compliance is neglected, even very small machine displacements produce a large error in the calculated strain. As an example, say the load frame displaces by 0.025 mm (.001 inch). If that displacement is assumed to

occur in the solder, then the strain will be off by 0.025/0.51 or 5%. Even fairly stiff machines, can displace by 0.025 mm at about 50-kg loads. In measuring bulk tensile strengths, this load frame displacement can easily be neglected because the solder is so soft and the gage length is generally long. In testing solder joints in shear, however, because the gage length (i.e. joint thickness) is very short, load frame displacements must be subtracted out.

To calculate the displacement occurring outside of the solder joints, Cu with the same dimensions as the double shear specimens (i.e. 13 x 1.8 x 100 mm) was pulled in tension and the total elongation (Cu plus machine elongations) measured as a function of the load. Since two sets of grips each with different compliances were used, this measurement had to be done for both. Using the Young's modulus for Cu, 120 GPa (18 x 10^6 psi), the elongation in the Cu between the grips was measured and subtracted from the total elongation. After testing a double shear specimen, the machine compliance for the ultimate load plus the Cu displacement for the dimensions of the specimen tested was subtracted from the total elongation to yield the shear displacement in the solder joint.

Prior to testing, the double shear specimens were polished to 0.05μm, the microstructure examined and the solder joint thickness and length measured using a travelling optical microscope with an accuracy of about ±.005 mm. The solder joints in the double shear specimen have an odd shape as shown in Figure 2.2. The length of the joint was taken as the average of the length of the two Cu/solder interfaces on either side of the joint. These values and equations (2.2) and (2.3) were used to calculate the stresses and strains. The shear strengths reported here are the ultimate values. Because testing of the solder joints is done in shear, these ultimate strengths do not represent the onset of necking. Instead, the load drop is due to the onset of cracking in the solder.

3.2.2.2. Fatigue Testing

Fatigue testing was done on a load frame originally designed by Fultz et al. [153,154] to be portable and for tensile testing in a magnetic field. Later it was modified by McCormack [54] for fatigue testing. Here, some minor modifications were done, but for the most part the same setup as used by McCormack was used here. One major change was in the grip design where concern over off-centered loading and displacements associated with pin-loading through zero load led to the design shown in Figure 3.4. These grips are made of annealed stainless steel and were machined to within .05 mm of the dimensions shown. Because grooves could not be machined into the gripping plates, a #100 mesh 304 stainless steel screen of about .3-mm thickness was used between the specimen and the grips to increase friction. No slipping of the specimen was observed during testing, and because the upper grip screws into the pull rod and the lower grip is clamped onto the compression frame base, no discontinuous displacements were seen in testing through zero load.

For ease of specimen alignment, the double shear specimen preparation was modified slightly. Prior to polishing, aligning holes of 3.2mm (1/8 inch) diameter were drilled through the center of the 6.4mm (1/4 inch) Cu plate at each end spaced 83mm apart as shown in Figure 3.5. The block was then assembled, dunked and machined as discussed above. After slicing and widening of the slots in the center plate of each specimen, part of the solder which filled these aligning holes during casting was drilled out with a 1.6mm (1/16 inch) drill bit, smaller than the original hole to prevent widening it. The remaining solder in each aligning hole was carefully removed by filing with a round 3.2mm (1/8 inch) file. Prior to clamping the specimen into the grips, pins were inserted through the aligning holes and a small (usually about 3 kg) preload was placed on the specimen. With the specimen under this preload, it was assumed to be aligned and the grips were then tightened. Prior to fatigue testing, the aligning pins were removed.

All fatigue testing was done in Houghton type K quench oil at 75 ± 2°C. Strain cycling was always centered about zero with amplitudes between about 5 and 10%. The shear displacement in the joints was measured using an extensometer positioned as shown in Figure 3.5. The strain was calculated using equation (2.3) and the joint thicknesses measured as discussed above. The strain rate was calculated by dividing strain range by half the cycle time and was usually about $1.5 \times 10^{-4} s^{-1}$. The stress ranges were calculated from the load ranges as were the shear strengths above.

3.2.3. Aging Results

Normalized shear strength as a function of time at room temperature is plotted in Figure 3.6. The shear strength is normalized by dividing the actual average strength by the average strength of the initial specimens from the same block. The average initial strength from all the blocks tested was 31MPa ± 1MPa. The elongations are plotted in Figure 3.7 and 3.8, and the results of aging at 110°C are shown in Figure 3.9. The microstructures of the aged specimens are shown in Figures 3.10 to 3.13.

The fatigue data is shown in Figure 3.14. In Figure 3.15, the microstructure of a fatigued 6-month old specimen is shown. In Figures 3.16 and 3.17, the same is shown for a 1.5-year old specimen.

3.2.4. Discussion

The shear strength data of Figure 3.6 shows that the strength decreases at room temperature by about 20-25% and does not begin to level off for about 40-50 weeks. The micrographs in Figure 3.10 show that for the first few months, there is relatively little change in the microstructure. There is more variation along any given joint than there is with aging. At about 9 months, some discontinuous coarsening at colony boundaries and some overall coarsening is evident, but there is no real dramatic change in the microstructure. After 15 months at room temperature, the overall microstructure looks

coarser and lamellar regions have begun to break up and disappear, but the initial colony structure is still discernible.

The elongations in Figure 3.7 show quite a bit more scatter than do the strengths. This scatter probably comes to a great extent from variations in the grip and load frame compliances from test to test. As stated above, very little error in the displacement can cause a larger error in the calculated strain. In addition, it seems that the elongation is much more sensitive to the microstructure than is the strength and that variations in the microstructure from specimen to specimen are likely to be at least in part responsible for some of the scatter.

The elongations normalized by dividing by the average initial elongation for each block are shown in Figure 3.8. The elongation remains fairly constant up to about 40-50 weeks. The fact that no significant microstructural changes were seen over that time period further suggests that elongation is more sensitive to the overall eutectic microstructure than is the strength.

Beyond about 50 weeks aging, the elongation increases in block 3 but remains constant in block 4. Figure 3.7 shows that the block 4 elongation is relatively high from the outset probably due to the more globular as-cast microstructure shown in Figure 3.11. After aging, the microstructure coarsens, but there is no gross change in the morphology and no resultant change in elongation.

In blocks 1-3, the initial microstructure is less degenerate, and thus, the initial elongation is lower. After about 50 weeks at room temperature, however, discontinuous coarsening at the colony boundaries increases the degeneracy of these specimens so that the elongations increase with further aging until they approach values similar to the originally more degenerate material.

Comparison of Figures 3.6 and 3.8 shows that the strength levels off at about the same time that the elongations begin to increase. If discontinuous microstructural coarsening is responsible for the increase in elongation, as is suggested by comparison of the

microstructures with aging and the elongations and also by comparison of block 3 and 4 elongations, then it cannot be responsible for the decrease in strength which occurs over shorter time periods. It is likely that removal of supersaturated Sn in the Pb-rich regions, as suggested by Lampe [151], is responsible for softening. Further evidence for this conclusion is that both block 3 and 4 age to the same fraction of their initial strengths even though the initial overall eutectic microstructure and thus the degree of coarsening is different.

A reasonable approximation for the time required for Sn to diffuse through the Pb-rich regions to the Sn-rich regions is given by the square of the diffusion distance divided by the diffusivity. Using the value of the diffusivity for the lattice diffusion of Sn in Pb-rich alloys measured by Oberschmidt et al. [155], at room temperature, Sn diffuses about .1 μm through the Pb-rich regions in about 70 weeks. The assumption that the softening occurring over a period of about 50 weeks is due to the removal of supersaturated Sn from the Pb-rich regions, then, seems reasonable. However, little evidence of Sn precipitation was seen; the precipitates that were seen were always near the boundary regions as shown, for example, in the bulk microstructure of Figure 2.7. In the lamellar regions, where the phase diameter (perpendicular to the lamellae) is small, Lampe's suggestion that Sn diffuse through the Pb to the Sn-rich regions is probably valid. Near the boundaries, however, the phase diameter sometimes increases. In those regions, because diffusion is slow at room temperature, precipitation is more likely. It is, of course, possible that precipitates are present but too small to be seen optically. In that case the strength decrease would be due to precipitate coarsening, and the return of the strength after annealing would be due to a return of a fine dispersion of Sn precipitates.

From the phase diagram in Figure 1.4, very little Pb is soluble in Sn even at the eutectic temperature, and no Pb-rich precipitates were ever seen within the Sn-rich regions. Softening of the Sn-rich regions, therefore, cannot be responsible for the overall softening. These results are somewhat surprising. By the lever rule, eutectic solder is about 2/3 Sn.

The microstructure then must consist of a matrix of the relatively hard Sn-rich phase, and it is unclear why microstructural changes within the Pb-rich phase should affect the strength. It could be that in the regions of the microstructure that are deforming the most, the Sn- and Pb-rich grains are somewhat equiaxed and can deform more or less independently. In that case, the softer Pb-rich regions would determine the strength. It would be interesting to anneal an aged eutectic specimen and test their strength to determine how much of their strength is recoverable and therefore not due to overall microstructural coarsening.

Figure 3.14 shows that the fatigue life of eutectic solder can be approximately doubled by aging for long times at room temperature. Comparing Figures 3.15 to Figures 3.16 and 3.17 shows that while a coarsened band does appear to form in the aged specimens, it is not as distinct and does not extend as far ahead of the fatigue crack as does the coarsened band in the younger specimens. In Figure 3.16 there is no obvious coarsening along the fatigue crack in the aged specimen. Revealing the coarsened band required extra final polishing to reveal grain boundaries before the localized recrystallization could be seen as it is in Figure 3.17. The difference is consistent with the idea that an increase in the degeneracy of the microstructure, suggested by the microstructural changes shown in Figure 3.10 and the elongation data of Figure 3.8 to occur after about 9 months at room temperature, should spread out the deformation and at least postpone formation of a coarsened band. Here, if the coarsened band does not extend excessively beyond the crack, then less deformation will concentrate within it and it will not be able to propagate as quickly as the coarsened band in unaged specimens.

Chilton et al. [8] also saw an initial increase in the fatigue life of 60Sn-40Pb solder with room temperature aging. After about 60 days, however, they saw a decrease in life due to what they said was the dissolution of the disruptive Pb-rich proeutectic. Here, eutectic was used so no primary Pb was present. But because the change in the eutectic microstructure with room temperature aging was not very dramatic, it is not expected that aging of 60Sn-40Pb joints made by the same procedure as was used here would be drastic

enough to cause a dissolution of the proeutectic phase. The fact that dissolution occurred in the alloy of Chilton et al. [8] is probably due to their processing resulting in a more degenerate and therefore less stable as-cast microstructure. This, in turn, suggests that before the effect of aging of a solder alloy can be evaluated, the as-cast microstructure of the particular joint must be carefully considered.

In Figure 3.9, the results of aging at 110°C show that softening levels off sooner than seen at room temperature, but at a much higher fraction of the initial strength. At room temperature, as shown in Figure 3.6, the strength drops by about 25% while at 110°C, as shown in Figure 3.9, it drops by only about 15%. Again, this result is consistent with the idea that softening is due to Sn precipitation and its resultant removal from solid solution in the Pb-rich regions. At 110°C, kinetic reactions are faster resulting in an earlier plateau, but more Sn is soluble so that the strength plateaus (when tested at room temperature) at a higher value. From the phase diagram of Figure 1.4, the concentration of Sn soluble in Pb at room temperature is about 2% while at 110°C, it is about 6%. The difference in the amount of Sn left in solid solution after aging at room temperature and at 110°C could easily account for the differences in strength plateaus. The micrographs of Figures 3.12 and 3.13 show that much more global spheroidization and coarsening has occurred than was seen at room temperature. After a week at 110°C, some lamellar regions still exist as shown in Figure 3.13, but there is evidence of discontinuous coarsening around these regions. After a month, there are fewer, smaller lamellar regions with greater coarsening between them. The fact that little difference in the strength resulted from the dramatically different microstructures of Figures 3.10 and 3.12 suggests that the precipitation of Sn has a much more dramatic effect on the overall strength than does the spheroidization of the microstructure. Unfortunately, there was too much scatter in the elongations measured here due to different unspecified grips used during testing and consequent different machine displacements, but the microstructure of Figure 3.12 is expected to deform much more uniformly than the room temperature aged specimens. For this reason, the fatigue life

of specimens aged at elevated temperatures is expected to be even better than those aged at room temperature.

3.2.5. Conclusions

Softening during aging at room temperature appears to be due to the removal of Sn from the Pb-rich regions of the eutectic Sn-Pb microstructure. When the phase diameter is small, as it is in lamellar regions, no Sn precipitates are seen, at least optically, with aging. It was concluded that Sn diffuses through the Pb-rich regions to the adjacent Sn-rich regions. In coarser regions such as near colony and grain boundaries where Sn precipitates were sometimes seen, removal of Sn from solid solution in the Pb-rich regions occurs by precipitation as well as diffusion to the Sn-rich regions. The resultant removal of supersaturated Sn from solid solution causes softening of the material with aging.

Some discontinuous coarsening at the colony and grain boundaries and the consequent decrease in volume fraction of the lamellar regions was seen with aging at room temperature but only after 40-50 weeks. This increase in the globular, degenerate material was accompanied by an increase in the elongation seen with aging. It was concluded that the elongation is more sensitive to the overall microstructural morphology (i.e. the amount of globular material) while the overall strength depends on the strength of the individual phase regions.

At 110°C, softening occurs more quickly than it does at room temperature due to the faster diffusion of Sn in the Pb-rich regions. The degree of softening, however, is not as great due to the greater solubility of Sn in Pb at higher temperatures. The strength after aging at 110°C levelled off at a greater value than it did after aging at room temperature despite the fact that the microstructure was much more spheroidized and coarsened after aging at the higher temperature.

The fatigue data above suggest that room temperature storage of soldered devices will not adversely affect the fatigue properties of the eutectic solder joints. In fact, the contrary

is true; the fatigue life of eutectic Sn-Pb solder increases with aging. Microstructural changes which increase the total elongation of the specimen are likely to be responsible for the increase in fatigue life due to an increase in the degeneracy of the microstructure. These changes, however, do not occur until about 40-50 weeks at room temperature at least for the initial microstructures seen in this study. For our specimen design, then, it would appear that the microstructure, in so far as the fatigue properties are concerned, is stable for about 9 months.

Because a greater degree of spheroidization of the microstructure is obtained in less time at higher temperatures, a high-temperature aging treatment is expected to more than double the fatigue life of near-eutectic Sn-Pb solder joints which fail by the formation of a coarsened band. This conclusion is, of course, only valid if it is possible to age the solder at elevated temperatures without damaging chips or other components on the completed board or without adversely affecting the solder/Cu interface strength. At higher temperatures, more Sn is soluble in the Pb-rich regions so that aging results in softening to a greater strength than seen at room temperature initially, but storage at room temperature after a high-temperature anneal should result in a decrease in strength approaching that seen with aging at room temperature.

3.3 Addition of Obstacles

All of the methods discussed above for improving fatigue life by homogenizing the microstructure also decrease the strength of the solder. In some applications, solder strength might be an important consideration. In addition, decreasing the strength increases the plastic strain applied to the solder in a thermal fatigue situation. The above methods, therefore, would likely have an even greater effect if they could be achieved without decreasing the strength of the alloy. The addition of obstacles to solder can potentially increase the strength. Therefore, these methods may have an even greater effect than those above. To determine the effect of the addition of obstacles on fatigue life, off-eutectic

alloys, where particles (i.e. the primary phase) are simply introduced during standard casting procedures, were studied. The results of Chilton et al. [8] who saw an increase in fatigue strength with aging until aging resulted in a dissolution of the Pb-rich proeutectic after about 60 days at room temperature suggest that the proeutectic are beneficial to the fatigue life. However, since off-eutectic alloys are known to have lower strengths as well as a broader melting range and a higher melting temperature than the eutectic, the addition of a particle with a third phase, different from both Pb and Sn, was also investigated.

3.3.1. Fatigue of the Off-Eutectic Alloys

3.3.1.1. Background

Relatively little research has been done on Sn-Pb solders with compositions intermediate between the near-eutectic and the high-Pb solid solution alloys. What data exist, however, does suggest that off-eutectic compositions have better fatigue resistance than either of the above groups [61,94,156,157] at least under some testing conditions. These off-eutectic alloys are probably not widely used because of the rather large pastey or solid-liquid two-phase region associated with them.

Published fatigue life data [61,94,156,157] suggests that the fatigue life does not simply increase in moving away from the eutectic composition. Instead, it peaks at a composition around 50 wt.% Sn. In fact, other mechanical properties, notably the bulk tensile and shear strengths and the solder joint shear strengths [156-162], sometimes show this trend with composition usually showing a local maximum, if not a global maximum, at 40 to 50 wt.% Sn. The following experimental work was geared toward explaining this off-eutectic peak in properties as well as to evaluate the effect of the proeutectic particles on the fatigue failure mechanism.

3.3.1.2. Experimental

Five Sn-Pb compositions were made by combining 99.9% pure Pb with commercial 63Sn-37Pb bar solder. Ingots were made by combining the appropriate amounts of each material and heating them to 375°C, about 50°C above the melting point of Pb.

Preparation of the double shear specimens, the fatigue testing apparatus and procedure, and the metallography of the near-eutectic alloys were all described in the previous section. The only difference here is with the Pb-rich alloys (5Sn-95Pb and 20Sn-80Pb). These alloys were polished in the way described above for the eutectic alloy, but the Pb-rich regions required etching as well. This etching was done in one of the two following ways. First, it was found that polishing on the silica colloidal solution, which is alkaline, for long times (30 min to 1 hr) etched the Pb-rich regions. Alternatively, a procedure similar to that used by Gifkins [163] and Slepian and Blann [164] was used. After final polish, the Pb-rich solder joint was chemically polished using a solution of 2 parts acetic acid, 3 parts H_2O_2 and 5 parts methanol. The joint was then repolished on the silica colloidal solution and chemically repolished until a smooth surface was obtained. Etching was done using a solution of 10g ammonium molybdate and 10g of citric acid in 100ml distilled water for about 45-50 seconds at room temperature.

3.3.1.3. Results and Discussion

Fatigue Data:

Typical load vs. cycle plots for each of the alloys at both strains tested are shown in Figure 3.18. As seen previously [37,40,56,165], the load drops continuously during cycling. As suggested by Solomon [37,40,56], this load drop appears to be due to cracking which starts very early with cycling at least at the higher 10% strain range used here. If softening occurred initially prior to cracking, then an increase in slope of the load vs. cycle curves would be expected upon crack initiation. Since no break was observed in the load vs. cycle at 10% strain range curves of Figure 3.18, it was concluded that

softening was due to cracking early in fatigue. Because testing was done under stroke control, the strain amplitude and, thus, the cracking rate increased with cycling. Therefore, the stress amplitude vs. cycle plots are not linear as they were for Solomon who used plastic strain control. The rate of increase in cracking rate would be greater for specimens with shorter lives since life was defined as a percentage load drop and the load drop is due to cracking, and as seen in Figure 3.18, the curvature increases as the life decreases. At 5% strain, there are more distinct slope changes in the load vs. cycle curves of Figure 3.18. The early stages of softening in these cases may be due to microstructural changes, and the increase in cyclic softening later during cycling may be due to the onset of cracking. Interrupted fatigue tests, however, would be necessary to confirm this supposition.

The fatigue data are plotted as life, defined as number of cycles to a 30% load drop, vs. applied strain in Figure 3.19. Because testing was done under stroke control and because the load dropped continuously with cycling, the applied strain increased during testing. The strain used in Figure 3.19 was taken as the initial strain amplitude measured using an extensometer as discussed in the previous section. Because the initial loads and strains are similar for each of the above tests and because the machine compliance is the same for all the fatigue tests, it is believed that the relative fatigue lives measured are accurate even if the absolute number of cycles to failure data are unsuitable for general fatigue life prediction. Solomon [40] showed that the Coffin-Manson coefficients calculated from best linear fit techniques could depend on whether life was plotted on the vertical or horizontal axis especially when the correlation to the best fit line was low. Because life is the dependent variable, the results shown in Figure 3.19 are plotted as life vs. strain rather than the more usual strain vs. life plot. As shown, 50Sn-50Pb showed the best fatigue resistance for all applied strains tested although the difference decreases at lower strains.

The Coffin-Manson constants are shown in Table I. The values for 5Sn-95Pb and 63Sn-37Pb are similar to those published for these alloys and discussed above. While 5Sn-95Pb has better fatigue resistance than 63Sn-37Pb at all strains tested here, this

difference decreases as strain decreases to the point that at applied total strain amplitudes below about 5%, 5Sn-95Pb is expected to have better fatigue resistance than 63Sn-37Pb. This trend is similar to that seen previously by Kitano et al. [67] who found that 5Sn-95Pb had better fatigue resistance than 63Sn-37Pb only at small strains. Solomon [65,66] also reported a greater Coffin-Manson exponent for a Pb-rich alloy containing Ag as well as Sn than for 60Sn-40Pb solder.

TABLE I

Coffin-Manson coefficient, M, and and exponent, z, as defined in Equation (1.2) for the Sn-Pb alloys tested

Alloy	z	M
5Sn-95Pb	0.61	1.12
20Sn-80Pb	0.46	0.58
40Sn-60Pb	0.33	0.35
50Sn-50Pb	0.43	0.71
63Sn-37Pb	0.27	0.19

The quarter-cycle stress as a function of strain amplitude and composition is plotted in Figure 3.20. As seen in previous published strength data [156-161], the strength does not decrease monotonically with decreasing Sn concentration; the 40Sn-60Pb alloy is stronger than the 50Sn-50Pb alloy at both strain amplitudes tested. Consistent with this result, the Coffin-Manson coefficients shown in Table I do not increase monotonically in moving away from the eutectic composition; the value for the 40Sn-60Pb alloy is lower than it is for the 50Sn-50Pb alloy. These data then suggest that the 40Sn-60Pb alloy is stronger and less ductile than the 50Sn-50Pb alloy even though it has more of the presumably softer and more ductile Pb-rich proeutectic phase. Microstructural explanations for this phenomenon are given below.

Initial Microstructures:

Proeutectic Regions

The initial microstructures are shown in Figures 3.21 and 3.22. With increasing Pb, the eutectic microstructure is increasingly replaced by Pb-rich proeutectic particles. As shown in Figure 3.23, these primary Pb-rich particles in the 50Sn-50Pb alloy are still rather small and somewhat equiaxed. In the 40Sn-60Pb alloy, the Pb-rich dendrites grow to rather large sizes and have a well-developed dendritic structure with obvious side arms. Also shown in Figure 3.23, these dendrites tend to line up at an angle across the solder joint probably in the direction of the predominant temperature gradient present during casting. Of course, not all of the Pb-rich dendrites are parallel in the 40Sn-60Pb alloy. This is probably due to local variations in the temperature gradient as well as to movement of the dendrites during solidification through the solid + liquid two-phase region.

In the 20Sn-80Pb alloy, the microstructure consists mostly of the primary Pb-rich dendrites. These Pb-rich islands, however, are surrounded by a film of eutectic material which formed in the final stages of solidification. The 5Sn-95Pb alloy consists, as expected, almost entirely of the Pb-rich α phase. Precipitation of Sn within the Pb-rich regions of both these Pb-rich alloys occurred uniformly throughout the bulk of the Pb with the broken lamellar, plate-shaped morphology reported by Frear [18] for cast 5Sn-95Pb alloys. The grain size in the 5Sn-95Pb alloy was about 25-50 μm and the Pb-rich phase size in the 20Sn-80Pb alloy was 50-100 μm.

Precipitation of Sn in the Pb-rich proeutectic regions was also seen in the eutectic rich alloys as shown in Figure 3.24. Although precipitation was never seen in well defined, planar lamellae, it was seen in faulted, less well defined lamellae and near colony boundaries (see, for example, Figure 2.7). Within the proeutectic of the 40Sn-60Pb and the 50Sn-50Pb, the precipitate sizes did not appear to vary continuously; they were either very coarse or very fine. Proeutectic with both these precipitate distributions are shown in Figure 3.24 and occur in all the off-eutectic alloys as seen in Figures 2.4, 2.8 and 3.21.

This distribution of size ranges is similar to that seen in two-step age-hardened alloys. The results of microprobe analysis showed that the regions with coarse precipitates are consistently a few percent higher in Sn than the regions with fine precipitation.

One method by which a two-step aging treatment could occur has to do with the undercooling required to nucleate eutectic solid during solidification. As reasoned above, Pb will continue to grow while the melt cools below the eutectic temperature. This layer of Pb will have the range of compositions shown in Figure 3.25 obtained by extrapolating the solidus below the eutectic temperature. Once the eutectic is nucleated, the temperature will increase toward the eutectic temperature. Only the Pb-rich layers formed during the undercooling will be rich in Sn at the eutectic temperature. Hence, only the outer layers of the Pb-rich proeutectic can precipitate Sn during the eutectic solidification. Because the eutectic temperature is high, coarse precipitates will form and continue to grow as the ingot cools to room temperature. At room temperature, Sn will be able to precipitate throughout the proeutectic, but because room temperature is relatively low, a fine dispersion forms instead. The precipitates seen in a cross section will therefore depend on where the primary Pb-rich particle is cut. Microprobe analysis of Pb-rich proeutectic particles containing coarse Sn precipitates consistently showed a few percent more Sn than those containing a fine dispersion toward the center of the proeutectic.

Eutectic Regions:

The effect of the proeutectic in the off-eutectic, eutectic-rich alloys appears to be an increase, at least locally, in the degeneracy of the eutectic surrounding the Pb-rich particle. Examples of this local degeneracy can be seen near the proeutectic particles in Figures 2.4a, 2.8, 3.21 and 3.23. It is probably due to the inability of Pb to nucleate the eutectic without an undercooling and the consequent lack of time in finding a preferred growth direction once the eutectic is nucleated and while the melt heats back to the eutectic temperature.

In moving away from the eutectic composition, then, the fraction of the softer Pb-rich phase increases and the degeneracy of the eutectic at least near the proeutectic increases.

Since both of these effects should soften the cast alloy, a monotonic decrease in strength is expected as the composition moves from the eutectic to the Pb-rich compositions. As discussed above, however, a peak in strength is sometimes seen at about 40-50 wt.% Sn. Here, as shown in Figure 3.20, the stress amplitude of the 40Sn-60Pb alloy was consistently higher than that of the 50Sn-50Pb but lower than that of the eutectic. Microhardness measurements, the results of which are given in Table II, showed that the strength of the eutectic regions in the 40Sn-60Pb alloy was higher than those of the 50Sn-50Pb alloy suggesting that they were more lamellar rather than more degenerate in the 40Sn-60Pb alloy. The indent used in the microhardness tests was on the order of the size of the proeutectic. Contributions to the hardness measurement in the eutectic regions are therefore expected from the proeutectic regions. Because the 40Sn-60Pb alloy has more of the softer proeutectic, the actual strength difference in the eutectic regions is probably even greater than measured. Also, in microhardness testing, the strain rate is relatively fast. At slower, more reasonable strain rates, the difference between the lamellar and degenerate eutectic will again be even greater. Micrographs, such as those shown in Figures 3.21 and 3.23 and at higher magnification in Figure 3.26 also suggest that the eutectic of the 40Sn-60Pb alloy is less degenerate with a better defined colony structure than the eutectic regions of the 50Sn-50Pb alloy. The effect, therefore, seems to be real.

TABLE II

Vickers microhardness measurements made using 10-g load. Values in parentheses indicate the number of measurements included in the averages shown.

Region	63Sn-37Pb	50Sn-50Pb	40Sn-60Pb
Eutectic	—	12.5±.7 (14)	14.3±.7 (18)
Lamellar Eut.	14.5±.4 (5)	—	—
Degenerate Eut.	13.4±.3 (4)	—	—
Proeutectic-Fine ppt.	N/A	13.9±.8 (6)	14.3±1.2 (5)
Proeutectic-Coarse ppt.	N/A	9.9±.4 (6)	9.3±.5 (7)

One explanation for this phenomenon involves the difference in shape of the proeutectic in the two alloys. The Pb-rich dendrites in the 40Sn-60Pb alloy are much larger with well developed side arms than those of the 50Sn-50Pb alloy which are much more equiaxed with more planar surfaces. It is possible that the more convoluted surface on the proeutectic in the 40Sn-60Pb alloy allows heterogeneous nucleation of Sn at a smaller undercooling than in the 50Sn-50Pb alloy. It would thus require less eutectic to form in order to raise the temperature back to the eutectic temperature. The liquid remaining at the eutectic temperature would have more time for solidification and, thus, for developing favorable lamellar growth directions than would that of the 50Sn-50Pb alloy. This effect would only be seen with solidification conditions allowing lamellar growth and development of a colony structure in the cast eutectic material. For very fast cooling rates, the microstructure will be more degenerate anyway, and such a subtle difference is not expected. Also, at fast testing strain rates, the difference in strength between the degenerate and colony eutectic microstructures decreases [132] so again the effect would be less. These reasons could explain why a peak in the strength of Sn-Pb solders is sometimes seen at the eutectic composition rather than at an off-eutectic composition. In fatigue, the less-degenerate structure of the 40Sn-60Pb alloy is expected to decrease the life (as was seen here) when failure occurs by formation of a coarsened band.

In the Pb-rich alloys, there is very little eutectic material. The fact that there is any at all in the 5Sn-95Pb alloy as seen in Figure 3.22 and at higher magnification in Figure 3.27, however, suggests that solidification occurred at a nonequilibrium rate causing coring of the Pb-rich proeutectic particles. If solidification occurs at a rate that is too fast to allow significant diffusion in the solid, then the liquid can reach the eutectic composition before the overall solid composition reaches the maximum solubility of 19.2 wt.% Sn shown in Figure 1.4. If this happens, eutectic can form in alloys even when it would not normally

based on the equilibrium phase diagram. This appears to be what happened in the case of the 5Sn-95Pb alloy.

Intermetallic Layers

As seen previously [18,97,140,141], the intermetallics which form on the Cu/63Sn-37Pb interface are the Cu_3Sn, ε, phase adjacent to the Cu and the Cu_6Sn_5, η, phase nearest the solder. This double intermetallic layer, shown in Figure 3.28 for two of the alloys studied, was also seen in all the other alloys except the 5Sn-95Pb alloy. Again, as seen before [18,166], only the Cu_3Sn intermetallic formed at the Cu/5Sn-95Pb interface.

Deformation Patterns in Fatigued Solder Joints:

Double shear specimens made with the five compositions tested were polished to 0.05μm prior to testing. Examination of the surface of the joint after fatigue without any further surface preparation resulted in the deformation patterns shown in Figures 3.29 to 3.31. As expected, the Pb-rich proeutectic in the off-eutectic, eutectic-rich 40Sn-60Pb and 50Sn-50Pb alloys broke up the microstructure to the point that the long straight shear bands seen in the eutectic alloy did not form. The deformation is much more uniform and spread out in these off-eutectic alloys.

In the 5Sn-95Pb alloy, a mosaic deformation pattern (Figure 3.30) similar to those reported previously was seen at the higher strain ranges near 10%. This pattern, however, was not the result of cracking. Figure 3.32 shows a 5Sn-95Pb solder joint repolished following fatigue at about 13% strain amplitude. The mosaic pattern has been erased, and only one main crack growing in from each stress concentration in the joint is seen. The mosaic pattern seen in these joints following fatigue at 75°C with a 13% strain amplitude is therefore the result of strain concentration rather than cracking.

At 5% strain amplitude, this mosaic deformation pattern was not seen (Figure 3.31). Instead, deformation appears to be concentrated along grain boundaries. This deformation pattern is similar to that reported by Frear [18] in the early stages of thermal fatigue cycling between -55 and 125°C. Both grain boundary migration and grain boundary sliding have

been reported [87-92] during fatigue of this alloy and could account for the observed deformation pattern of Figure 3.32. Also, these deformation modes would be expected to be dominant over slip mechanisms at lower strain amplitudes.

Fatigue Failure Mechanisms:

Pb-Rich Alloys

Microstructures of fatigued Pb-rich alloys are shown in Figure 3.33 where it is evident that fatigue failure in the 20Sn-80Pb alloy involves localized microstructural changes similar to near-eutectic alloys. Cracking was always observed to begin at the stress concentration in the joint and propagate along the joint through regions of the microstructure which had recrystallized. This recrystallization is evident in Figure 3.33 by the broken up eutectic regions near the crack. The more equiaxed Sn and Pb grains in these regions were not present in the as-cast microstructure. These recrystallized regions did not extend very far ahead of the crack and could simply be due to strain localization ahead of the fatigue crack. The fact that there are no major deformation bands near the interface in the as-fatigued specimen of Figure 3.30 further suggests that this locallized recrystallization is due to the propagating crack and not to strain localization prior to cracking. There is evidence of local recrystallization ahead of the fatigue crack in the 5Sn-95Pb alloy as well. For example, the small grains surrounding the large grains ahead of the cracks in Figure 3.33 suggest that recrystallization has occurred at least locally ahead of the crack. In both of the Pb-rich alloys at all strain amplitudes tested, failure occurred intergranularly as shown in Figure 3.32 for the 5Sn-95Pb alloy and in Figure 3.34 for the 20Sn-80Pb alloy. This is in apparent conflict with the observed deformation pattern seen for the higher strain amplitudes in the 5Sn-95Pb alloy (Figure 3.30) which appeared to be due to planar slip. Probably at the higher strains, the mosaic pattern was due to grain boundary processes occurring with preference for the grain boundaries parallel and perpendicular to the applied shear strain, but it is also possible that local recrystallization ahead of the propagating fatigue crack allowed the material ahead of the crack to deform by grain boundary sliding

resulting in grain boundary failures even though the bulk of the material was deforming intragranularly. Transgranular cracking seen by other investigators [67-73] under similar testing conditions is probably due to the higher strain rates that are generally used than were used here.

Eutectic-Rich Alloys

As shown in Figure 3.35, all three eutectic-rich alloys failed by the formation of a coarsened band. Figure 3.36 shows a coarsened band in a 40Sn-60Pb alloy at higher magnification. Cracking within the coarsened band followed Sn-Sn grain boundaries and Pb-Sn phase boundaries and appeared to begin, as shown in Figure 3.37, at the Sn-Sn grain boundaries as suggested previously by Frear et al. [18,53,133].

In the off-eutectic alloys, the coarsened band often stopped at proeutectic particles such as shown in Figure 3.38 suggesting, as expected, that the primary Pb-rich phase regions have a beneficial effect on the fatigue resistance of these alloys. Obviously, the effect of these particles on the deformation patterns discussed above inhibits failure by the formation of a coarsened band. The shorter the shear band that forms in the alloy, the less strain that will be able to concentrate within it and the longer it will take for the material within the band to recrystallize. This result is evident in the fatigue data presented in Figure 3.19 where both the 50Sn-50Pb and 40Sn-60Pb alloys have longer fatigue lives than the 63Sn-37Pb alloy at all strains tested. At lower strains, however, the difference decreases. It is likely that the driving force for recrystallization at these lower strains becomes insufficient to overcome recovery in the deforming regions so that failure occurs by a different mechanism. When failure occurs by a mechanism which does not involve the formation of a coarsened band, it is reasonable to expect the fatigue life to scale with the strength of the alloy under total-strain-controlled conditions. If the lines shown in Figure 3.19 are extrapolated, this is indeed what is seen. The strongest alloy, 63Sn-37Pb, would have the greatest fatigue resistance and the weakest alloy, 50Sn-50Pb, would have the least resistance. Further effects of these particles on the failure mechanism can be better

understood by determining why the fatigue resistance of the 40Sn-60Pb alloy is lower than the 50Sn-50Pb alloy even though it has a higher fraction of the Pb-rich particles.

Although the coarsened band is observed to stop at proeutectic particles (Figure 3.38), it is more often observed to cut through them as seen, for example, in Figures 3.35 and 3.36. This is not entirely unexpected. The Pb-rich proeutectic are much softer than the surrounding eutectic regions and are thus relatively deformable. When the deformation concentrates into bands around the proeutectic particle, it will eventually be cut by the geometric strain localization mechanism discussed above for the bypassing of obstacle regions in the near-eutectic alloys. Once the deformation in the proeutectic concentrates, it too will recrystallize, soften and allow further strain concentration. The difference in the fatigue resistance of 40Sn-60Pb and 50Sn-50Pb must have something to do with the ability of the proeutectic in these alloys to withstand bypassing by the above mechanism.

As stated above, the eutectic regions of the 40Sn-60Pb alloy are more lamellar with the typical colony structure seen in near-eutectic alloys than those of the 50Sn-50Pb alloy. These less degenerate eutectic regions in the 40Sn-60Pb alloy will better concentrate the deformation within colony boundaries than the more degenerate eutectic of the 50Sn-50Pb alloy. Thus, in the 40Sn-60Pb alloy, even though there are more obstacles, the deformation will be more concentrated and able to cut through them.

Coring in the proeutectic during nonequilibrium solidification will cause the proeutectic in the 50Sn-50Pb alloy to have more overall Sn and potentially greater strength than that of the 40Sn-60Pb alloy. If it is assumed that no diffusion occurs in the solid and if an average partition coefficient is used, then only a few percent difference between the 40Sn-60Pb and the 50Sn-50Pb proeutectic particles is expected. Because some diffusion is expected, however, this difference is expected to be even less. Also, the aging data in the previous section suggest that the Sn in solution in the Pb contributes more to the strength of the alloy than the Sn precipitated. Since the proeutectic in the 40Sn-60Pb and 50Sn-50Pb alloys

have the same Sn solubility at the same temperature, the effect of these small concentration differences on the strength is not likely to be great.

The results of microhardness testing in the proeutectic of the 40Sn-60Pb and 50Sn-50Pb alloys are given in Table II above. As shown, the strengths of the proeutectic are similar so long as particles with similar precipitate distributions are compared. The size of the indents, however, were on the order of the size of the proeutectic so the strength was averaged over the entire particle. Also, the 40Sn-60Pb eutectic regions are harder than those of the 50Sn-50Pb alloy which may increase the apparent hardness of the Pb-rich regions in the 40Sn-60Pb alloy.

One interesting result of the microhardness tests is that the hardest proeutectic in the 50Sn-50Pb alloy were harder than the eutectic regions of that alloy. In that case, the proeutectic would be much less bypassable obstacles than the softer ones. Published data [157-161] suggest that while Pb is softer than near-eutectic alloys at room temperature, it becomes stronger at higher temperatures. This reversal is most likely due to the difference in the melting points of the two different alloys and suggests that the difference in strength of the hard proeutectic and eutectic regions of the 50Sn-50Pb alloy may be even greater at the higher fatigue testing temperature of 75°C. So again, the fact that the eutectic regions in the 50Sn-50Pb alloy are softer and more degenerate than those of the 40Sn-60Pb alloy seems to be of more importance than the difference in Sn concentration within the proeutectic.

In addition to its effect on the surrounding eutectic morphology, the shape of the proeutectic particles is liable to have an additional effect on fatigue failure. As discussed above, the proeutectic in the 40Sn-60Pb alloy are elongated and tend to line up across the solder joint. As shown in Figure 3.23, the more equiaxed shape of the proeutectic in the 50Sn-50Pb alloy will provide more strain concentration than the 40Sn-60Pb particles which are lined up almost perpendicular to the applied shear strain. The 50Sn-50Pb

proeutectic, then, will cause the deformation around it to spread out into the surrounding eutectic material and thus postpone strain localization through the proeutectic.

3.3.1.4. Conclusions

Fatigue failures at 75°C with strain ranges between about 5 and 10% in the Pb-rich 20Sn-80Pb and 5Sn-95Pb alloys occurs by localized recrystallization ahead of the propagating fatigue crack. Cracking through this recrystallized region occurs intergranularly at all strain ranges tested.

In the off-eutectic but eutectic-rich alloys, the presence of the Pb-rich proeutectic particles prevents the formation of long straight shear bands seen in the shear deformation of near-eutectic solder joints. The proeutectic, however, also affects the morphology of the surrounding eutectic material. In both the 50Sn-50Pb and 40Sn-60Pb alloys, the Pb-rich proeutectic caused the nearby eutectic to be more degenerate than regions removed from the proeutectic. In the 40Sn-60Pb alloy, however, the more convoluted surface of the proeutectic particles allows nucleation of Sn and therefore eutectic at a smaller undercooling than the more equiaxed proeutectic of the 50Sn-50Pb alloy. Formation of eutectic at a smaller undercooling, in turn, allows slower growth of the eutectic and more time for the developing of a preferred growth direction. The resultant eutectic microstructure is more lamellar and less uniform than it would be with greater undercooling. The more heterogeneous eutectic microstructure in the 40Sn-60Pb alloy allows more concentration of the strain and easier bypassing of the proeutectic even though there are more of them than in the 50Sn-50Pb alloy. Also, the more degenerate eutectic in the 50Sn-50Pb alloy is softer to the point that some of the proeutectic in the 50Sn-50Pb alloy, although not significantly stronger than the proeutectic of the 40Sn-60Pb alloy, are stronger than the surrounding eutectic material which increases the effective resistance of the proeutectic to strain concentration. Other likely effects include added strength at the center of the proeutectic in the 50Sn-50Pb alloy due to greater Sn concentration from nonequilibrium

cooling and greater strain concentration around the more equiaxed 50Sn-50Pb proeutectic particles.

Everything that makes 40Sn-60Pb less resistant to fatigue failures by the formation of a coarsened band is a result of the fact that the Pb-rich proeutectic particles are deformable and therefore can be "cut" by the coarsened band. Once strain localizes within a proeutectic particle, the effective length of the coarsened band increases, and more strain can be concentrated within it. It then has greater ability to bypass other proeutectic particles. For this reason, even greater improvements are expected with less deformable particles.

3.3.2. Addition of Hard Particles of a Third Phase

3.3.2.1. Background

The idea of adding particles to solder is not a new one although the reasoning behind it has generally been different from that proposed here. Any problems encountered in adding particles usually involve flux entrapment and a consequent increase in the void density or segregation problems upon reflow (remelting) due to density differences between the particle and the solder. Below, a method is developed for the addition of particles with a density similar to solder without the use of fluxes.

There are several requirements for third-phase particles if they are to be successfully introduced uniformly to a solder joint. First, they must have a density similar to solder to prevent segregation upon reflow of the joint. Second, they must be wet by liquid solder to prevent rejection of the particle upon reflow. Third, they must be stable at typical soldering temperatures to prevent their dissolving or melting during soldering or reflow.

The particles introduced can be either elemental or compound. The advantages of an elemental powder is that wetting can be predicted fairly accurately with a phase diagram by requiring that the element form a compound with Sn or Pb. Also, the particle size and distribution of a powder is easily controlled. One potential problem with an elemental

powder is that if the element involved has a strong affinity for Sn or Pb, then it might dissolve even below its melting point. This dissolution is known to occur with gold and silver in Sn-Pb solders [167,168]. Compound powders, on the other hand, are difficult to introduce to solder without the use of fluxes. Theoretically, one way of doing that would be to precipitate the compound from the melt. That procedure, however, would require the identification of two elements which when present together in the solder melt are insoluble in the melt and precipitate a compound with a density similar to the melt. Even if two such elements were identified, control of the particle size would be more difficult in a precipitation process than with introducing powders. For these reasons, it was decided that elemental powders would be the best initial approach.

In deciding which elemental powders would be investigated, the following restrictions were made. The element was required to have a melting point above 500°C to prevent melting during soldering. Because Sn and Pb proeutectic do not show significant segregation during soldering, the density was required to be between Sn and Pb. To further restrict the density range, the density of liquid Pb rather than solid Pb was used as an upper limit. The element was required to have an existing phase diagram with Sn or Pb which showed that intermetallic formation occurred with either Sn or Pb. Elements forming low-melting intermetallics (melting point less than about 500°C) were eliminated to minimize the chance of the powders dissolving into the solder melt. And, finally, to narrow down the choices, all dangerous, toxic, expensive and rare elements were eliminated.

3.3.2.2. Results and Discussion

The above restrictions led to the choice of niobium (Nb) as the elemental powder to be added. The density of Nb is 8.55 g/cm^3, well within the set limits (7.30 g/cm^3 for Sn and 10.7 g/cm^3 for liquid Pb). The density of eutectic Sn-Pb solder can be approximated using the law of mixtures since the eutectic microstructure breaks up into approximately pure Sn and Pb regions. The weight fraction of each phase is given by the lever rule and the phase

diagram in Figure 1.4 and is .55 for Sn and .45 for Pb. The density, then, is given approximately by:

$$\rho^{-1} = \frac{(0.45\ g_{Pb}/g_{tot})}{(11.4\ g_{Pb}/cc_{Pb})} + \frac{(0.55 g_{Sn}/g_{tot})}{(7.3\ g_{Sn}/cc_{Sn})}$$

$$\rho = 8.7\ g/cc.$$

The density of liquid eutectic solder is likely to be lower, but in any case, it should be close to the value for Nb.

To grind Nb, which is a fairly ductile metal, into a fine powder form, NbH, which is brittle, was used. NbH was ball milled for several hours to obtain powders ranging in size from a few to 10μm in diameter. It was reasoned that due to the reduced surface area of larger powder sizes, if Nb powders of this size could be introduced, then larger ones could as well. The ground NbH powders were then reduced to Nb in a hydrogen furnace. The hydrogen (H) in NbH sits on ordered interstitial sites [169] so that when, under vacuum at high temperatures, the H is driven off, Nb metal is left. The dehydriding, in this case, was done at 1100°C.

The Nb-Sn phase diagram is shown in Figure 3.39. At all temperatures and compositions, Nb and Pb are completely miscible [170]. At reasonable soldering temperatures, the intermetallic which will form on the Nb powders in the presence of Sn is $NbSn_2$. To prevent oxidation of the clean Nb powders, Sn was melted within the vacuum furnace at 400°C under Ar and the Nb introduced prior to removal from the furnace. Once cool, the Sn-coated powders were added to solder with enough extra Pb to balance the Sn coating the Nb powders, leaving a nearly eutectic composition. Unfortunately, as shown in Figure 3.40, the pretin layer was completely reacted and what was left of the original Nb powders was present as small Nb particles embedded in large intermetallic particles.

Energy Dispersive X-ray (EDX) analysis showed the intermetallic to be approximately 33% Sn and verified that the particles within the intermetallic were relatively pure Nb. It was concluded that the intermetallic was $NbSn_2$. Following pretinning, the powders were slowly cooled in the vacuum furnace. It is likely that the excessive amount of $NbSn_2$ formed during this slow cool. Because the furnace could not be made to cool down any faster, another approach had to be devised.

Following dehydriding of the NbH powders, the clean Nb powders were wrapped under Ar in Sn foil. Because the furnace opened from the top and because Ar is heavier than air, the powders could be wrapped without excessive exposure to air. These Sn wrapped powders were then immediately encapsulated in a quartz tube with solder of the appropriate composition which was backfilled with Ar. The quartz tube was placed in a furnace at 400°C until the Sn foil melted. It was then removed, shaken vigorously and quenched in water. Micrographs showing particles in this quenched ingot are presented in Figure 3.41. Chemical analysis by EDX confirmed that these particles were still Nb.

A small piece of this quenched ingot was then added to eutectic solder at 230°C and air cooled. A particle in this ingot is shown in Figure 3.42. Lamellae in this micrograph can be seen to grow out from the particle at a 90° angle. Since lamellae always grow perpendicular to the solidifying interface, this observation indicates that the Nb particle, as expected, is wet by the solder. This wetting occurred without the use of fluxes, and no void formation was seen in this bulk ingot.

3.3.2.3. Conclusions

By reasoning given in the previous section, the addition of relatively undeformable particles of sizes on the order of the sizes of the proeutectic in 50Sn-50Pb solder to near-eutectic solders is expected to greatly improve the low-cycle fatigue life of these alloys. Potential problems with added particles are segregation due to density mismatches and void

nucleation due to flux entrapment. Both of these problems can be avoided by using Nb powders. A method of introducing these powders to Sn-Pb solders was presented.

4. CONCLUSIONS

Fatigue failures in the slowly cooled near-eutectic solder joints studied here are accompanied by the formation of a band of coarsened material running parallel to the direction of the applied shear strain. This coarsened band results from the concentration of the deformation into long, straight shear bands which form along the relatively soft colony boundaries which happen to line up parallel to the applied shear strain. The longer and straighter the shear band, the more deformation that can concentrate within it. Localized recrystallization within the band begins near the largest stress concentration and is followed by strain-assisted coarsening. These localized microstructural changes result in localized softening and further deformation concentration in the recrystallized material of the band and, analogous to a crack, in adjacent unrecrystallized material within the band. In regions of the joint where no shear band parallel to the applied shear strain forms ("obstacles"), the coarsened band can cut across by geometric strain localization, where strain localizes because the region is surrounded by approximately coplanar bands, or by mode II crack-like propagation of the relatively soft coarsened band. As the length of the coarsened band increases, the amount of deformation within it increases until eventually cracking, which was seen to occur along Sn-Sn grain boundaries and Sn-Pb phase boundaries, begins. The longer the initial band, the easier the "obstacles" will be bypassed and the less resistant the solder will be to fatigue. Hence, the best methods of improving fatigue life in these alloys involve the elimination of the long, straight shear bands which form during deformation. Two general ways for doing that were proposed. The first involves homogenization of the microstructure, and the second involves particle additions.

Homogenization of the microstructure was shown to improve fatigue life by aging eutectic solder at room temperature for about a year and a half. It was concluded that

discontinuous coarsening at colony boundaries which increased the degeneracy of the microstructure beginning after about 9 months at room temperature spread out the deformation sufficiently during fatigue to inhibit failure by formation of a coarsened band. Localized recrystallization was seen ahead of the fatigue crack in aged solder, but it was not as distinct and did not extend as far ahead of the crack as did the band in the unaged joints.

Softening to about 70-75% of the initial shear strength occurred with room temperature aging levelling off after about 40-50 weeks. Since the microstructural changes mentioned above did not occur until after the strength levelled off, it was concluded that softening occurred through a mechanism other than discontinuous microstructural coarsening. It has been proposed before that room temperature aging causes softening of Sn-Pb alloys by precipitation of Sn in the Pb-rich regions and the resultant decrease in solid solution strengthening. Using published diffusion data, it was shown that Sn diffusion in bulk Pb could occur over a distance of about 0.1μm in about 70 weeks suggesting that the above mechanism is possible. Since no precipitation was seen within lamellar or otherwise fine regions of the microstructure, it was concluded that when the interphase separation is small, supersaturated Sn in the Pb-rich regions diffuses to adjacent Sn-rich regions; otherwise, it precipitates. In either case, Sn is removed from solid solution and results in softening.

At 110°C, softening occurs more rapidly than at room temperature but only decreases the strength by about 15%. The greater strength after the higher temperature aging treatment is due to the greater solubility of Sn in Pb at higher temperatures. Aging at this higher temperature resulted in more coarsening and a more degenerate microstructure than at room temperature and these microstructural changes are expected to be more beneficial to fatigue resistance than those seen after aging at room temperature for much longer times.

The addition of particles was shown to improve the fatigue life of near-eutectic solders by studying fatigue of the off-eutectic alloys which are essentially eutectic alloys with varying amounts of added particles (the proeutectic). All eutectic-rich alloys tested with

strain ranges between 5 and 10% at 75°C with strain rates on the order of $10^{-4}s^{-1}$ failed by formation of a coarsened band as seen in the near-eutectic alloys, but the fatigue lives were as much as 5 times better in the proeutectic-containing alloys than in the eutectic. As expected, the proeutectic particles break up the microstructure and prevent the long, straight shear bands seen to accelerate failure in the near-eutectic alloys from forming.

The 40Sn-60Pb alloy is stronger than the 50Sn-50Pb alloy under the conditions used here, but has a lower fatigue resistance even though it is further off the eutectic composition and, thus, has more of the Pb-rich proeutectic. It was found that the eutectic regions of the 40Sn-60Pb alloy were less degenerate and had a better defined colony structure than did those of the 50Sn-50Pb alloy. These less degenerate regions in the 40Sn-60Pb alloy are harder but, due to the colony structure, concentrate deformation more than those of the 50Sn-50Pb alloy. Hence, even though there is more of the proeutectic, they are more easily bypassed in the 40Sn-60Pb alloy.

The difference in the microstructure of the eutectic regions in the two off-eutectic but eutectic rich alloys studied was proposed due to the difference in shape of the proeutectic which forms in these alloys. In the 50Sn-50Pb alloy, the proeutectic are relatively small and equiaxed while in the 40Sn-60Pb alloy, they are dendritic with well-developed side arms. It was proposed that the more convoluted surface of the proeutectic in the 40Sn-60Pb alloy allowed nucleation of the eutectic at a smaller undercooling thus, allowing more time for growth of the eutectic and development of a preferred lamellar growth direction.

The 40Sn-60Pb alloy showed less resistance to fatigue than the 50Sn-50Pb alloy because the proeutectic particles were deformable and thus, bypassable by the coarsened band. For this reason, relatively undeformable particles are expected to have an even greater effect on the fatigue resistance than the Pb-rich proeutectic. A procedure for the addition of Nb powders, which have a density similar to eutectic Sn-Pb solder, to solder without the use of fluxes, which can cause porosity problems in solder joints, was developed and discussed.

Fatigue failures in 5Sn-95Pb and 20Sn-80Pb solder joints also involved localized recrystallization, but this recrystallization was only seen near the tip of the fatigue crack. Cracking occurred intergranularly in both alloys at the strain ranges between 5 and 10% tested.

5. REFERENCES

1. J.W. Munford, "The Influence of Several Design and Material Variables on the Propensity for Solder Joint Cracking," *IEEE Transactions on Parts, Hybrids, and Packaging*, PHP-11(1975), 296-304.

2. R.N. Wild, "Fatigue Properties of Solder Joints," Welding Research Supplement, *Welding Journal*, 51 (1972), 521s-526s.

3. R.W. Rohde and J.C. Swearengen, "Deformation Modeling Applied to Stress Relaxation of Four Solder Alloys," *Journal of Engineering Materials and Technology*, 102 (April, 1980), 207-214.

4. F.W. Oberin, "Solder Joint Cracking in Potted High Voltage Modules," Micro Electronic Packaging Technology: Materials and Processes, ed. by W.T. Shieh, ASM(1989), 189-202.

5. P.M. Hall, T.D. Dudderar and J.F. Argyle, "Thermal Deformations Observed in Leadless Ceramic Chip Carriers Surface Mounted to Printed Wiring Boards," *IEEE Transactions on Components, Hybrids, and Manufacturing Technology*, CHMT-6, #4 (December, 1983), 544-552.

6. D. Frear, D. Grivas and J.W. Morris, Jr., "Parameters Affecting Thermal Fatigue Behavior of 60Sn-40Pb Solder Joints," *Journal of Electronic Materials*, 18 (1989), 671-680.

7. R.N. Wild, "Some Factors Affecting Leadless Chip Carrier Solder Joint Fatigue Life II," 12th Annual Electronics Manufacturing Seminar Proceedings, Naval Weapons Center Report #NWC TP 6896 (1988), 271-199.

8. A.C. Chilton, M.A. Whitmore and W.B. Hampshire, "Isothermal Mechanical Fatigue of a Model SMD Joint," in Micro Electronic Packaging Technology, ed. by W.T. Shieh, ASM(1989), 159-176.

9. A.C. Chilton, M.A. Whitmore and W.B. Hampshire, "Fatigue Failure in a Model SMD Joint," *Soldering and Surface Mount Technology*, #3 (Oct., 1989), 21-24.

10. H.D. Solomon, V. Brzozowski and D.G. Thompson, "Prediction of Solder Joint Fatigue Life," GE Internal Report #88CRD101 (April, 1988).

11. T.A. Krinke and D.K. Pai, "Factors Affecting Thermal Fatigue Life of LCCC Solder Joints," *Welding Journal*, 67 (Oct., 1988), 33-40.

12. W. Engelmaier, "Surface Mount Solder Joint Long-term Reliability: Design, Testing, Prediction," *Soldering and Surface Mount Technology*, #1(February, 1989), 14-22.

13. W. Engelmaier, "Effects of Power Cycling on Leadless Chip Carrier Mounting Reliability and Technology," *Electronic Packaging and Production*, 23, #4(April, 1983), 58-63.

14. W. Engelmaier, "Fatigue Life of Leadless Chip Carrier Solder Joints During Power Cycling," *IEEE Transactions on Components, Hybrids, and Manufacturing Technology*, CHMT-6 (Sept., 1983), 232-237.

15. D.K. Pai and T.A. Krinke, "A Solution to Solder Joint Failure in Leadless Ceramic Chip Carriers," *Surface Mount Technology*, 3 (Sept., 1989), 27-35.

16. Capt. R.E. Settle, Jr., "A New Family of Microelectronic Packages for Avionics," *Solid State Technology*, (June, 1978), 54-58.

17. J.W. Lampe, "The Interrelationships of Design, Materials, and Processes for Surface Mount Assemblies in Military Applications," *Surface Mount Technology*, 3, #7(November, 1989), 22-27.

18. D.R. Frear, "Microstructural Observations of the Sn-Pb Solder/Cu System and Thermal Fatigue of the Solder Joint," Ph.D. Thesis, University of California, Berkeley, CA, (1987).

19. P.M. Hall, "Solder Post Attachment of Ceramic Chip Carriers to Ceramic Film Integrated Circuits," *IEEE Transactions on Components, Hybrids, and Manufacturing Technology*, CHMT-4, #4 (December, 1981), 403-410.

20. G. Cherian, C. Wynn and H. White, "New Solder Column Alloy Improves Reliability of Chip Carrier Assemblies," presented at the 18th International SAMPE Technical Conference, October, 1986.

21. H.B. Ellis, "Aspects of Surface Mounted Chip Carrier Solder Joint Reliability," 11th Annual Electronics Manufacturing Seminar Proceedings, Naval Weapons Center report #NWC TP 6789, 377-407.

22. P.A. Ainsworth, "The Formation and Properties of Soft Soldered Joints," *Metals and Materials*, 5 (1971), 374-379.

23. J.H. Lau and D.W. Rice, "Solder Joint Fatigue in Surface Mount Technology: State of the Art," *Solid State Technology*, Oct. (1985), pp. 91-104.

24. M.E. Fine and D.A. Jeannotte, "Soft Solder -- General Principles and Fatigue Life Estimation," Micro Electronic Packaging Technology: Materials and Processes, ed. by W.T. Shieh, ASM (1989). 147-157.

25. E. Baker, "Understanding Cyclical Thermal Stress in Electronic Assemblies: The Key to Improving Accelerated-Life Testing," *Insulation/Circuits*, 19, (October, 1975), 49-56.

26. J.L. Marshall, "Characterization of Solder Fatigue in Electronic Packaging," *Brazing and Soldering*, #15 (Fall, 1988), 4-9.

27. E.E. de Kluizenaar and M.M.F. Verguld, "The Strength of Soldered Joints on Surface Mounted Devices," *Soldering and Surface Mount Technology*, 1 (February, 1989), 52-57.

28. J.R. Wilcox, R. Subrahmanyan and Che-Yu Li, "Thermal Stress Cycles and Inelastic Deformation in Solder Joints," Micro Electronic Packaging Technology: Materials and Processes, ed. by W.T. Shieh, ASM (1989), 203-211.

29. R. Subrahmanyan, J.R. Wilcox and Che-Yu Li, "A Damage Integral Approach to Solder Joint Fatigue," Micro Electronic Packaging Technology: Materials and Processes, ed. by W.T. Shieh, ASM (1989), 213-221.

30. R. Subrahmanyan, J.R. Wilcox and Che-Yu Li, "A Damage Integral Approach to Thermal Fatigue of Solder Joints," *IEEE Transactions on Components, Hybrids, and Manufacturing Technology*, CHMT-12, #4(December, 1989), 480-491.

31. K.C. Norris and A.H. Landzberg, "Reliability of Controlled Collapse Interconnections," *IBM J. Res. Develop.*, (May, 1969), 266-271.

32. M. Miyazaki, S. Yoshioka and A. Hijakata, "Evaluation of Thermal Fatigue Strength in Lap Type Solder Joints," *Zairyo*, 30 (April, 1981), 330-335.

33. M.C. Shine, L.R. Fox and J.W. Sofia, "A Strain Range Partitioning Procedure for Solder Fatigue," *Brazing and Soldering*, #9 (1985), 11-14.

34. M.C. Shine and L.R. Fox, "Fatigue of Solder Joints in Surface Mount Devices," Low Cycle Fatigue, ASTM STP 942, ed. be H.D. Solomon, G.R. Halford, L.R. Kaisand and B.N. Leis, ASTM, Philadelphia (1988), 588-610.

35. M.C. Shine, "Method of Predicting Fatigue Lifetimes of Metallic Structures," United States Patent #4947341 (August 7, 1990).

36. H.D. Solomon, "Creep Strain Rate Sensitivity and Low Cycle Fatigue of 60/40 Solder," *Brazing and Soldering*, #11(1986), 68-75.

37. H.D. Solomon, "Fatigue of 60/40 Solder," IEEE Trans. on *Components, Hybrids and Manufacturing Technology*, 9(1986), 423-432.

38. H.D. Solomon, "The Influence of Hold Time and Fatigue Cycle Wave Shape on the Low Cycle Fatigue of 60/40 Solder," Proceedings of the 38th Electronic Components Conference, IEEE (May, 1988), 7-13.

39. H.D. Solomon, "Low-Frequency, High-Temperature Low Cycle Fatigue of 60Sn-40Pb Solder," Low Cycle Fatigue, ASTM STP 942, ed. be H.D. Solomon, G.R. Halford, L.R. Kaisand and B.N. Leis, ASTM, Philadelphia (1988), 342-370.

40. H.D. Solomon, "Strain-Life Behavior in 60/40 Solder," Transactions of the ASME, *Journal of Electronic Packaging*, 111, #2 (June, 1989), 75-82.

41. H.D. Solomon, "Low Cycle Fatigue of Surface-Mounted Chip-Carrier/Printed Wiring Board Joints," *IEEE Transactions on Components, Hybrids, and Manufacturing Technology*, CHMT-12 (December, 1989), 473-479.

42. J.W. Evans, "An Overview of Thermally Induced Low Cycle Fatigue in Surface Mounted Solder Joints," *Surface Mount Technology*, (Feb., 1989), 35-39.

43. M. Kitano, S. Kawai and I. Shimizu, "Thermal Fatigue Strength Estimation of Solder Joints of Surface Mount IC Packages," *Soldering and Surface Mount Technology*, 2 (June, 1989), 4-8.

44. N.F. Enke, T.J. Kilinski, S.A. Schroeder and J.R. Lesniak, "Mechanical Behaviors of 60/40 Tin-Lead Solder Lap Joints," *IEEE Transactions on Components, Hybrids, and Manufacturing Technology*, CHMT-12, #4 (December, 1989), 459-468.

45. S. Majumdar and W.B. Jones, "How Well Can we Predict the Creep-Fatigue Life of a Well-Characterized Material," in Solder Mechanics — A State of the Art Assessment, ed. by D.R. Frear, W.B. Jones and K.R. Kinsman, TMS (1991), 273-360.

46. B.I. Sandor, "Life Prediction of Solder Joints," in Solder Mechanics — A State of the Art Assessment, ed. by D.R. Frear, W.B. Jones and K.R. Kinsman, TMS (1991), 363-419.

47. S.S. Manson, "Behavior of Minerals [Materials] Under Stress and Strain Cycling," Thermal Stress and Low-Cycle Fatigue, Ch. 4, McGraw-Hill (1966), p.125-192.

48. L.F. Coffin, Jr., "A Study of the Effects of Cyclic Thermal Stresses on a Ductile Metal," *Trans. ASME*, 76 (1954), 931-950.

49. L.F. Coffin, Jr., "Introduction to High-Temperature Low-Cycle Fatigue," *Experimental Mechanics*, 8 (May, 1968), 218-224.

50. C. Laird, "Cyclic Deformation of Metals and Alloys," Treatise on Materials Science and Technology, 6, Plastic Deformation of Materials, ed. by R.J. Arsenault, Academic Press, NY (1975), 101-162.

51. K. Bae, A.F. Sprecher, Z. Guo, H. Conrad and D.Y. Jung, "Effect of Compliance on the Fatigue of Solder Joints in Surface-Mounted Electronic Packages," in Micro Electronic Packaging Technology, ed. by W.T. Shieh, ASM(1989), 109-119.

52. V.D. Coombs, Testing for Prediction of Material Performance in Structures and Components, ASTM STP #515 (1972), 3-21.

53. D. Frear, D. Grivas, M. McCormack, D. Tribula and J.W. Morris, Jr., "Fatigue and Thermal Fatigue Testing of Pb-Sn Solder Joints,"Proceedings of the 3rd Annual Electronic Packaging and Corrosion in Microelectronics Conference, 3(1987), ASM, 269-276.

54. M. McCormack, "Initial Research Regarding Isothermal Shear Fatigue of Solder Joints," MS Thesis, University of California, Berkeley, CA, (1984).

55. D. Frear, D. Grivas, M. McCormack, D. Tribula and J.W. Morris, Jr., "Fatigue and Thermal Fatigue of Pb-Sn Solder Joints," Effect of Load and Thermal Histories on Mech. Behavior, TMS (1987), 113-126.

56. H.D. Solomon, "Low Cycle Fatigue of 60/40 Solder -- Plastic Strain Limited vs. Displacement Limited Testing," Electronic Packaging: Materials and Processes, ed. by J.A. Sartell, ASM(1985), 29-48.

57. J.R. Taylor and D.J. Peddar, "Joint Strength and Thermal Fatigue in Chip Carrier Assembly," *Int. J. Hybrid Microelectronics*, 5 (1982), 209-214.

58. E.C. Cutiongco, S. Vaynman, M.E. Fine and D.A. Jeannotte, "Isothermal Fatigue of 63Sn-37Pb Solder," Trans. ASME *Journal of Electronic Packaging*, 112 (June, 1990), 110-114.

59. R.C. Weinbel, J.K. Tien, R.A. Pollak and S.K. Kang, "Creep-Fatigue Interaction in Eutectic Lead-Tin Solder Alloy," *J. Mat. Sci.*, 22 (1987), 3901-3906.

60. L.R. Fox, J.W. Sofia and M.C. Shine, "Investigation of Solder Fatigue Acceleration Factors," *IEEE Transactions on Components, Hybrids, and Manufacturing Technology*, CHMT-8, #2 (June, 1985), 275-282.

61. R.N. Wild, "Some Fatigue Properties of Solders and Solder Joints," IBM Technical Paper No. 74Z000481 (1975).

62. J.K. Tien, B.C. Hendrix and A.I. Attarwala, "Creep-Fatigue Interactions in Solders," *IEEE Transactions on Components, Hybrids, and Manufacturing Technology*, 12, #4 (Dec., 1989), 502-505.

63. D.R. Frear and W.B. Jones, "Cyclic Deformation of 60Sn-40Pb Solder Joints During Thermomechanical Fatigue," Proc. NEPCON '90, Anaheim, CA (1990), 1340.

64. D.R. Frear, "Thermomechanical Fatigue in Solder Materials," in Solder Mechanics — A State of the Art Assessment, ed. by D.R. Frear, W.B. Jones and K.R. Kinsman, TMS (1991), 191-237.

65. H.D. Solomon, "Room Temperature Low Cycle Fatigue of a High Pb Solder (Indalloy 151)," Micro Electronic Packaging Technology: Materials and Processes, ed. by W.T. Shieh, ASM(1989), 135-146.

66. H.D. Solomon, "High and Low Temperature Strain-Life Behavior of a Pb Rich Solder," Transactions of the ASME *Journal of Electronic Packaging*, 112 (June, 1990), 123-128.

67. M. Kitano, T. Shimizu, T. Kumazawa and Y. Ito, "Statistical Fatigue Life Estimation: The Influence of Temperature and Composition on Low-Cycle Fatigue of Tin-Lead Solders," Statistical Research on Fatigue and Fracture, *Current Japanese Materials Research*, 2(1987), 235-251.

68. H.S. Rathore, R.C. Yih and A.R. Edenfeld, "Fatigue Behavior of Solders Used in Flip-Chip Technology," *Journal of Testing and Evaluation*, 1 (1973), 170-178.

69. S. Vaynman, M.E. Fine and D.A. Jeannotte, "Isothermal Fatigue of Low Tin Lead Based Solder," *Met. Trans. A*, 19A (1988), 1051-59.

70. S. Vaynman, "Effect of Strain Rate on Fatigue of low-Tin Lead-Base Solder," *IEEE Transaction on Components, Hybrids and Manufacturing Technology*, CHMT-12, #4 (Dec., 1989), 469-472.

71. S. Vaynman, M.E. Fine and D.A. Jeannotte, "Prediction of Fatigue Life of Lead-Base Low Tin Solder," Proc. 37th Electronic Component Conf., IEEE (1987), 598-603.

72. S. Vaynman, M.E. Fine and D.A. Jeannotte, "Isothermal Fatigue Failure Mechanisms in Low Tin Lead Based Solder," Effects of load and Thermal Histories on Mechanical Behavior of Materials, TMS (1987), 127-38.

73. S. Vaynman, M.E. Fine and D.A. Jeannotte, "Low-Cycle Isothermal Fatigue Life of Solder Materials," in Solder Mechanics — A State of the Art Assessment, ed. by D.R. Frear, W.B. Jones and K.R. Kinsman, TMS (1991), 155-189.

74. D.S. Stone, "The Creep-Fatigue Interaction in Solders and Solder Joints," Trans. ASME, *Journal of Electronic Packaging*, 112 (1990), 100-103.

75. K.U. Snowden, "The Effect of Atmosphere on the Fatigue of Lead," *Acta Metallurgica*, 12 (1964), 295-303.

76. K.U. Snowden, "The Effect of Cycle Frequency and Atmospheric Corrosion on the Fatigue of Lead," *Philosophical Magazine*, 10 (1964), 435-440.

77. K.U. Snowden, "Fatigue Crack Formation in Bicrystals of Lead," *Phil. Mag.*, 14 (1966), 1019-1029.

78. R. Berriche, S. Vaynman, M.E. Fine and D.A. Jeannotte, "The Effect of Environment on Fatigue of Low Tin Lead Base Alloys," Electronic Packaging and Corrosion in Microelectronics, ASM International (1987), 169-174.

79. G.J. Stone and V. Raman, "Inhibition of Cyclic Grain Boundary Migration Through Cellular Precipitation in Pb-5 Pct. Sn Alloy," *Met. Trans. A*, 19A (1988), 2355-2358.

80. R.C. Weinbel, E.A. Schwarzkopf and J.K. Tien, "Effect of Frequency on the Cyclic Creep and Fracture of a Lead-Rich Lead-Tin Solder Alloy," *Scripta Metall.*, 21 (1987), 1165-8.

81. N.D. Zommer, D.L. Feucht and R.W. Heckel, "Reliability and Thermal Impedance Studies in Soft Soldered Power Transistors," *IEEE Transactions on Electron Devices*, ED-23(1976), 843-850.

82. T. Takenaka, F. Kobayashi and T. Netsu, "Reliability of Flip-Chip Interconnections," Proceedings of the 1984 International Symposium on Microelectronics, International Society for Hybrid Microelectronics, Montgomery, AL (1984), 419-423.

83. E. Levine and J. Ordonez, "Analysis of Thermal Cycle Fatigue Damage in Microsocket Solder Joints," *IEEE Transactions on Components, Hybrids and Manufacturing Technology*, CHMT-4, #4 (Dec., 1981), 515-519.

84. D.R. Frear, D. Grivas and J.W. Morris, Jr., "Thermal Fatigue in Solder Joints," *Journal of Metals*, 40(1988), 18-22.

85. L.S. Goldmann, R.D. Herdzik, N.G. Koopman, and V.C. Marcotte, "Lead-Indium for Controlled-Collapse Chip Joining," *IEEE Transactions on Parts, Hybrids, and Packaging*, PHP-13(1977), 194-198.

86. S.K. Kang, N.D. Zommer, D.L. Feucht and R.W. Heckel, "Thermal Fatigue Failure of Soft-Soldered Contacts to Silicon Power Transistors," *IEEE Transactions on Parts, Hybrids, and Packaging*, PHP-13(1977), 318-321.

87. T.G. Langdon and R.C. Gifkins, "Cyclic Grain Boundary Migration During High Temperature Fatigue -- I. Microstructural Observations," *Acta Metall.*, 31 (1983), 927-938.

88. T.G. Langdon, D. Simpson and R.C. Gifkins, "Cyclic Grain Boundary Migration During High Temperature Fatigue -- II. Measurements of Grain Boundary Sliding," *Acta Metall.*, 31 (1983), 939-946.

89. P.J. Greenwood, T.C. Reiley, V. Raman and J.K. Tien, "Cavitation in a Pb/Low-Sn Solder During Low Cyclic Fatigue," *Scripta Metallurgica*, 22 (1988), 1465-8.

90. V. Raman and T.C. Reiley, "Dynamic Recrystallization During High Temperature Fatigue," *Scripta Metallurgica*, 20 (1986), 1343-1346.

91. H.S. Betrabet and V. Raman, "Microstructural Observations in Cyclically Deformed Pb-Sn Solid Solution Alloy," *Met. Trans.*, 19A (1988), 1437-1441.

92. V. Raman and T.C. Reiley, "Cyclic Deformation and Fracture in Pb-Sn Solid Solution Alloy," *Met. Trans.*, 19A (1988), 1533-1545.

93. K.U. Snowden and J.N. Greenwood, "Rectangular Cracking in Lead," *Trans. TMS-AIME*, 212 (February, 1958), 91-92.

94. E.R. Bangs and R.E. Beal, "Effect of Low Frequency Thermal Cycling on the Crack Susceptibility of Soldered Joints," Welding Research Supplement, *Welding Journal*, 54 (1975), 377s-383s.

95. B.D. Dunn, "The Resistance of Space-Quality Solder Joints to Thermal Fatigue," *Circuit World*, 6 (1979), 16-27.

96. W.M. Wolverton, "The Mechanisms and Kinetics of Solder Joint Degradation," *Brazing and Soldering*, 13 (1987), 33-38.

97. L.K. Quan, "Tensile and Shear Behavior of Alloyed Sn-Pb Solder Joints," M.S. Thesis, University of California, Berkeley (1988).

98. D.A. Porter and K.E. Easterling, Phase Transformations in Metals, Van Nostrand Reinhold, UK (1981).

99. G.A. Chadwick, "Eutectic Alloy Solidification," *Progress in Materials Science*, 12 (1963), 97-182.

100. R. Elliot, Eutectic Solidification Processing: Crystalline and Glassy Alloys, Butterworths, Boston (1983).

101. J.D. Hunt and K.A. Jackson, "Binary Eutectic Solidification," *Transactions of the Metallurgical Society of AIME*, 236 (June, 1966), 843-852.

102. K.A. Jackson and J.D. Hunt, "Lamellar and Rod Eutectic Growth," *Transactions of the Metallurgical Society of AIME*, 236 (August, 1966), 1129-1142.

103. D.J.S. Cooksey, D. Munson, M.P. Wilkinson and A. Hellawell, "The Freezing of Some Continuous Binary Eutectic Mixtures," *Philosophical Magazine*, 10 (1964), 745-769.

104. F.R. Mollard and M.C. Flemings, "Growth of Composites from the Melt — Part II," *Transactions of the Metallurgical Society of AIME*, 239 (October, 1967), 1534-1546.

105. B.E. Sundquist and L.F. Mondolfo, "Heterogeneous Nucleation in the Liquid-to-Solid Transformation in Alloys," *Transactions of the Metallurgical Society of AIME*, 221 (February, 1961), 157-164.

106. V. de L. Davies, "Mechanisms of Crystrallization in Binary Eutectic Systems," *Journal of the Institute of Metals*, 93 (1964-65), 10-14.

107. L.F. Mondolfo, "Nucleation in Eutectic Alloys," *The Journal of the Australian Institute of Metals*, 10, #2 (1965), 169-177.

108. A. Ohno, T. Motegi and K. Ishibashi, "Formation Mechanism of Eutectic Grains," Proceedings of Solidification and Casting of metals, Metals Society, London (1979), 203-207.

109. J.A. Spittle, "Endogenous-Exogenous Freezing Characteristics of Pure and Impure As-Cast Zn-Al Alloys," *Metal Science Journal*, 11 (December, 1977), 578-585.

110. R.W. Kraft, "Technique for Determining Orientation Relationships and Interfacial Planes in Polyphase Alloys: Application to Controlled Eutectic Specimen," *Transactions of the Metallurgical Society of AIME*, 221 (August, 1961), 704-711.

111. R.W. Kraft, "Crystallography of Equilibrium Phase Interfaces in Al-$CuAl_2$ Eutectic Alloys," *Transactions of the Metallurgical Society of AIME*, 224 (February, 1962), 65-74.

112. R.H. Hopkins and R.W. Kraft, "Nucleation and Growth of the Pb-Sn Eutectic," Trans. *TMS-AIME*, 242 (1968), 1627-1633.

113. B. Labulle and C. Petipas, "Crystallographic Study of Thin Pb-Sn Lamellar Eutectic Ribbons," *Journal of Crystal Growth*, 28 (1975), 279-287.

114. J.D. Verhoeven, D.P. Mourer and E.D. Gibson, "The Morphology and Crystallography of Directionally Solidified Pb-Sn Eutectic Alloys," *Metallurgical Transactions A*, 8A (August, 1977), 1239-1247.

115. J.D. Hunt and J.P. Chilton, "An Experimental Investigation of the Undercooling at the Solid/Liquid Interface of the Lead-Tin Eutectic," *Journal of the Institute of Metals*, 92 (1963-64), 21-25.

116. R.W. Kraft, "Controlled Eutectics," *Journal of Metals,* 2 (1966), 192-200.

117. J.D. Hunt, "Developments in Eutectics," *Journal of Crystal Growth,* 3,4 (1968), 82-91.

118. A.S. Yue, "Microstructure of Magnesium-Aluminum Eutectic," *Transactions of The Metallurgical Society of AIME,* 224 (October, 1962), 1010-1015.

119. R.W. Kraft and D.L. Albright, "Crystallographic Substructure of Lamellar Al-$CuAl_2$ Eutectic," *Transactions of the Metallurgical Society of AIME,* 224 (December, 1962), 1176-1184.

120. J.D. Hunt, "The Lamella → Rod Transformation in Eutectics," *Journal of the Institute of Metals,* 94 (1966), 125-129.

121. W.A. Tiller, "Polyphase Solidification," Liquid Metals and Solidification, ASM, Ohio (1958), 276-318.

122. H.W. Kerr and W.C. Winegard, "Solidification of Eutectic Alloys," *Journal of Metals,* 18 (1966), 563-569.

123. H.W. Weart and D.J. Mack, "Eutectic Solidification Structures," *Trans. AIME,* 212 (1958), 664-670.

124. J.P. Chilton and W.C. Winegard, "Solidification of a Eutectic Made from Zone-Refined Lead and Tin," *Journal of the Institute of Metals,* 89 (1960-61), 162-164.

125. M.C. Flemings, Solidification Processing, McGraw-Hill, NY (1974).

126. R.W. Kraft and D.L. Albright, "Microstructure of Unidirectionally Solidified Al-$CuAl_2$ Eutectic," *Transactions of the Metallurgical Society of AIME,* 221 (February, 1961), 95-102.

127. D. Tribula, "A Microstructural Study of Creep and Thermal Fatigue Deformation in 60Sn-40Pb Solder Joints," Ph.D. Thesis, University of California, Berkeley (1990).

128. J.W. Morris, Jr., D. Tribula, T.S.E. Summers and D. Grivas, "The Role of Microstructure in Thermal Fatigue of Pb-Sn Solder Joints," Solder Joint Reliability: Theory and Application, to be published by Van Nostrand Reinhold, NY (1991).

129. M. Cagnon, M. Suery, A. Eberhardt and B. Baudelet, "High Temperature Deformation of the Pb-Sn Eutectic," *Acta Metallurgica,* 25(1977), 71-75.

130. D.A. Porter, K.E. Easterling and G.D.W. Smith, "Dynamic Studies of the Tensile Deformation and Fracture of Pearlite," *Acta Metallurgica,* 26(1978), 1405-1422.

131. G. Frommeyer, "Metallic Composite Materials," Physical Metallurgy, ed. by R.W. Cahn and P.Haasen, Elsevier Science Publishers BV (1983), 1852-1883.

132. Z. Mei, J.W. Morris, Jr., M.C. Shine and T.S.E. Summers, "Effects of Cooling Rate on Mechanical Properties of Near-Eutectic Tin-Lead Solder Joints," to be published in the *Journal of Electronic Materials.*

133. D. Frear, D. Grivas and J.W. Morris, Jr., "A Microstructural Study of the Thermal Fatigue Failures of 60Sn-40Pb Solder Joints," *Journal of Electronic Materials*, 17(1988), 171-180.

134. J.W. Morris, Jr., D. Grivas, D. Tribula, T. Summers and D. Frear, "Research on the Mechanism of Thermal Fatigue in Near-Eutectic Pb-Sn Solders," 13th Annual Electronics Manufacturing Seminar Proceedings, NWC TP 6986 (March, 1989), 275-297. Also published in *Soldering and Surface Mount Technology*, #3 (Oct., 1989), pp.4-10 and p.20.

135. D. Tribula, D. Grivas, D. Frear and J.W. Morris, Jr., "Observations on the Mechanisms of Fatigue in Eutectic Pb-Sn Solder Joints," *Journal of Electronic Packaging*, 111(1989), 83-89.

136. D. Tribula, D. Grivas, D.R. Frear and J.W. Morris, Jr., "Microstructural Observations of Thermomechanically Deformed Solder Joints," Welding Research Supplement, *Welding Journal*, 68 (1989), 404s-409s.

137. D. Tribula and J.W. Morris, Jr., "Creep in Shear of Experimental Solder Joints," Trans. ASME *Journal of Electronic Packing*, 112 (June 1990), 87-93.

138. J.W. Morris, Jr., D. Tribula, T.S.E. Summers and D. Grivas, "The Metallurgical Mechanisms of Solder Fatigue," presented at the National Electronic Packaging and Production Conference (NEPCON) West '90, Anaheim, CA, February 23, 1990, and to be published in the Proceedings.

139. J.W. Morris, Jr. and Z. Mei, "Toward New Solders with Improved Fatigue Resistance" in Solder Mechanics — A State of the Art Assessment, ed. by D.R. Frear, W.B. Jones and K.R. Kinsman, TMS (1991), 239-270.

140. -, "Copper-Tin Intermetallics," *Circuits Manufacturing* (September, 1980), 56-64.

141. L. Quan, D. Frear, D. Grivas and J.W. Morris, Jr., "Tensile Behavior of Pb-Sn Solder/Cu Joints," *Journal of Electronic Materials*, 16 (1987), 203-208.

142. D. Frear, D. Grivas and J.W. Morris, Jr., "The Effect of Cu_6Sn_5 Whisker Precipitates in Bulk 60Sn-40Pb Solder," *Journal of Electronic Materials*, 16(1987), 181-186.

143. L.D. Graham and R.W. Kraft, "Coarsening of Eutectic Microstructures at Elevated Temperatures," *Transactions of the Metallurgical Society of AIME*, 236 (January, 1966), 94-102.

144. J.A. Eady and W.C. Winegard, "Microstructural Stability of the Pb-Sn Eutectic," *Canadian Metallurgical Quarterly*, 10, #3 (1971), 213-214.

145. M.G. Blanchin, A. Guinier, C. Petipas and G. Sauvage, "Fine Structure Investigation in Lead Rich Phase of Pb-Sn Lamellar Eutectic," [in French], *Acta Metallurgica*, 20 (November, 1972), 1251-1258.

146. M. Frebel and B. Otte, "A Discontinuous Coarsening Reaction in a Unidirectionally Solidified Pb-Sn Eutectic," *Scripta Metallurgica*, 9 (1975), 1317-1320.

147. M. Frebel, G. Duddek, W. Graf, M.N. Faridani and B. Otte, "The Influence of Grain Boundaries on the Thermal Stability of Lamellar Microstructures," *Berichte Der Bunsen-Gesellschaft Für Physikalische Chemie*, 265 (1978), 259-265.

148. F.A. McClintock and G.R. Irwin, Plasticity Aspects of Fracture Mechanics, ASTM STP 381 (1965), 84-113 as referenced by D. Broek, Elementary Engineering Fracture Mechanics, Martinus Nifhoff Publishers (1982), 99.

149. W.A. Baker, "The Creep Properties of Soft Solders and Soft-Soldered Joints," *Journal Inst. Metals*, 65 (1939), 277-300.

150. L.N. Larikov, "A Resistance Study of the Natural Ageing of Lead-Tin Alloys," *The Journal of the Institute of Metals*, 25, #4 (December, 1957), 247, translated from Russian *Doklady Bolgar. Akad. Nauk*, 9, #3 (1956), 53-56.

151. B.T. Lampe, "Room Temperature Aging Properties of Some Solder Alloys," Welding Research Supplement, *Welding Journal*, 55 (Oct., 1976), 330s-340s.

152. S.S. Ahluwalia, "Effect of Natural Ageing on the Mechanical Properties of the Soldered Joint Used in the Electronics Industry," *Soldering and Surface Mount Technology*, #1 (February 1989), 43-46.

153. B. Fultz and J.W. Morris, Jr., "Effects of High Magnetic Fields on the Flow Stress of 18-8 Stainless Steels," *Acta Metallurgica*, 34, #3 (March,1986), 379-384.

154. B. Fultz, R. Kopa and J.W. Morris, Jr., "Software Feedback Control for Materials Testing Systems," *Journal of Metals*, 38, #4 (April, 1986), 58.

155. J. Oberschmidt, K.K. Kim and D. Gupta, "Grain-Boundary Diffusion in Some Pb-Sn Alloys," *J. Appl. Phys.*, 53, #8 (August, 1982), 5672-5677.

156. D.M. Jarboe, "Thermal Fatigue Evaluation of Solder Alloys," Technical Communications Bendix Kansas City: BDX-613-2341 (February, 1980).

157. H. Inoue, Y. Kurihara and H. Hachino, "Pb-Sn Solder for Die Bonding of Silicon Chips," IEEE Trans., Components, Hybrids and Manufacturing Technology, CHMT-9, #2 (June 1986), 190-194.

158. —, Soldering Manual, AWS (1978).

159. H.H. Manko, Solders and Soldering, McGraw-Hill Book Company, New York (1979).

160. Metals Handbook — Desk Edition, ed. by H.E. Boyer and T.L. Gall, ASM, Ohio (1985), 12.3.

161. Solder Alloy Data, ITRI Publication #656 (1986).

162. G. Becker, "Testing and Results Related to the Mechanical Strength of Solder Joints," IPC-TP-288, Institute for Interconnecting and Packaging Electronic Circuits (1979).

163. R.C. Gifkins, "Chemical Polishing of Pb and Its Alloys," *Metallurgia*, 63 (1961), 209-210.

164. R.M. Slepian and G.A. Blann, "Improved Preparation of Pb and Pb Alloys," *Metallography*, 12 (1979), 353-356.

165. T.S.E. Summers and J.W. Morris, Jr., "Isothermal Fatigue Behavior of Sn-Pb Solder Joints," Transactions of the ASME, *Journal of Electronic Packaging*, 112 (June, 1990), 94-99.

166. D. Grivas, D. Frear, L. Quan and J.W. Morris, Jr., "The Formation of Cu_3Sn Intermetallic on the Reaction of Cu with 95Pb-5Sn Solder," *Journal of Electronic Materials*, 15(1986), 355-359.

167. W.G. Bader, "Dissolution of Au, Ag, Pd, Pt, Cu and Ni in a Molten Tin-Lead Solder," Welding Research Supplement, *Welding Journal*, 48, #12 (1969), 551s-557s.

168. H.M. Berg and E.L. Hall, "Dissolution Rates and Reliability Effects of Au, Ag, Ni and Cu in Lead Base Solders," in Proc. 1978 Reliability Physics Symposium (1973), 10-20.

169. D.G. Westlake, C.B. Satterthwaite and J.H. Weaver, "Hydrogen in Metals," *Physics Today*, (November, 1978), 32-39.

170. R.P. Elliot, Constitution of Binary Alloys, First Supplement, McGraw-Hill Book Company, NY (1965).

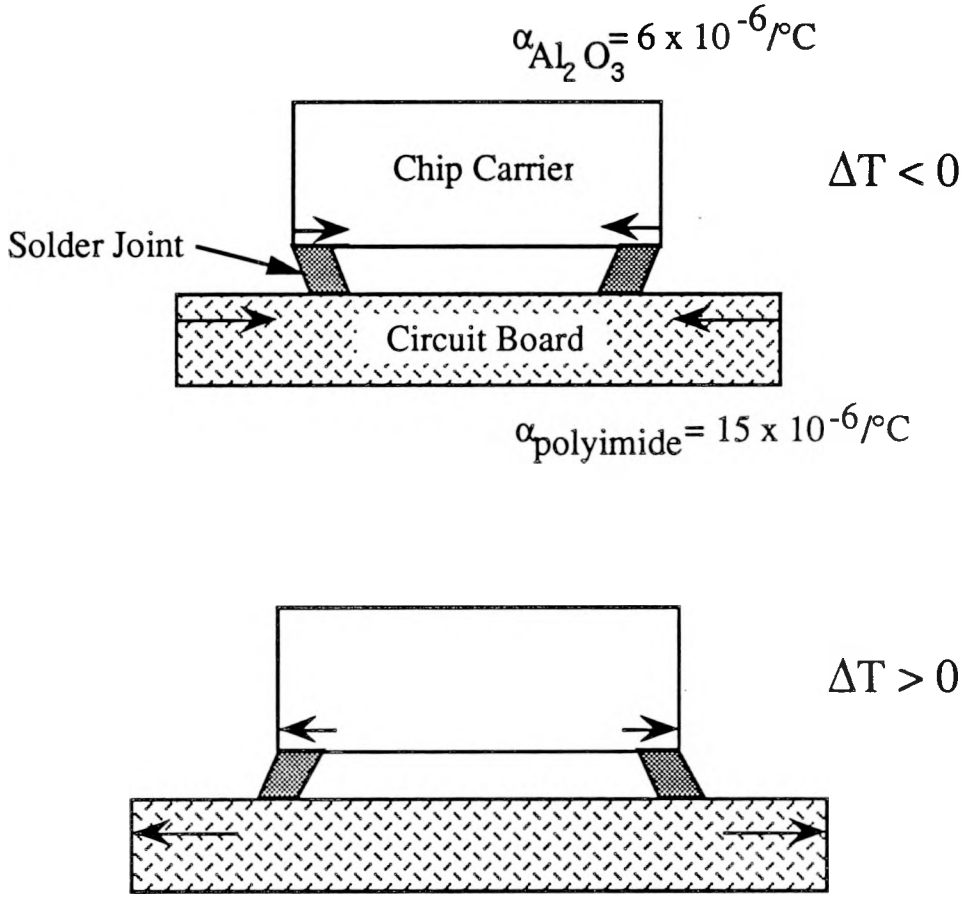

Figure 1.1. Schematic diagram illustrating the origin of thermal fatigue in surface-mounted components. For simplicity, a leadless chip carrier is drawn. The thermal expansion coefficients for one of the more severe cases of a ceramic chip carrier bonded to a polymer circuit board are given as examples.

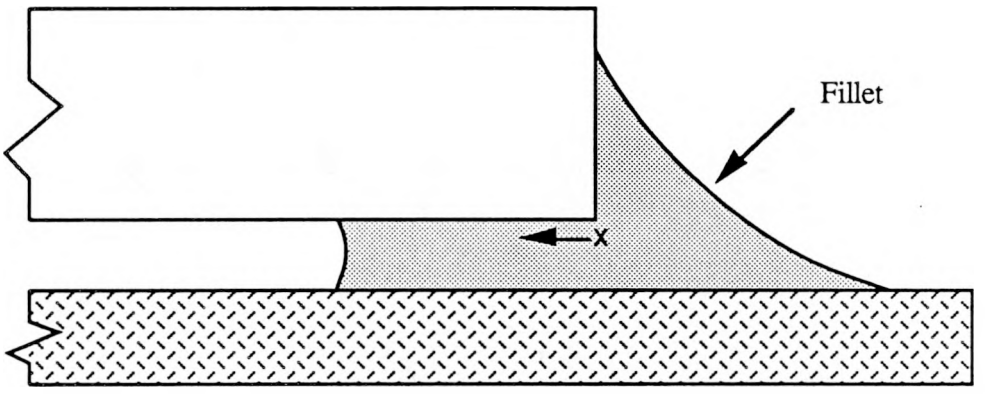

Figure 1.2. Schematic illustration of a leadless ceramic chip carrier cross section showing the typical crack initiation site and the fillet region through which final crack propagation generally occurs.

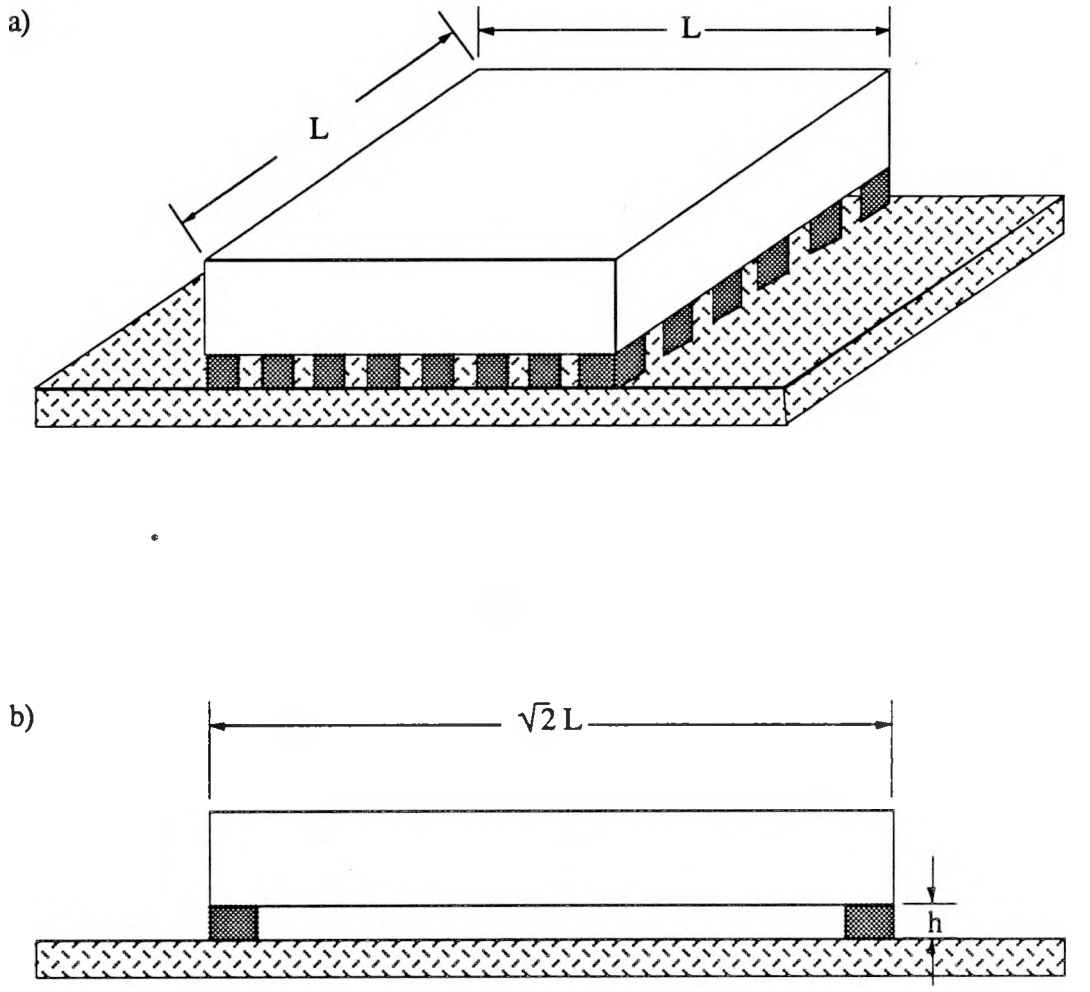

Figure 1.3. Schematic illustration of a leadless surface-mounted component. In (a), the entire chip carrier is shown while, in (b), a cross section through the package diagonal is shown. The dimensions used in equation 1.1 are labelled.

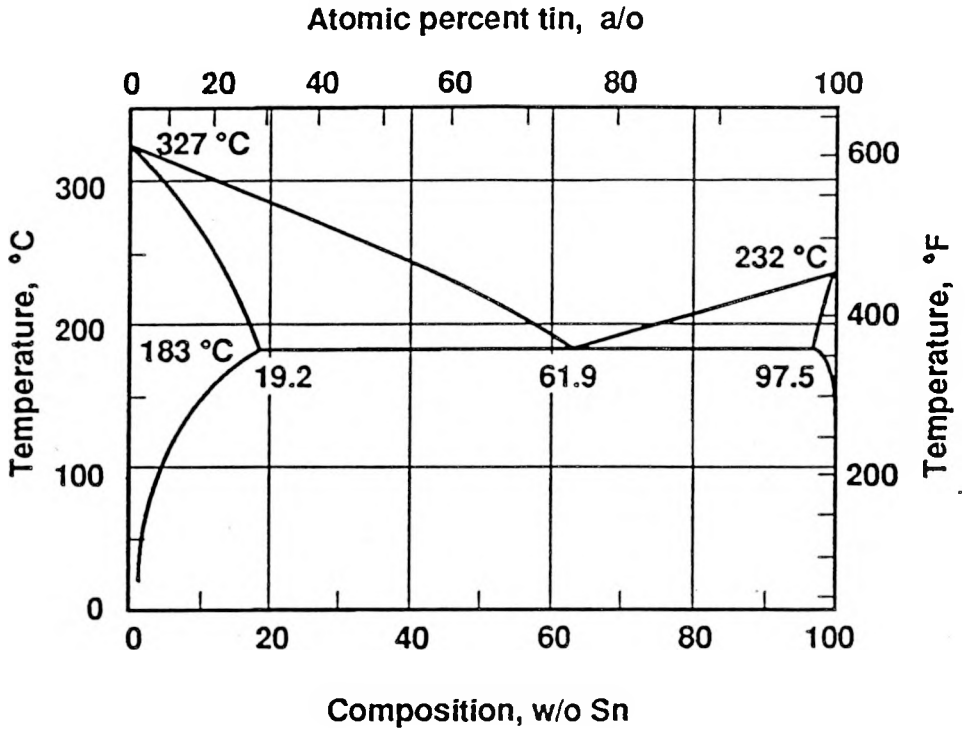

Figure 1.4. The Pb-Sn binary phase diagram. Sn and Pb make up a simple eutectic system with a eutectic composition of 61.9 wt.% Sn and a eutectic temperature of 183°C. [Adapted from the Pb-Sn phase diagram published in Binary Alloy Phase Diagrams, Vol. 2, ed. by T.B. Massalski, ASM, Ohio (1986)]

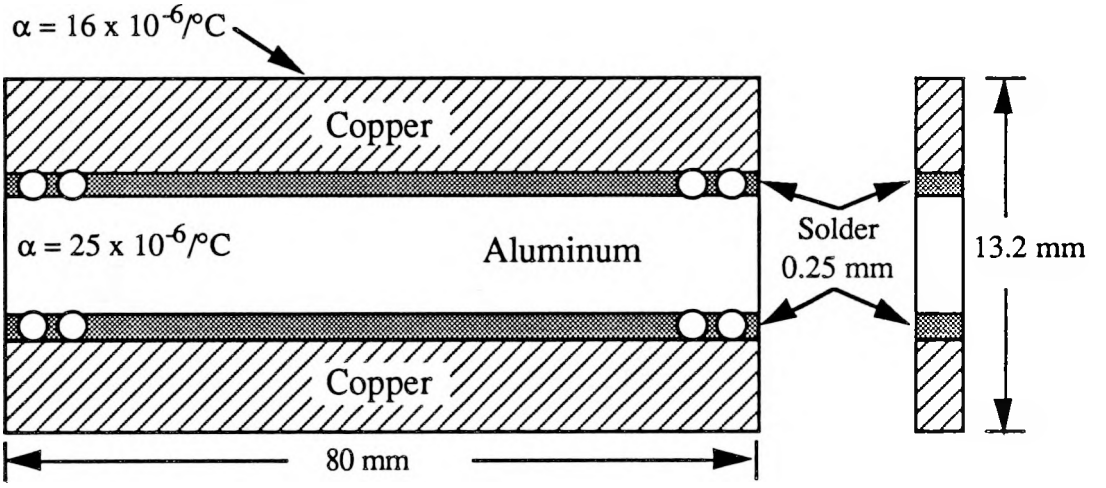

Figure 2.1. Thermal fatigue specimen. Due to the difference in the thermal expansion coefficients of Cu and Al, the two solder joints are sheared with zero strain in the center and a maximum strain at the ends of the specimen when cycled between two temperature baths.

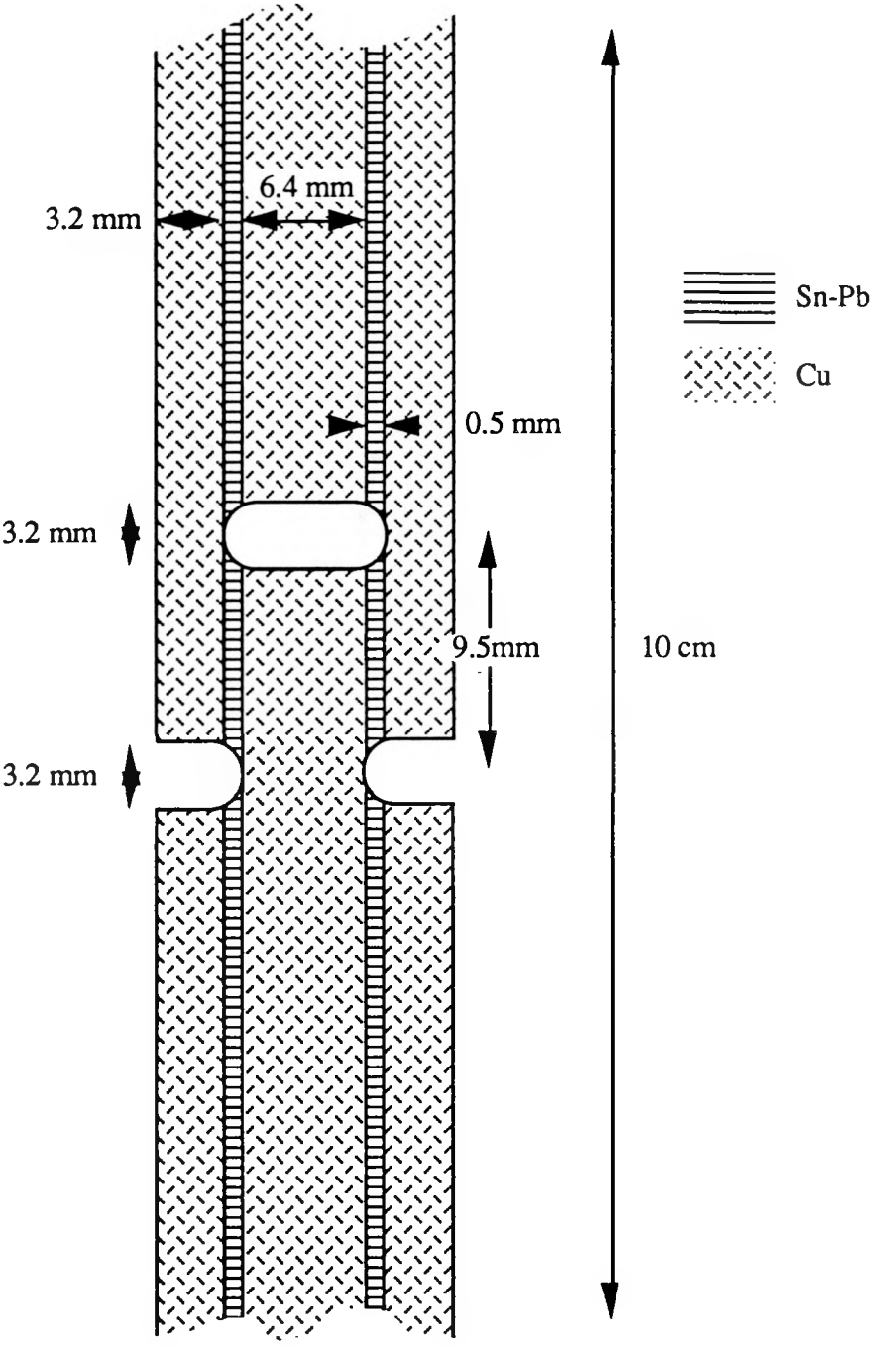

Figure 2.2. Double shear specimen. The specimen is about 1.6 mm thick and is machined so that the two central solder joints are sheared when the entire specimen is placed in tension.

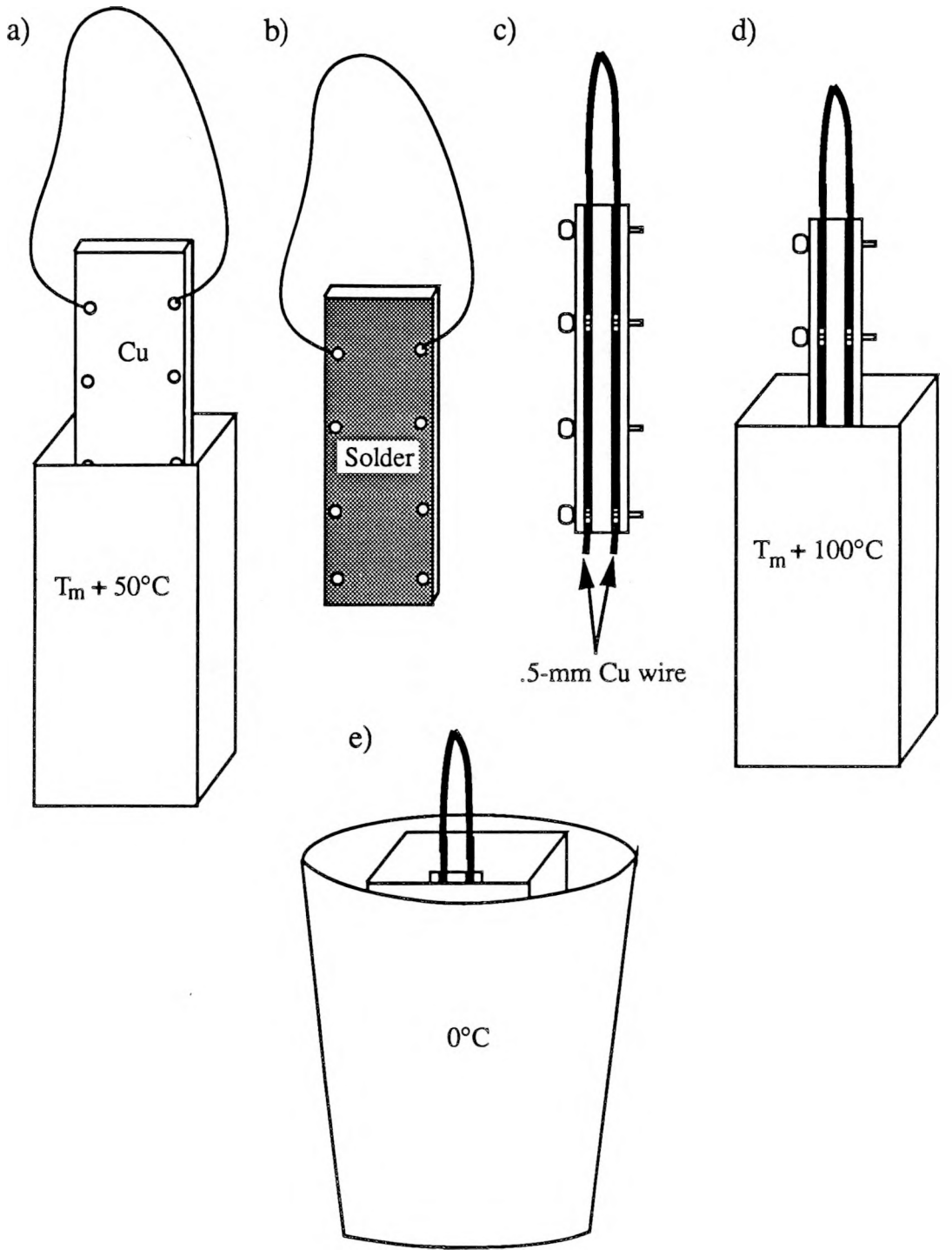

Figure 2.3. Schematic illustration of the modified casting procedure. a) Polished and etched Cu plates are dipped in flux and then in solder at 50°C above the melting point of the solder and, b), allowed to air cool. c) This pretinned block is assembled with .5-mm (20-mil) wire spacers and, d), dunked in solder at 100°C above its melting point. e) Finally, the block within the solder within the two crucibles is quenched in ice water.

a)

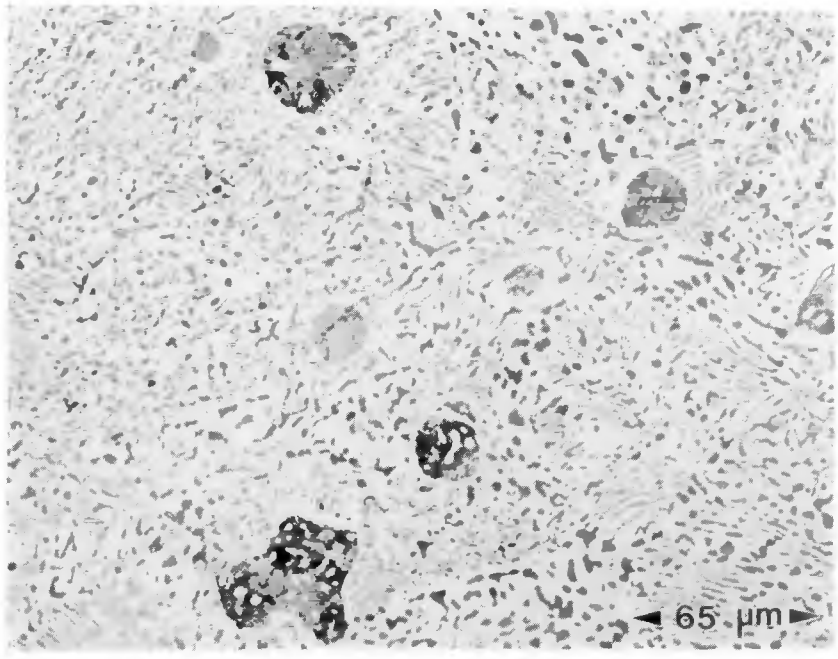

b)

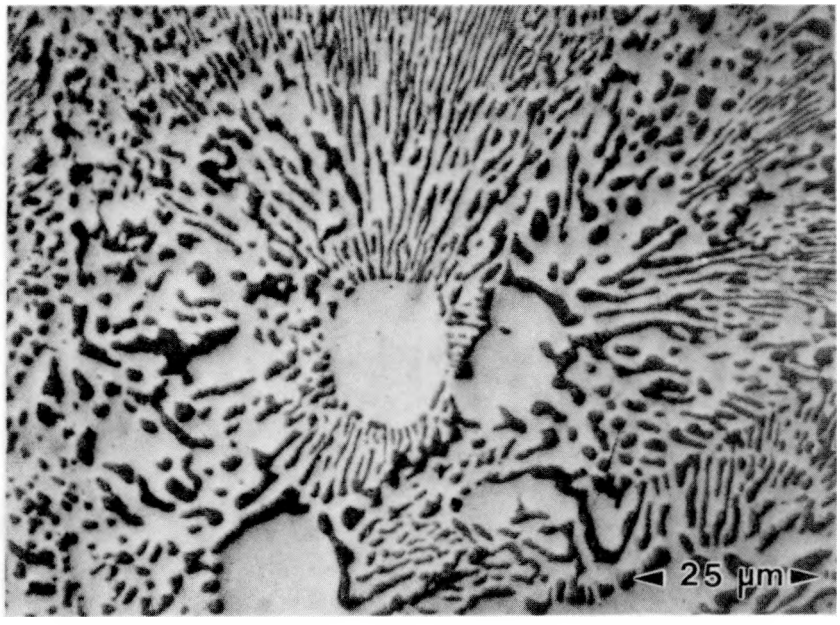

Figure 2.4. Eutectic regions surrounding proeutectic particles in a) Pb-rich (50Sn-50Pb) and b) Sn-rich (63Sn-37Pb) off-eutectic alloys. "Sn halos" can be seen surrounding the Pb-rich regions in a). In b), the Sn-rich proeutectic are much more effective at nucleating the lamellar eutectic material.

XBB 912-987A

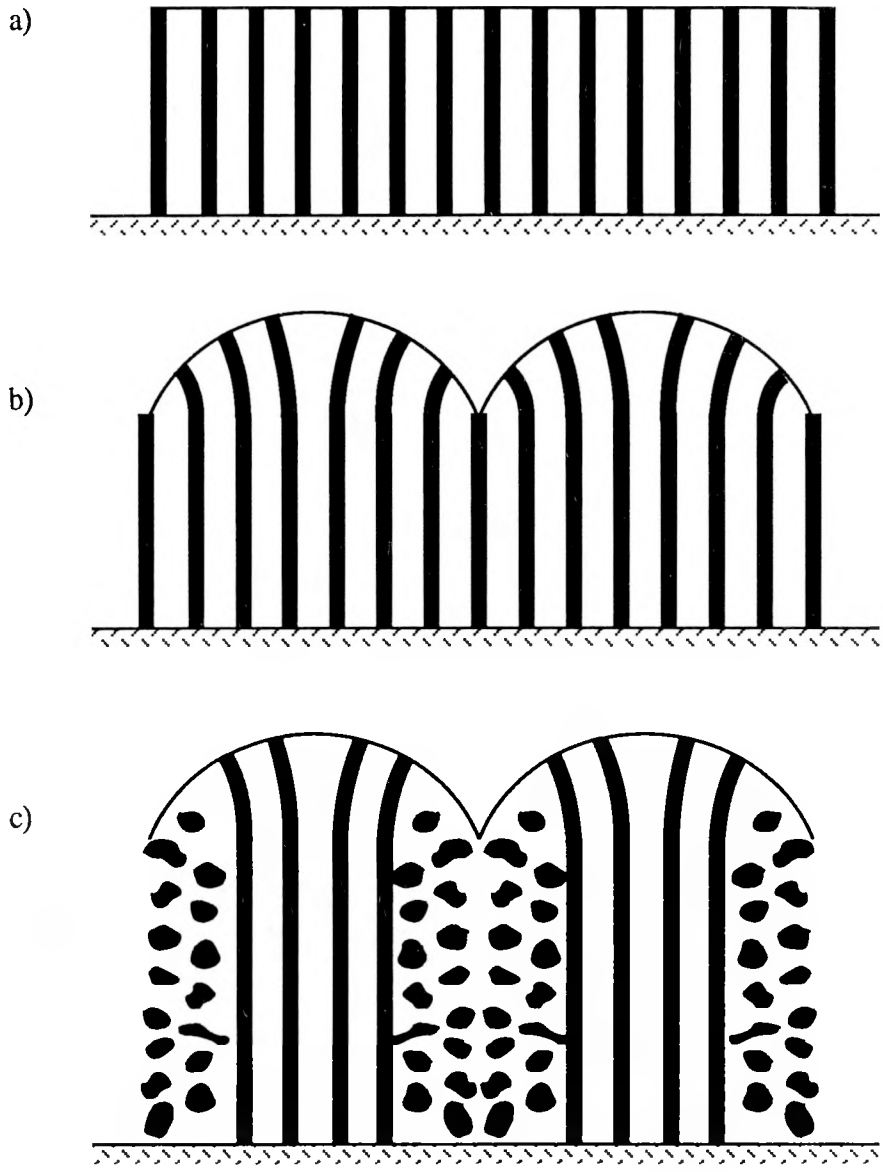

Figure 2.5. Diagram illustrating the development of a colony structure. In a), lamellae grow out of a substrate from which it nucleated. During solidification, impurities are rejected to the liquid (partition coefficient less than 1, the usual case) from both solidifying phases. Eventually, this impurity segregation can lead to a cellular breakdown of the solidifying interface as in b). Due to the curvature of the interface, the lamellae, which always grow perpendicular to the interface, must bend. c) Growing on higher energy planes, these curved lamellae in the cell or colony boundaries sometimes break down into a more globular structure with a lower overall surface area.

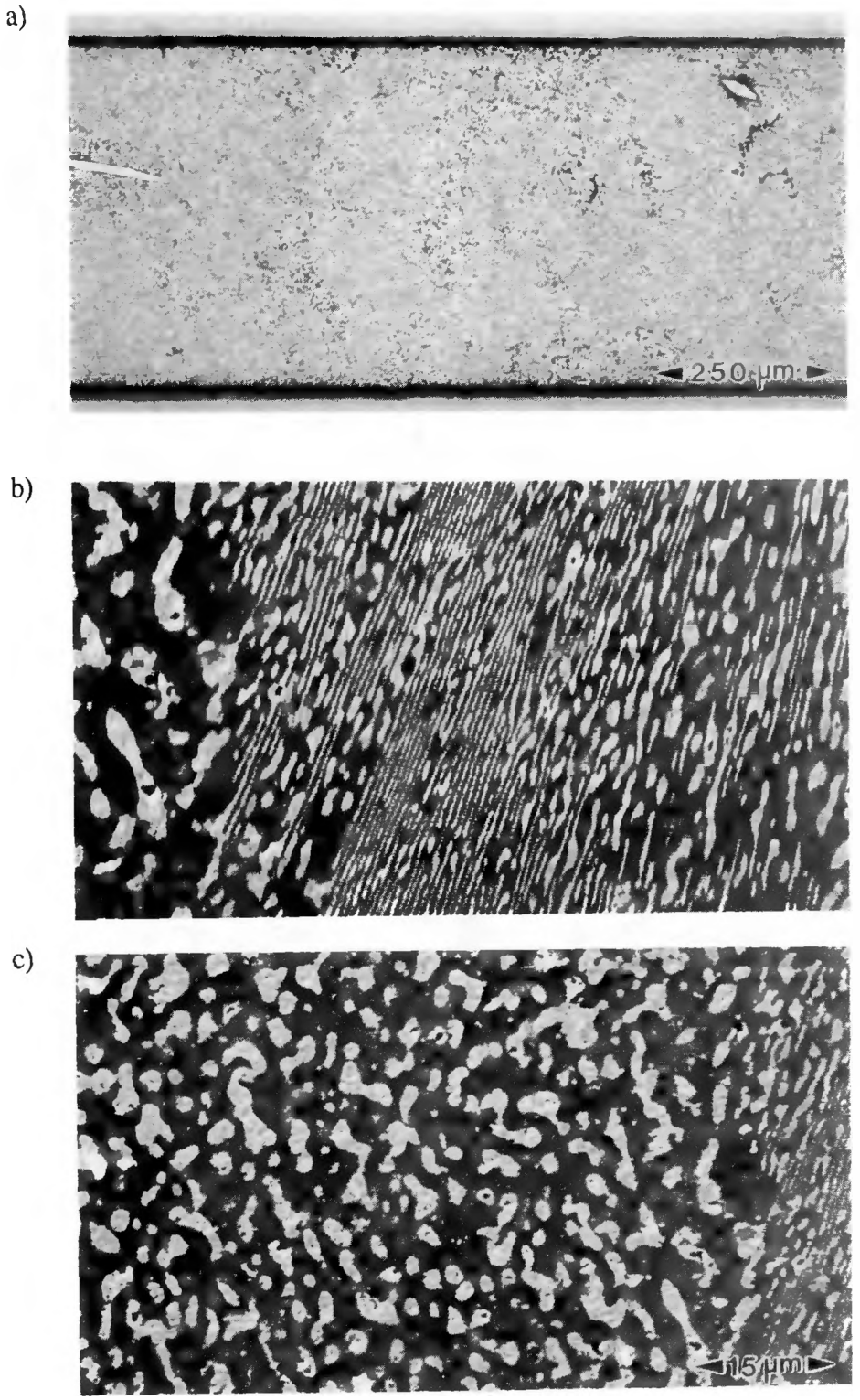

Figure 2.6. a) As-cast eutectic joint microstructure. The micrographs in b) and c) were taken on a scanning electron microscope and thus have contrast reversed to that in the optical micrograph of a). In b), a more lamellar region is shown. The parallel lamellae separated by globular regions are evidence of cellular solidification. In c), a more globular region is shown.

XBB 914-2863

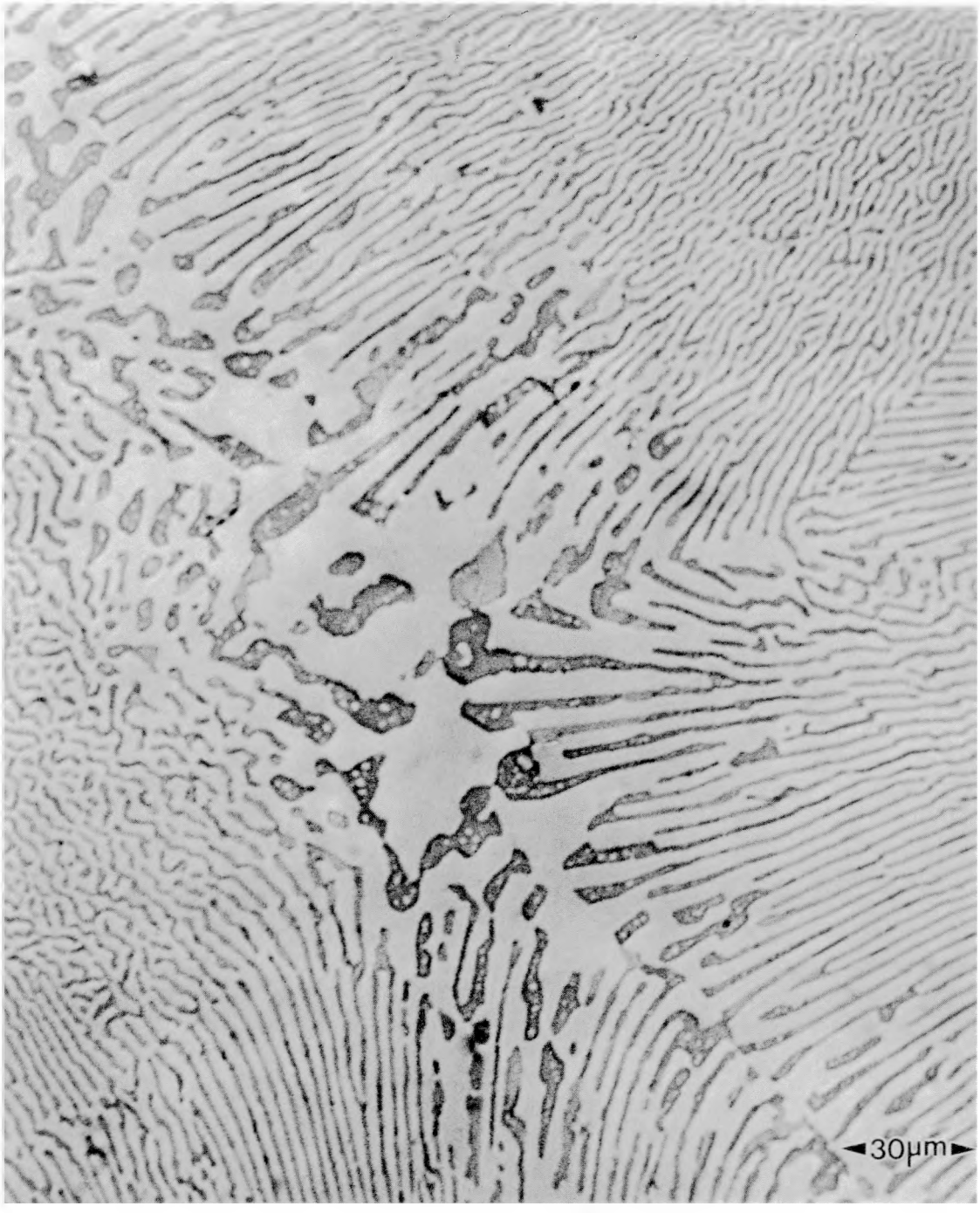

Figure 2.7. Eutectic grain/colony boundary region. This picture was taken from a bulk, air-cooled 63Sn-37Pb ingot and illustrates the microstructure within a boundary. In a eutectic microstructure, the boundaries are not planar as they are in a single-phase alloy. They consist of two phases and have a thickness associated with them due to the irregularities in the structure caused by solidification as two interfaces approach one another (eutectic grain boundary) or as the interface becomes curved during cellular solidification (colony boundary).

XBB 912-961A

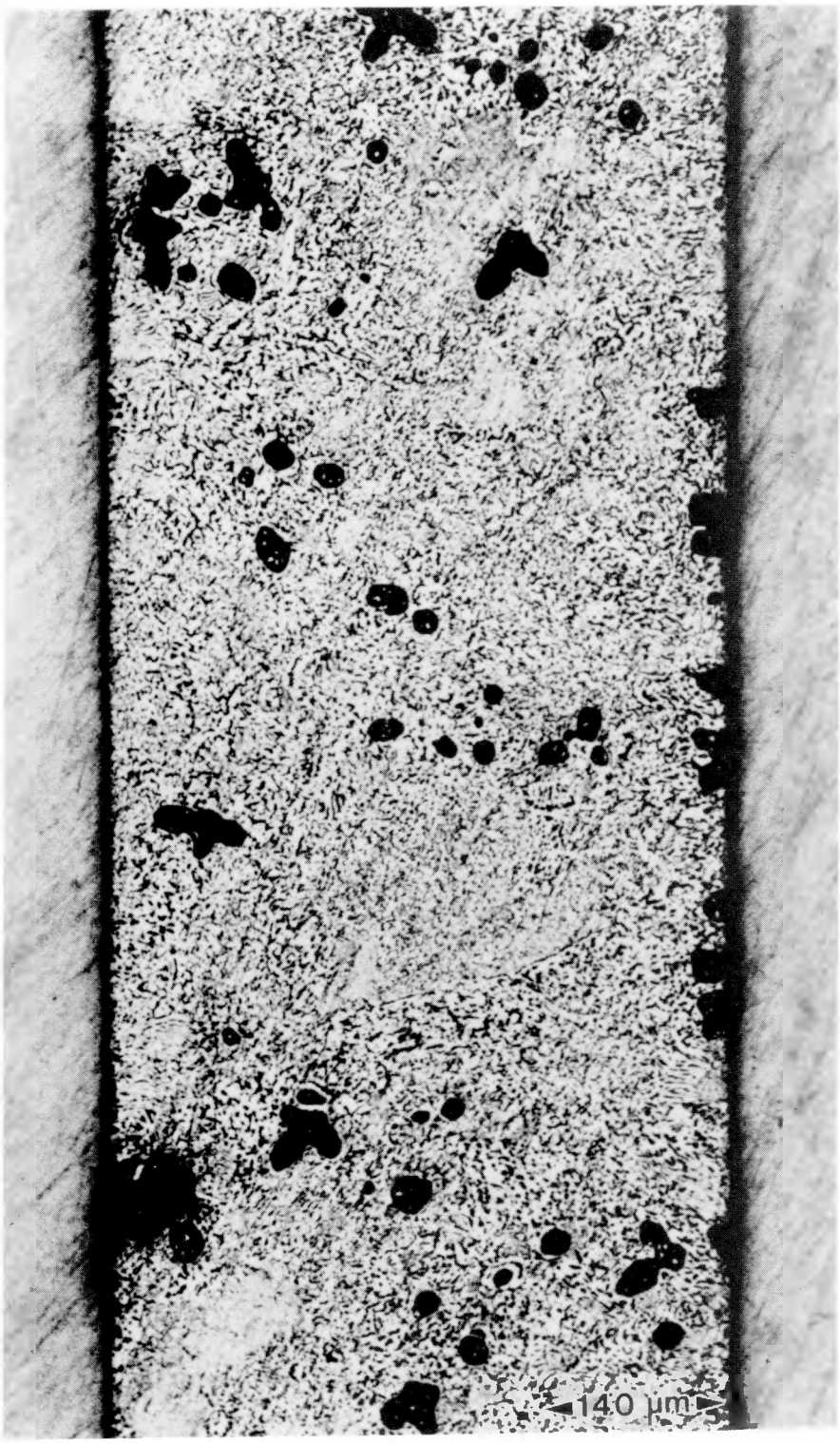

Figure 2.8. As-cast 60Sn-40Pb solder joint in a double shear specimen made of copper.

XBB 912-979A

a)

b)

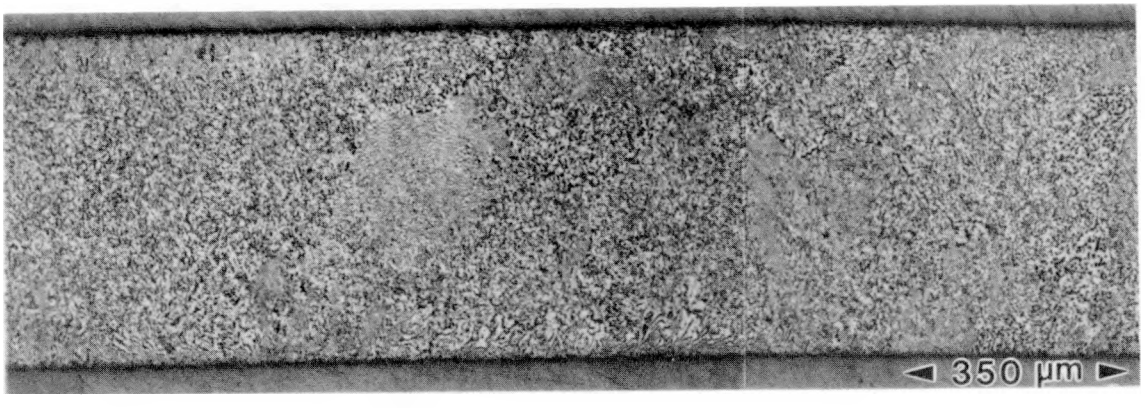

Figure 2.9. Eutectic double shear specimen polished and crept at 75°C with a 20-kg load into the secondary, steady-state creep regime. Nonuniform deformation results in the surface relief shown in a). Long straight shear bands exist in part of the joint. Repolishing of the specimen in b) shows that these long shear bands do not correspond to a coarsened band but must be present due to inhomogeneities in the as-cast microstructure.

XBB 911-434A

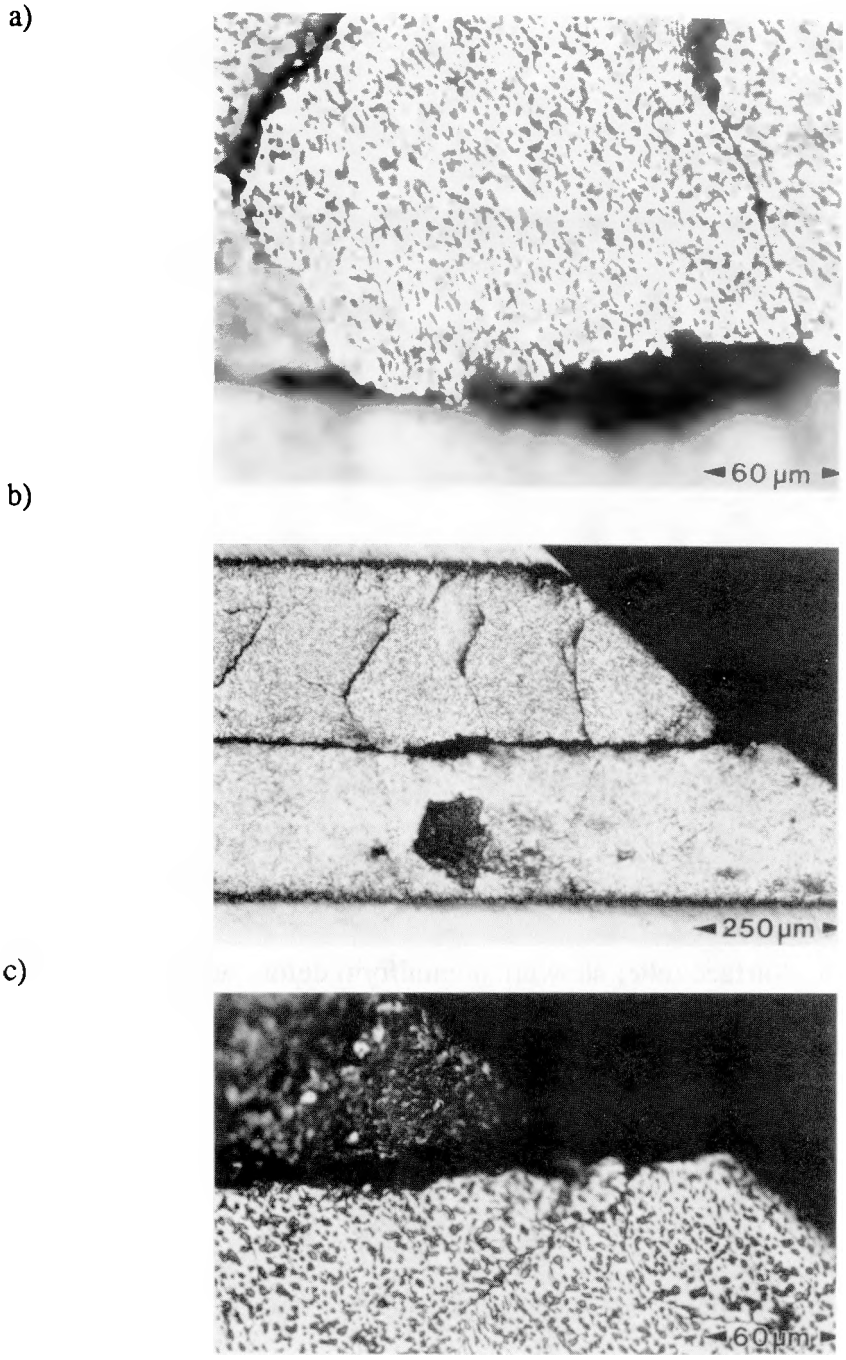

Figure 2.10. Eutectic double shear specimen polished and crept at 75°C with a 20-kg load into the secondary, steady-state creep regime. Nonuniform deformation results in the surface relief shown. In a), the colonies appear to move as blocks. The fact that the entire colony is in focus and that there are large steps on the surface at the boundaries indicates that most of the deformation occurs in the boundaries. In b), a step at the surface of the solder joint indicates how much deformation can concentrate within the shear bands when they are relatively long and straight. In c), the step in b) is shown at higher magnification.

XBB 913-1895A

Figure 2.11. Surface relief showing nonuniform deformation following creep of a 63Sn-37Pb solder joint. In some regions of the joint (A), long straight shear bands form allowing a great amount of deformation to concentrate there. In other regions (B), no colony boundaries line up to form fairly straight paths parallel to the direction of the applied shear strain.

XBB 913-1893A

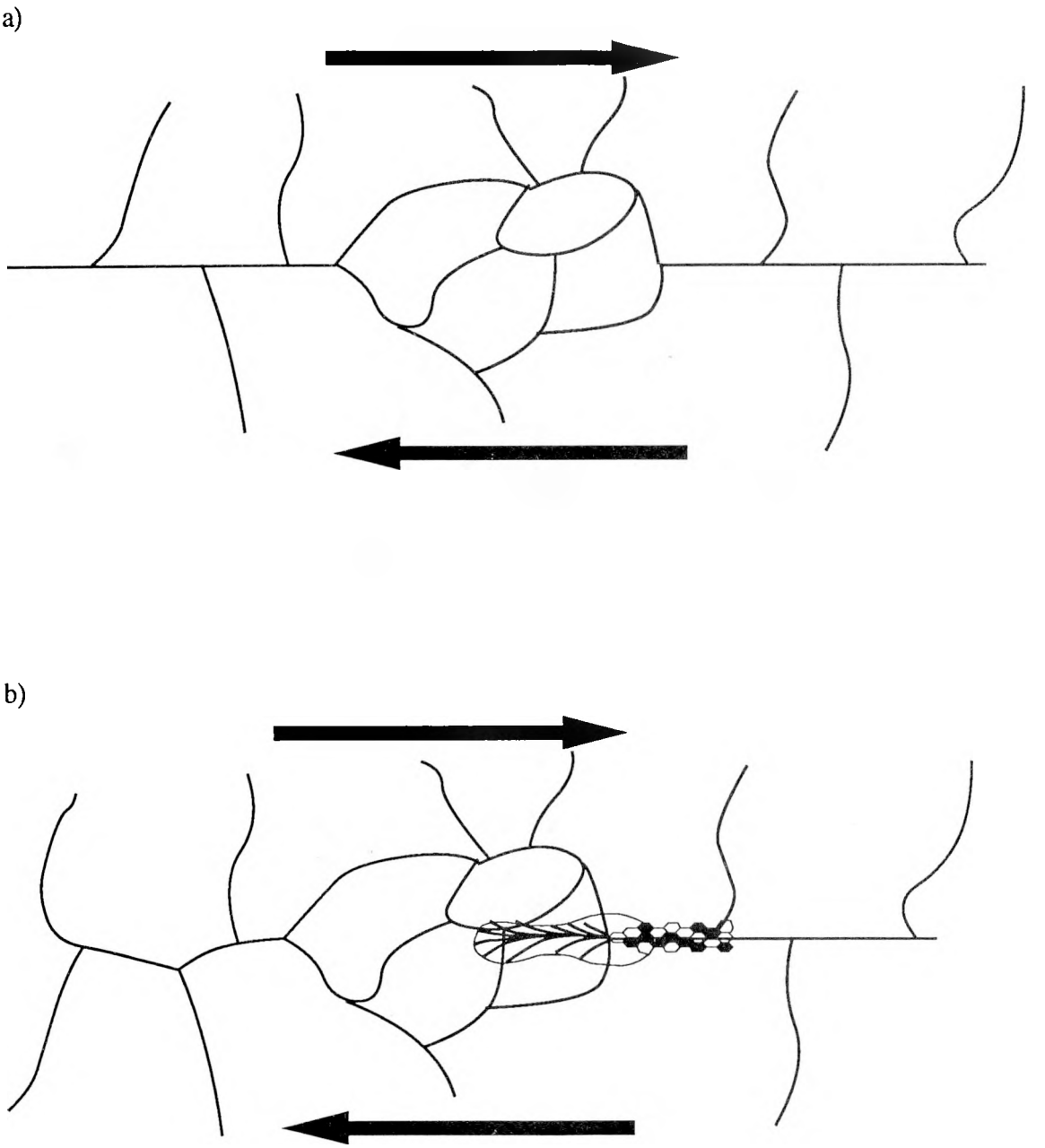

Figure 2.12. Methods by which an "obstacle" region can be cut by a shear band or coarsened band. a) If two shear bands line up parallel to the applied shear strain but separated by a less-deformable "obstacle" region, then deformation will concentrate within the "obstacle" region simply due to the geometry of the loading locally (i.e. geometric strain localization). b) If only one shear band is present, then a coarsened band can cross the obstacle by mode II crack-like propagation.

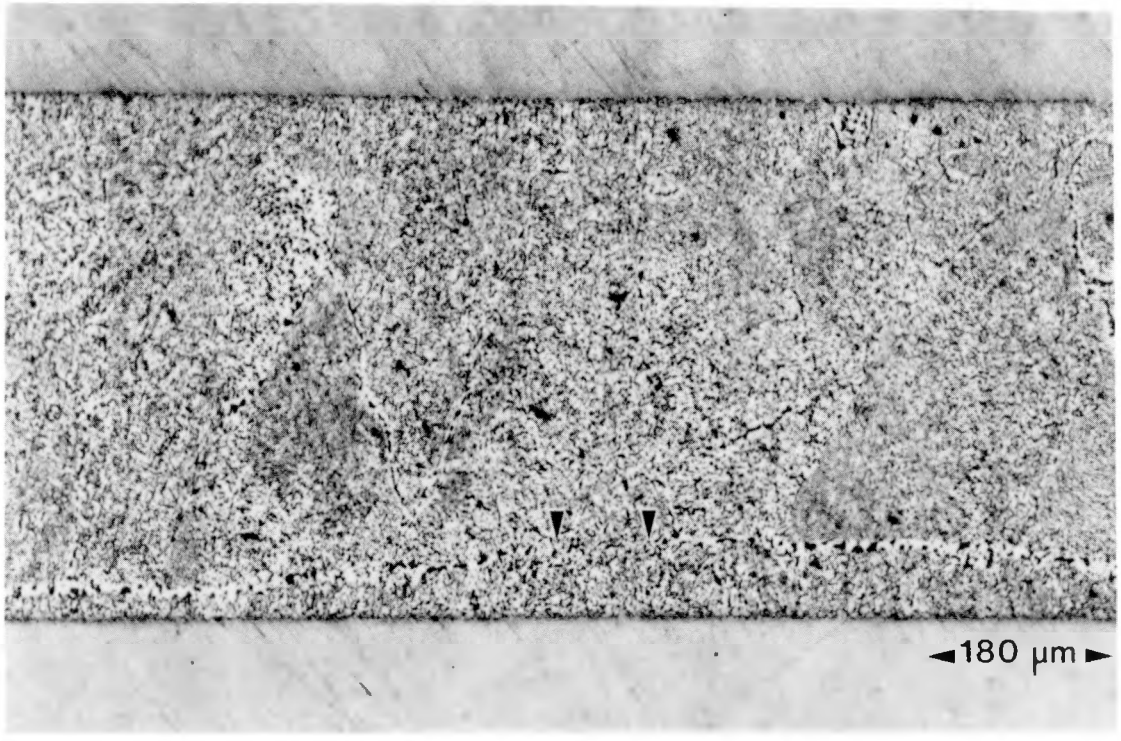

Figure 2.13. Coarsened band in a 63Sn-37Pb solder joint isothermally fatigued with 6% strain amplitude at 75°C. The coarsened band propagated along colony boundaries which lined up approximately parallel to the applied shear strain, but propagated around the "obstacle" region denoted by arrows where no colony boundaries lined up with the shear band. The deformation pattern following fatigue of this joint probably looked similar to that in Figure 2.11. If fatigue had been continued, this "obstacle" would eventually have been cut by one of the mechanisms shown in Figure 2.12.

XBB 912-972A

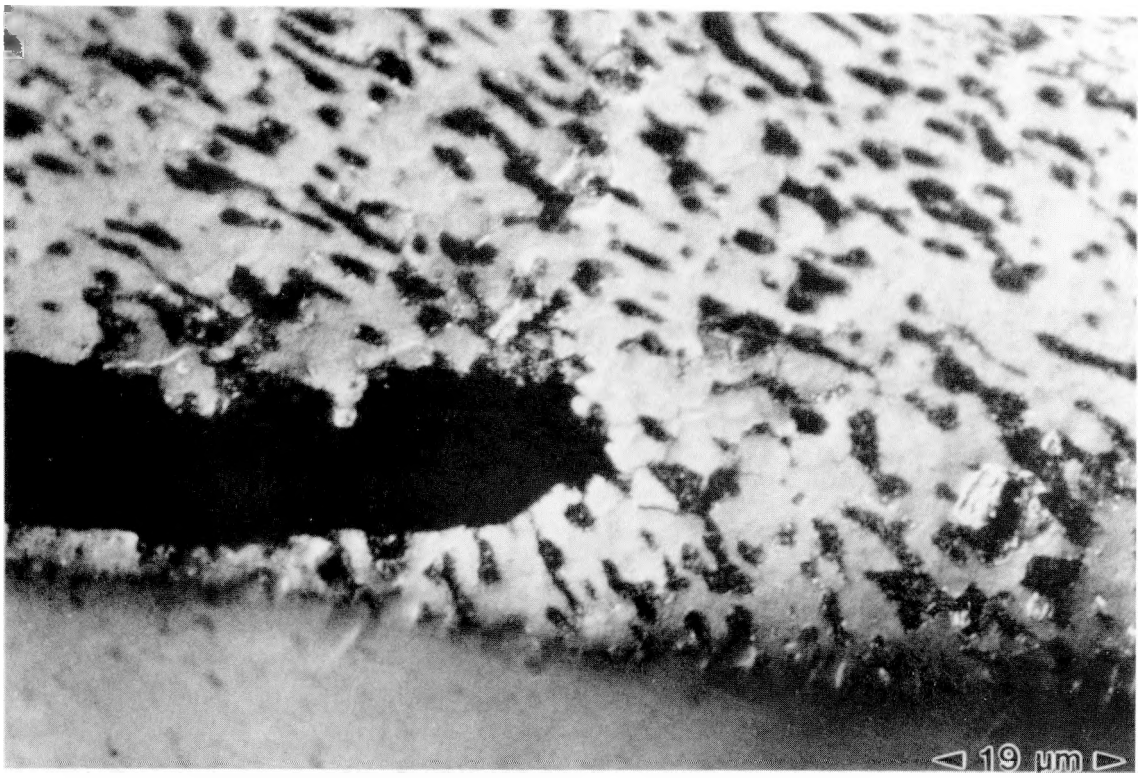

Figure 2.14. Crack in sheared 63Sn-37Pb solder joint. In the as-polished condition, Sn-Sn grain boundaries are seen ahead of the blunt crack. Because grain boundaries are not generally revealed during polishing in the as-cast condition, these visible grains are likely the product of recrystallization ahead of the crack. If so, the recrystallization zone ahead of the crack is on the order of the crack tip opening displacement.

XBB 912-966A

a)

b)

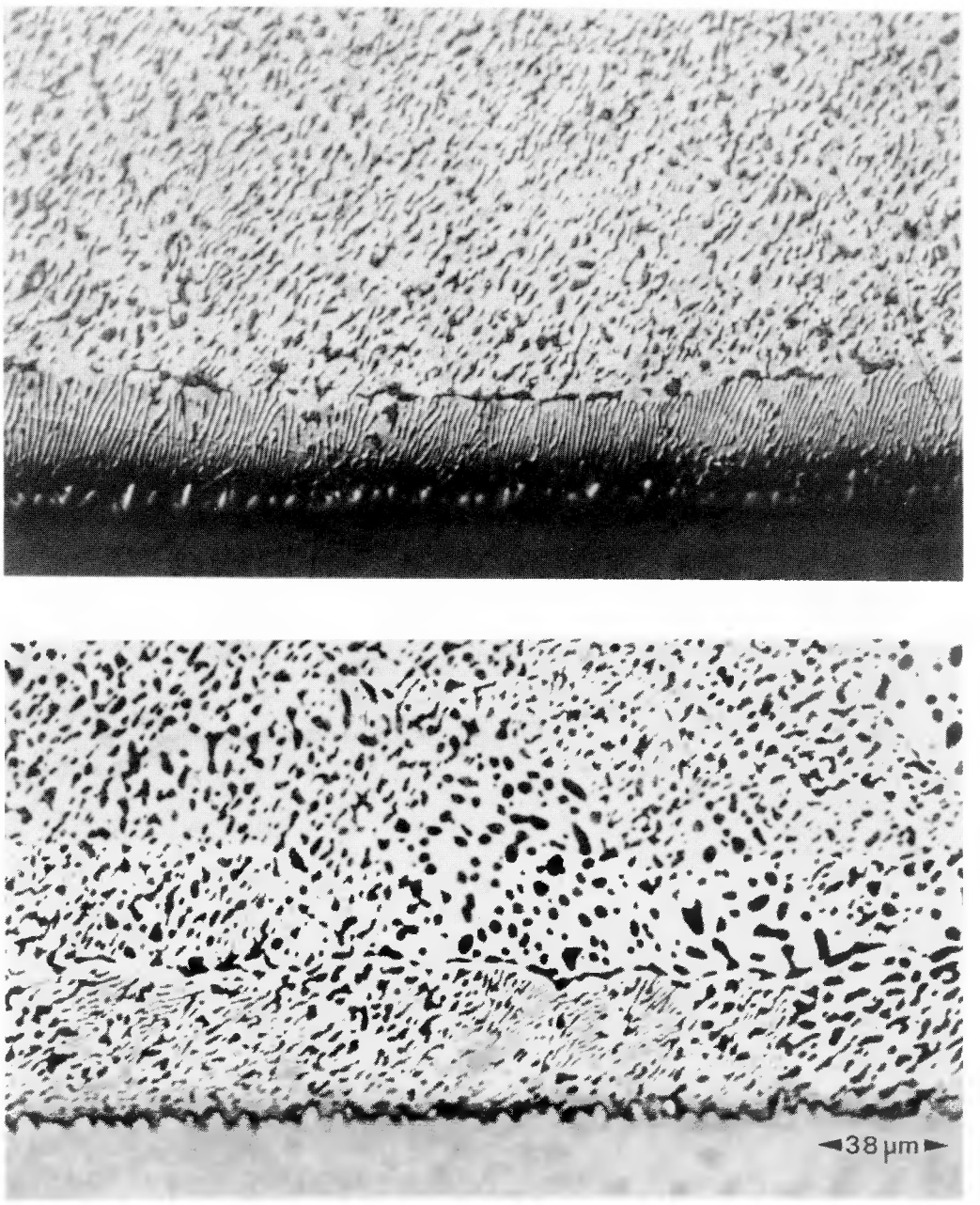

Figure 2.15. Two examples of Sn-Pb eutectic colonies nucleated at the Cu(intermetallic)/solder interface. This heterogeneous nucleation results in a colony boundary which runs along the joint. Sometimes the colonies are very distinct as in a), but at other times, they are somewhat degenerate and less clear as in b). In both cases, however, the boundaries are relatively soft and approximately parallel to any applied shear strain.

XBB 912-981A

Figure 2.16. Coarsened band which formed along colony boundaries in a eutectic Sn-Pb solder joint isothermally fatigued with a 10% strain range at 75°C.

XBB 913-1892A

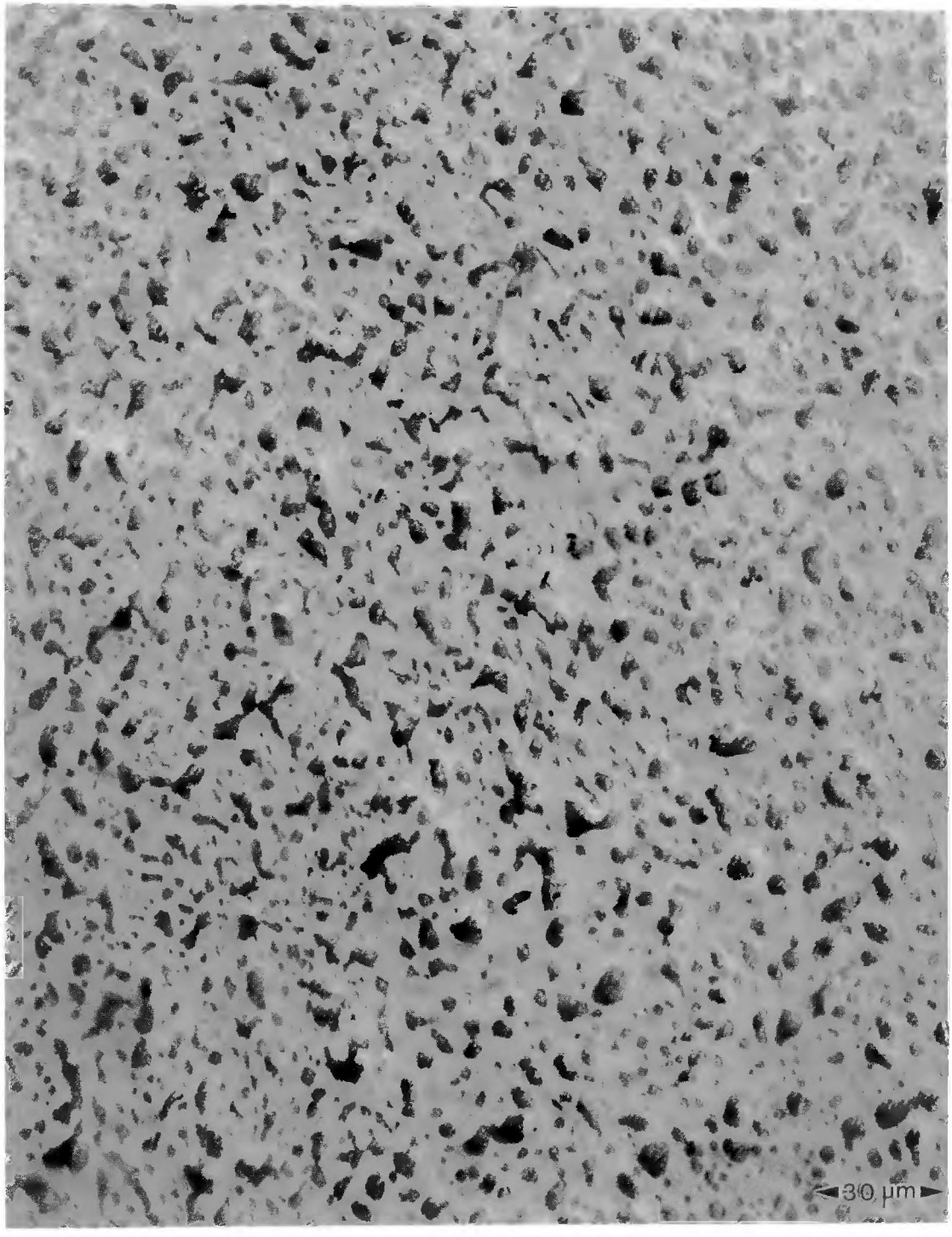

Figure 3.1. Water-quenched bulk 63Sn-37Pb ingot. Quenching results in a fairly uniform dispersion of Pb grains within a Sn matrix.

XBB 912-985A

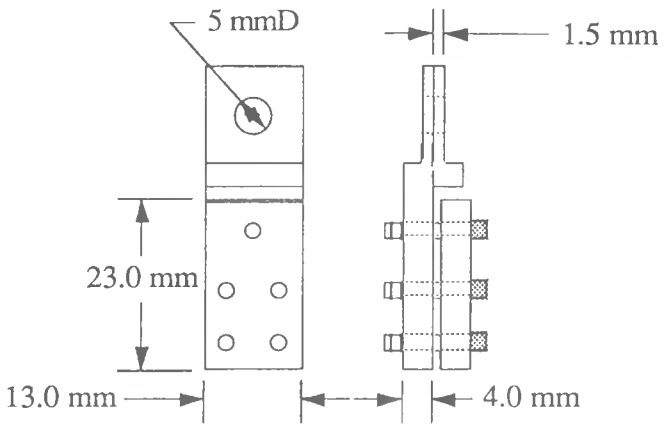

Figure 3.2. One set of grips used to measure solder joint shear strengths. Grooves cut at a 45° angle 0.1 mm deep were cut into the inside of each of the gripping plates. The screws used had 4/40 thread.

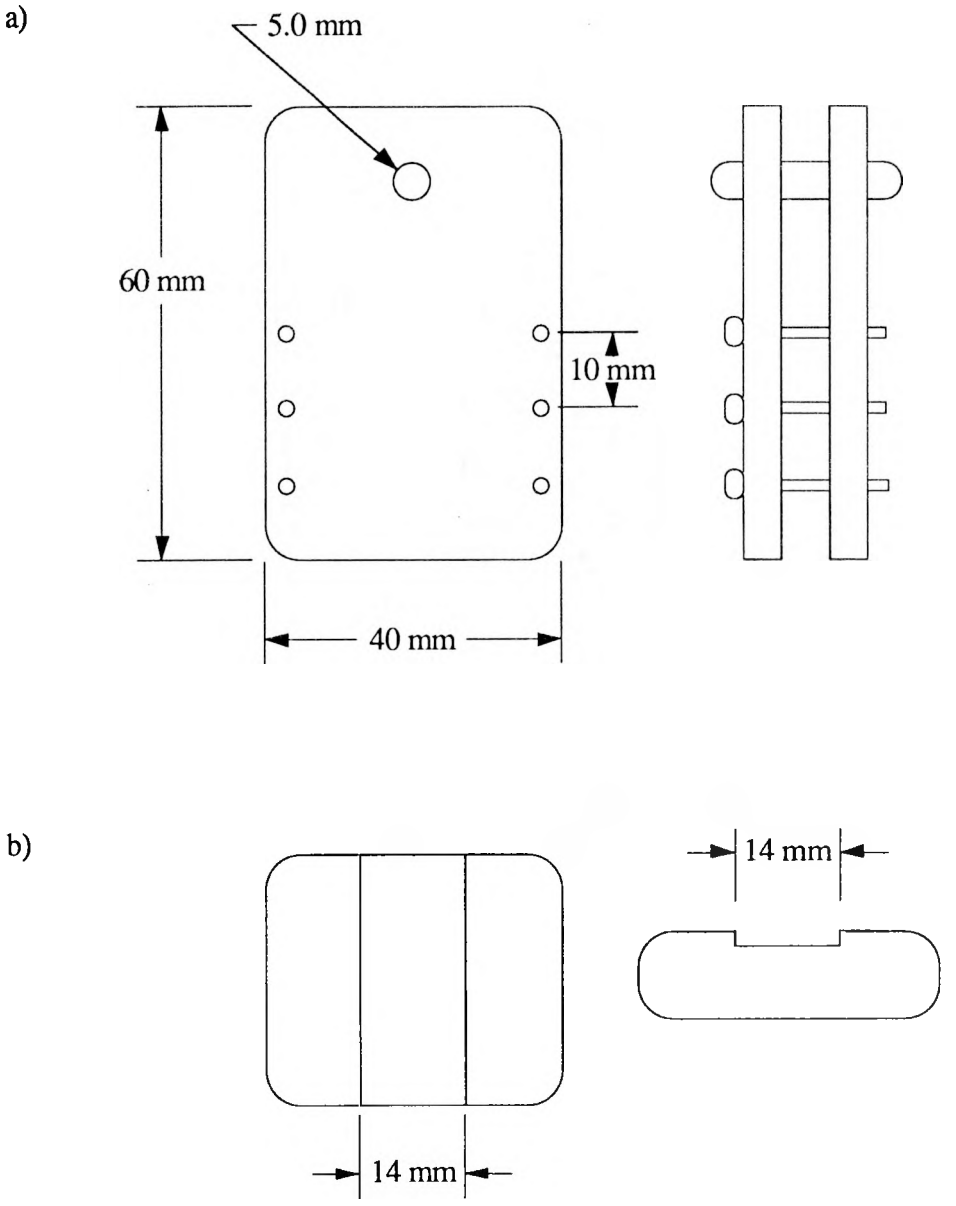

Figure 3.3. a) Specimen grips used for solder joint shear strength measurements. This design allowed room for wider specimens and less bending of the specimen during testing than the grips of Figure 3.2. b) This plate, machined as shown, was used for centering the double shear specimen within the grips.

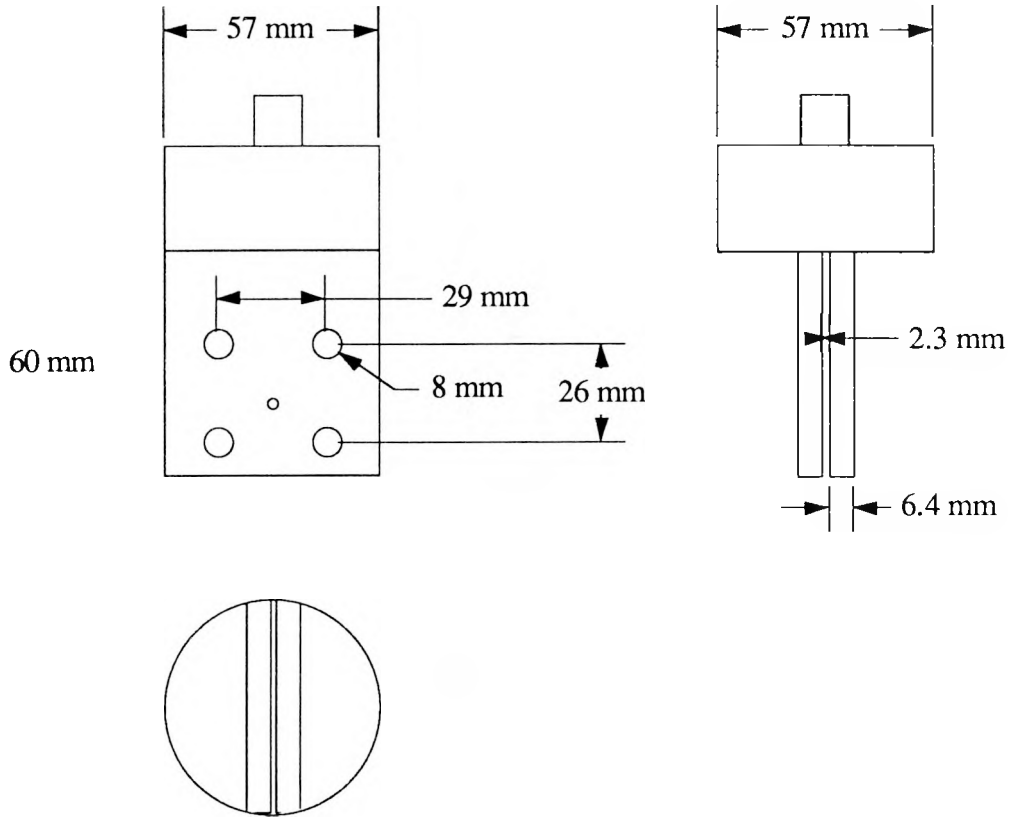

Figure 3.4. Grips designed and made to allow centered loading of a specimen during stroke-controlled fatigue. Stainless #100 mesh screens were used between the specimen and the gripping plates to increase the friction there. The upper grip was attached to the pull rod with a threaded junction, and the bottom grip was attached to the compression frame with a clamp to minimize through-zero load displacements.

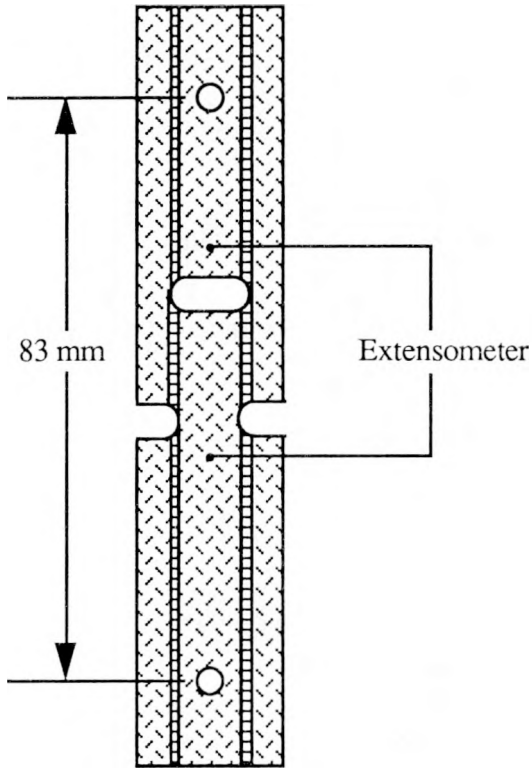

Figure 3.5. Double shear specimen modification for specimen alignment in isothermal fatigue grips. Aligning holes were centered in the 6.4-mm (1/4-inch) Cu plate prior to assembling and dunking the block. Solder within the holes was later removed by carefully filing without increasing the size of the hole. An extensometer was placed between pins positioned as shown on either side of the deforming solder joints.

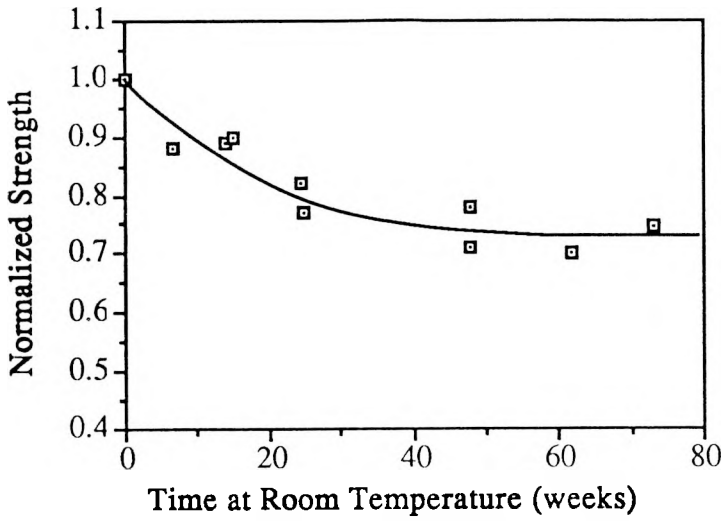

Figure 3.6. Normalized shear strengths (shear strength of aged specimens divided by initial strength of specimens from the same batch) of 63Sn-37Pb solder joints aged at room temperature. The average initial shear strength tested 9 days after casting was 31 ± 1 MPa.

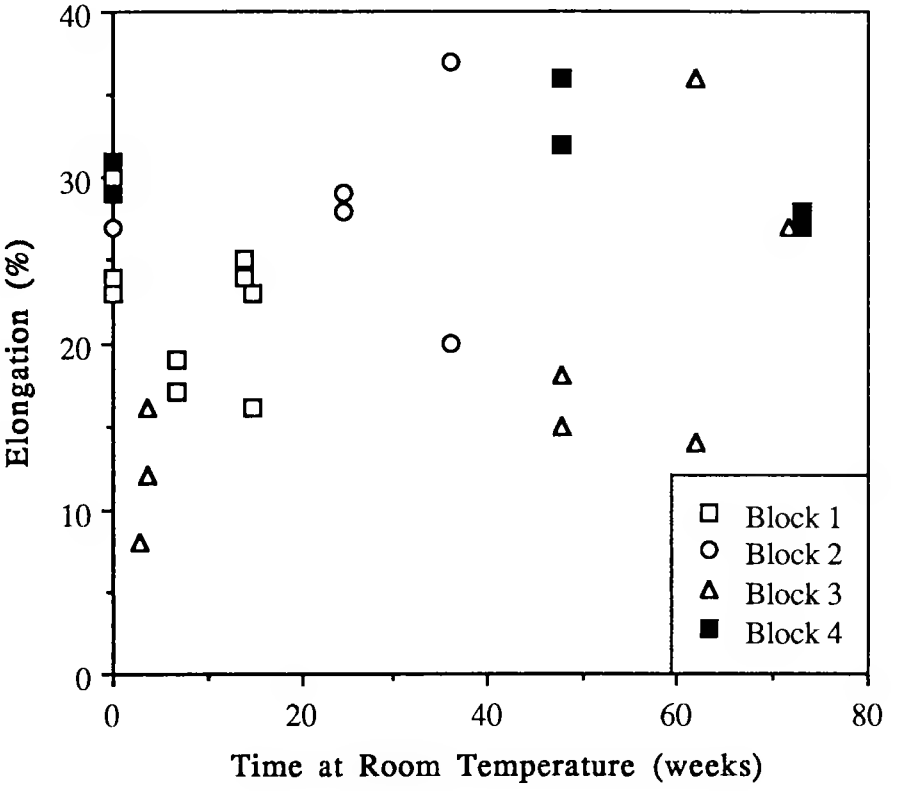

Figure 3.7. Elongation to maximum load of 63Sn-37Pb solder joints as a function of room temperature aging time.

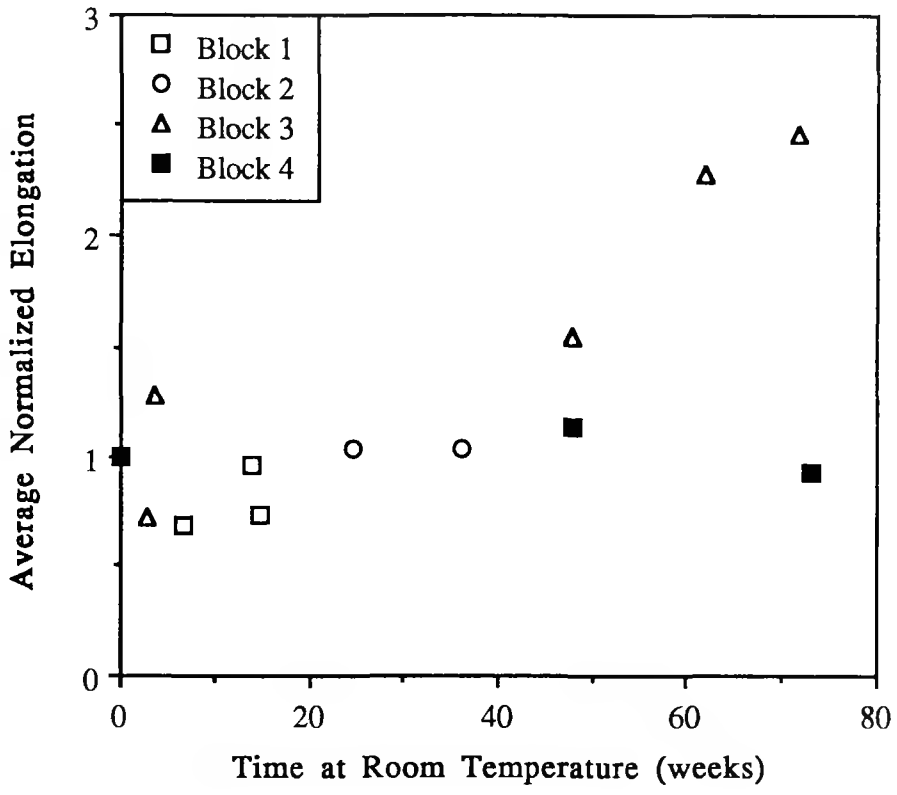

Figure 3.8. Average elongations of aged 63Sn-37Pb solder joints divided by the average initial elongation for each block, or batch, of specimens.

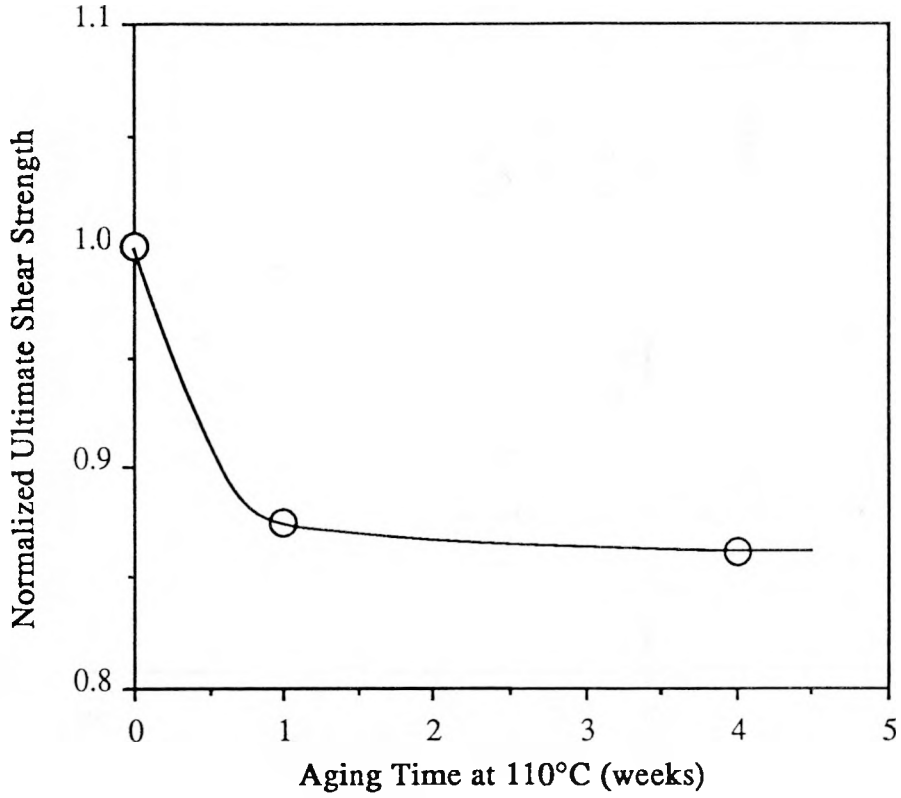

Figure 3.9. Normalized shear strengths of 63Sn-37Pb solder joints aged at 110°C. Each point represents the average of two specimens except the intial strength which was 31 MPa for one specimen.

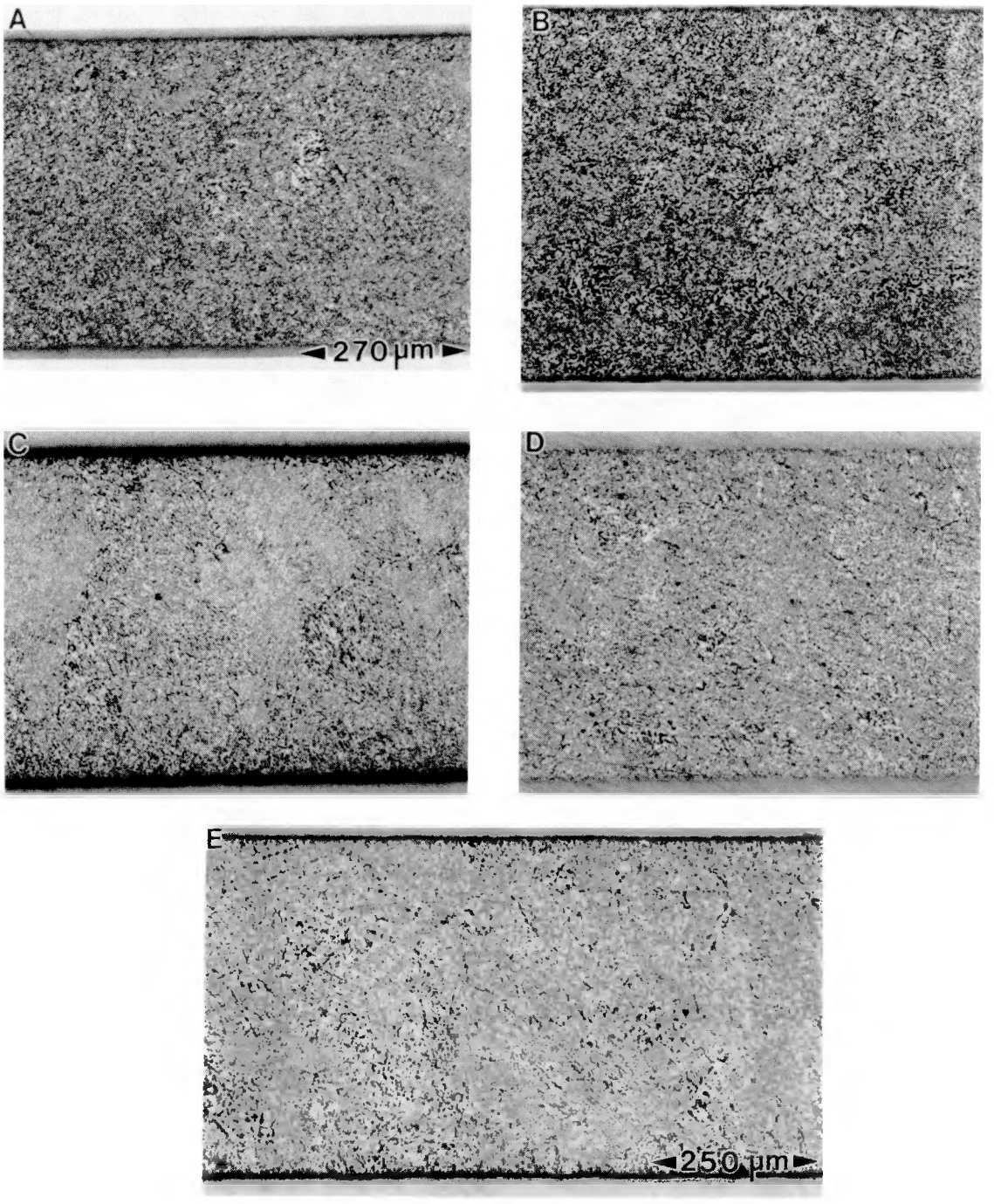

Figure 3.10. Double shear specimen 63Sn-37Pb solder joint microstructures typical of a) the initial condition and after aging at room temperature for b) 3 months, c) 6 months, d) 9 months and e) 15 months.

XBB 914-2864

a)

b)

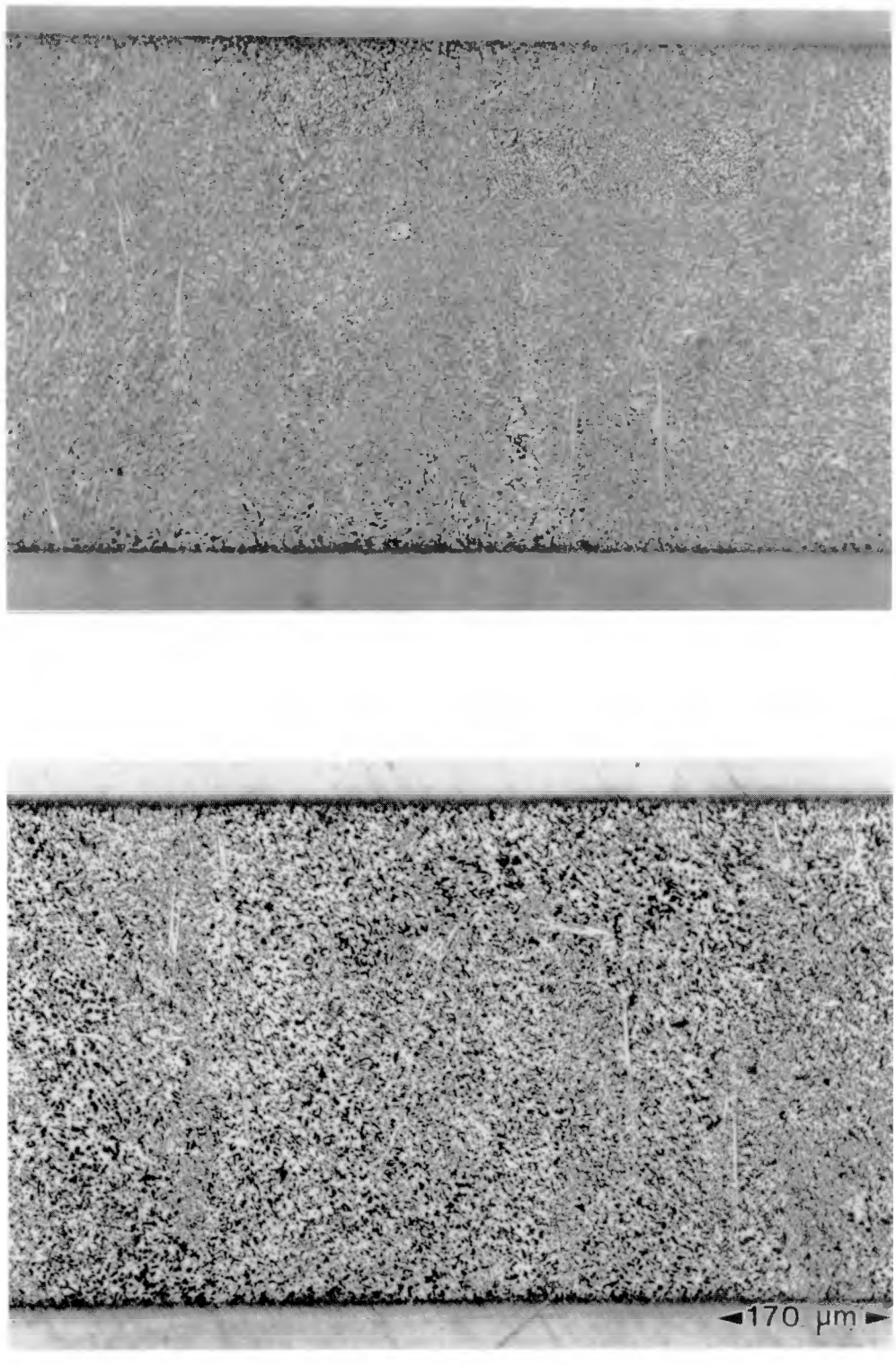

Figure 3.11. Typical Block 4 63Sn-37Pb solder joint microstructures for the a) initial condition and b) after aging 15 months at room temperature.
XBB 912-1891A

a)

b)

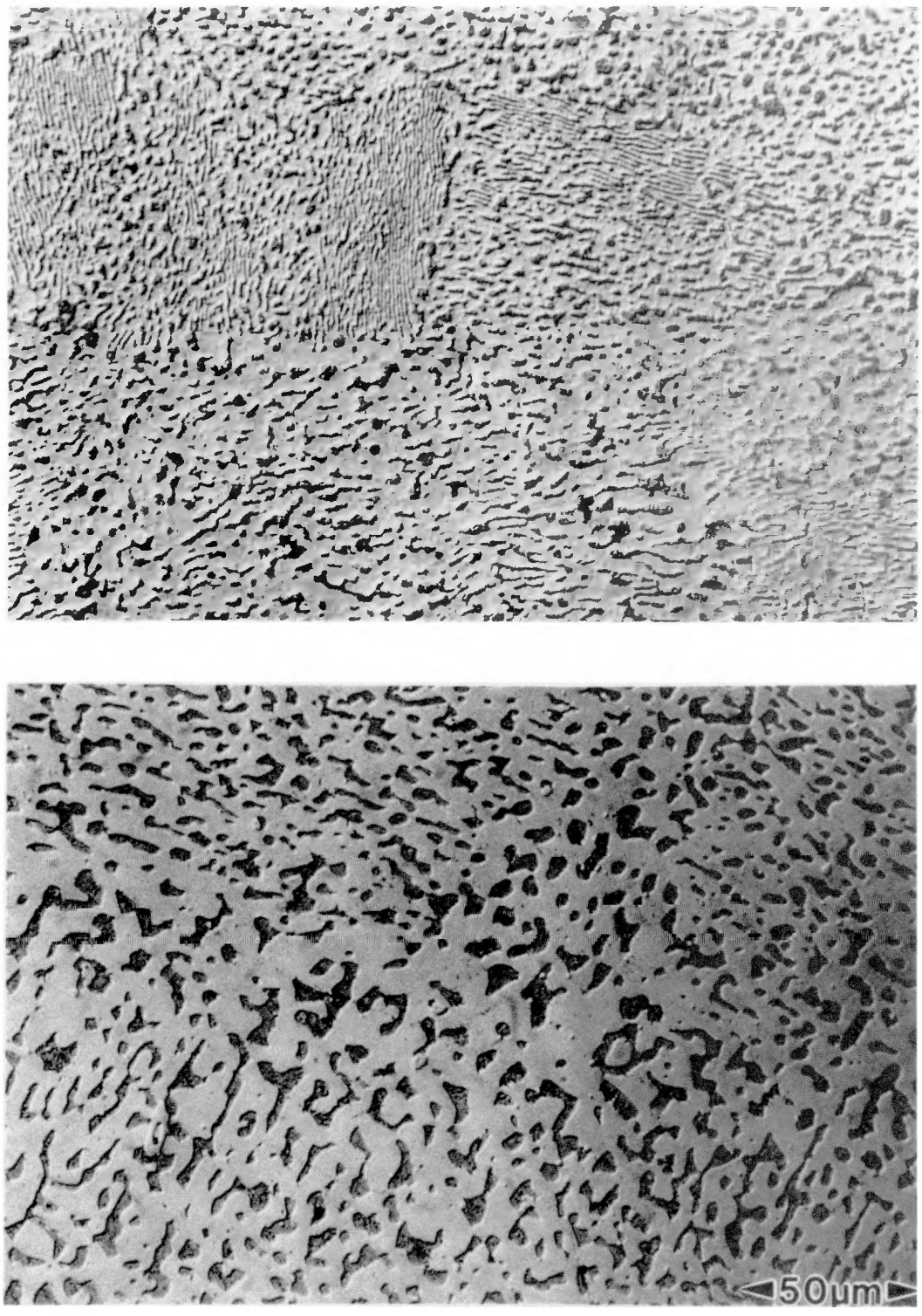

Figure 3.12. Typical 63Sn-37Pb solder joint microstructures a) 9 days after casting and b) after 1 month at 110°C.

XBB 911-431A

a)

b)

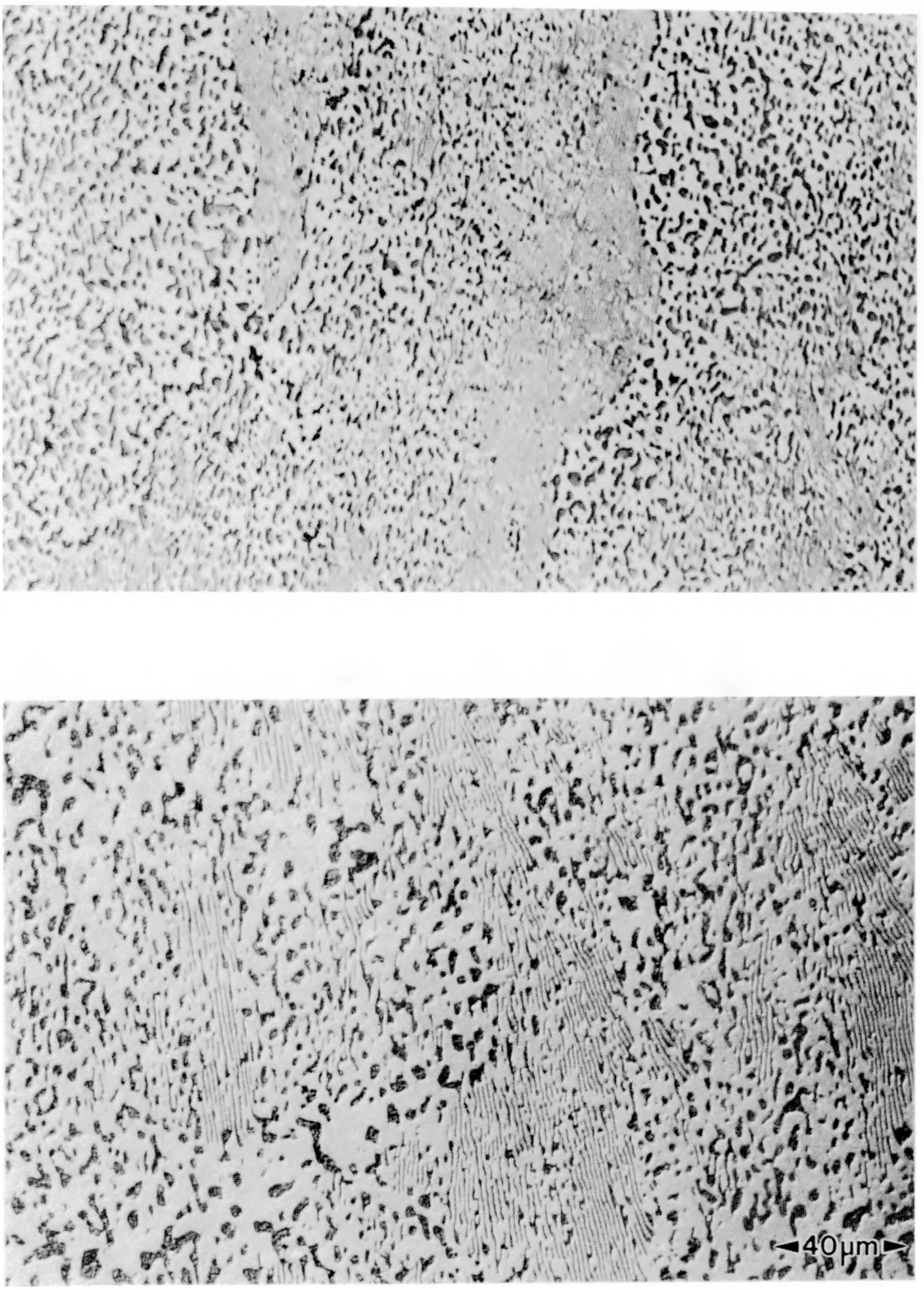

Figure 3.13. Typical 63Sn-37Pb solder joint microstructures after a) 1 week and b) 1 month at 110°C.

XBB 912-1889A

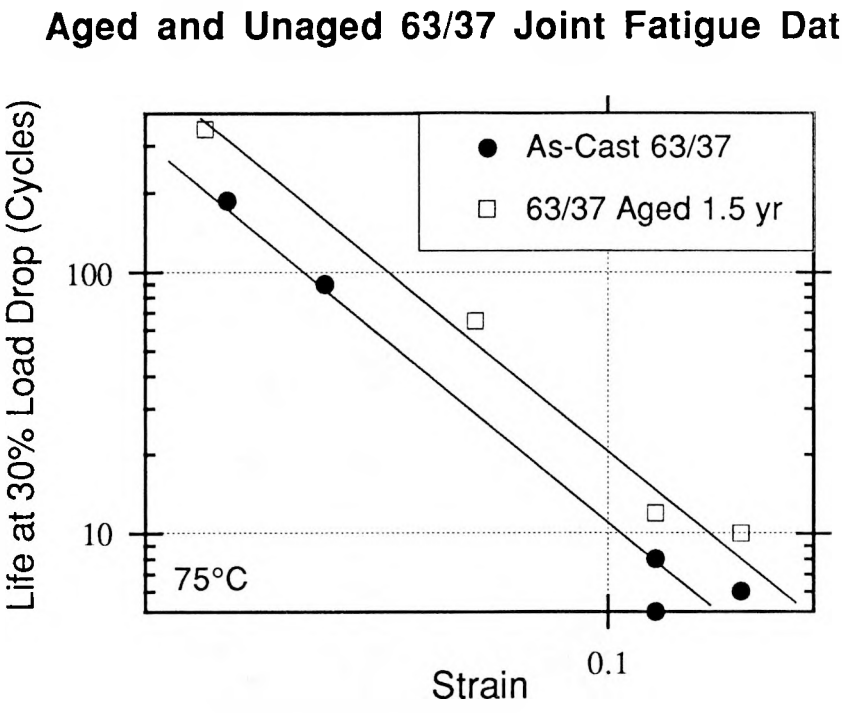

Figure 3.14. Fatigue life (cycles to 30% drop in load) as a function of strain range for 6- and 18-month old 63Sn-37Pb double shear specimens.

Figure 3.15. Coarsened band running along a 6-month old 63Sn-37Pb solder joint fatigued at 75°C with a 10% strain range to 30% load drop. XBB 898-6545B

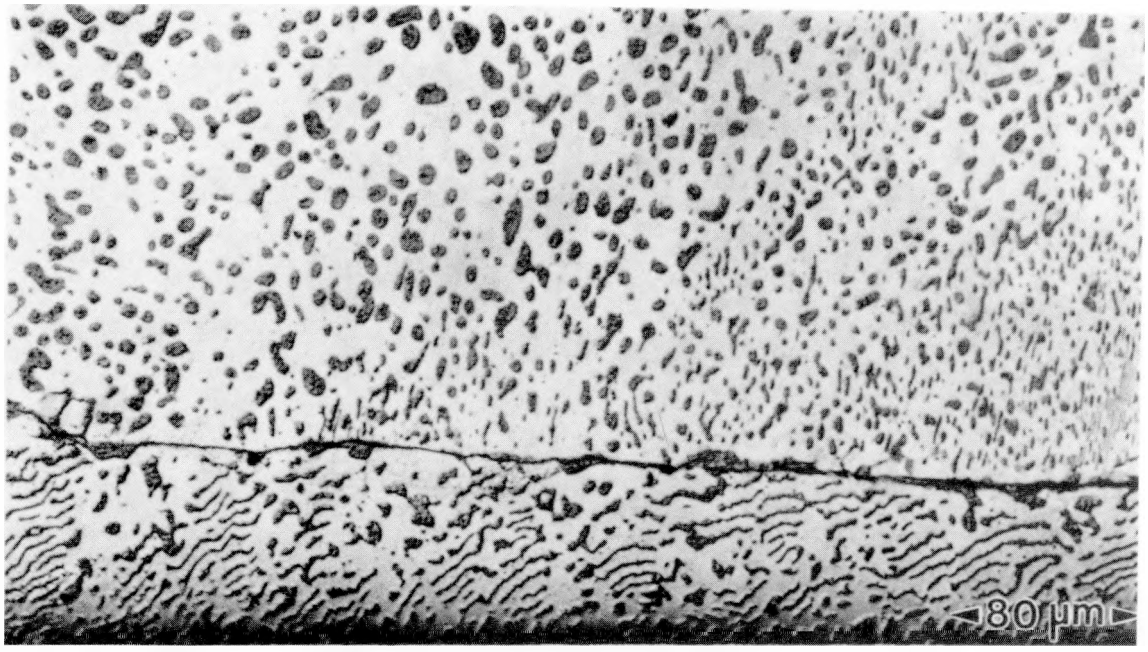

Figure 3.16. Fatigue crack running through a 1.5-year old 63Sn-37Pb solder joint fatigued at 75°C with a 10% strain range to 30% load drop.

XBB 911-432A

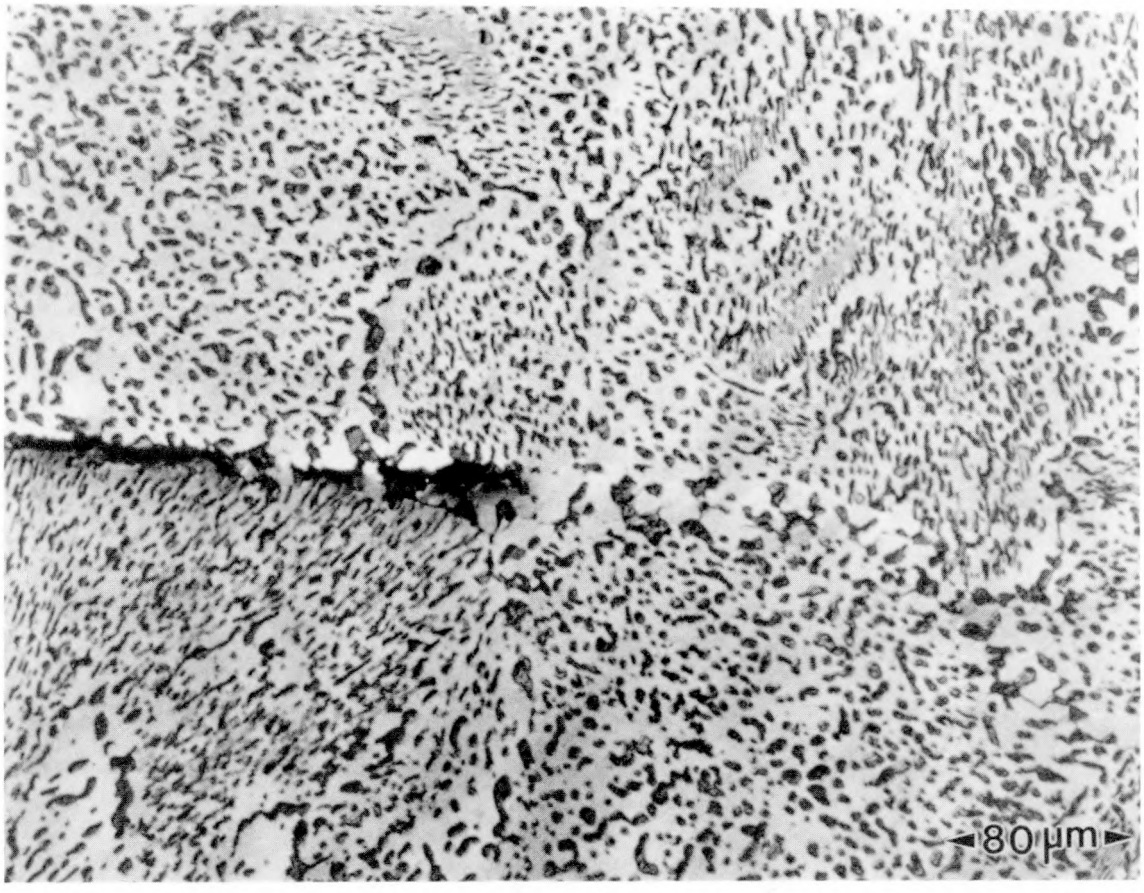

Figure 3.17. Microstructure near a crack in a 1.5-year old 63Sn-37Pb solder joint fatigued at 75°C with a 10% strain range to 30% load drop polished to reveal Sn-Sn grain boundaries.

XBB 912-968A

a)

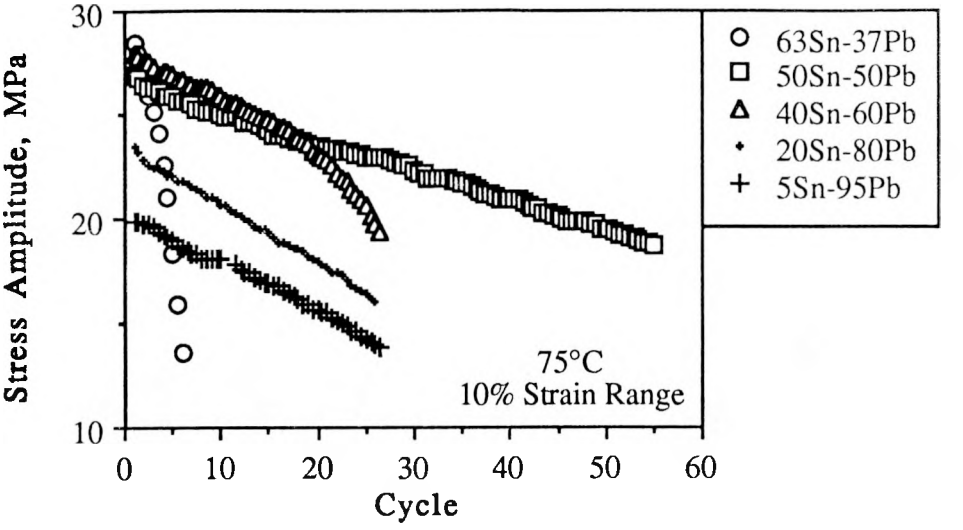

b)

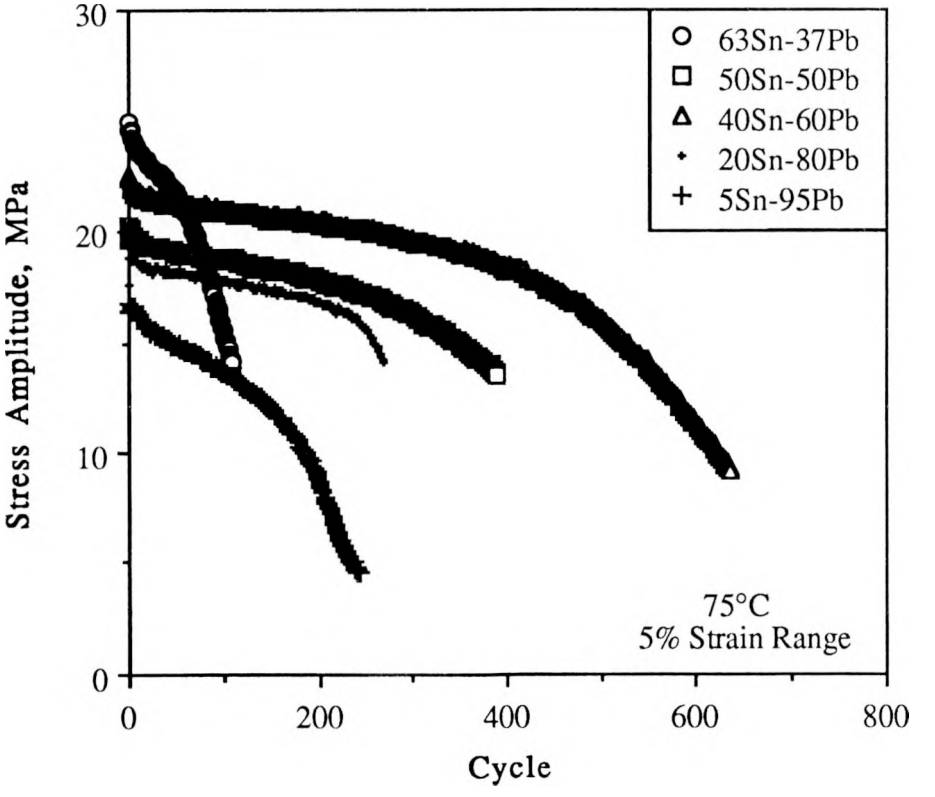

Figure 3.18. Typical stress amplitude vs. cycle curves for isothermal fatigue of the Sn-Pb solders shown at 75°C with a strain range near a) 10% and b) 5%.

a)

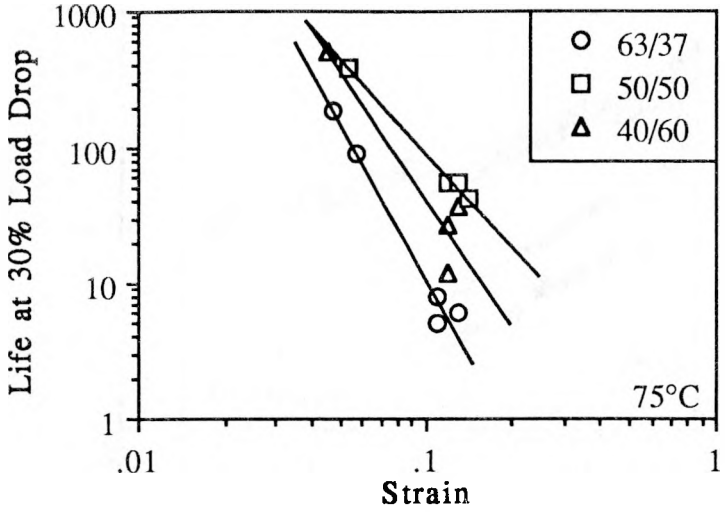

b)

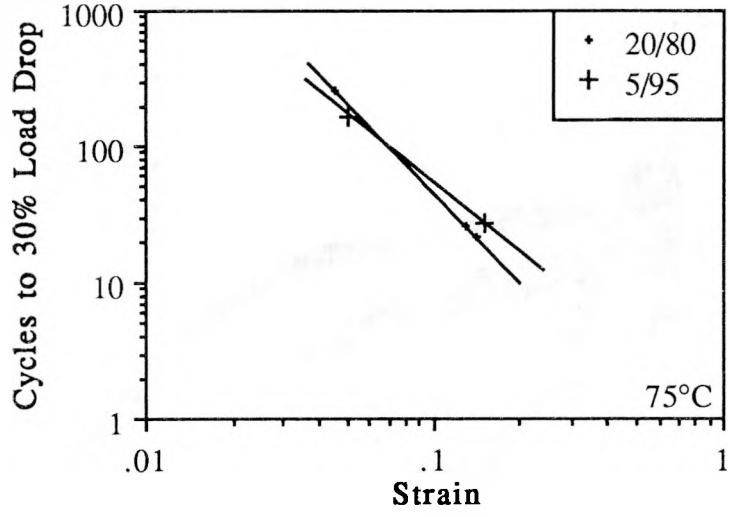

Figure 3.19. Isothermal fatigue life, defined as the number of cycles to a 30% drop in stress amplitude, as a function of applied strain range for the a) eutectic-rich and b) Pb-rich Sn-Pb solders shown tested at 75°C under stroke control.

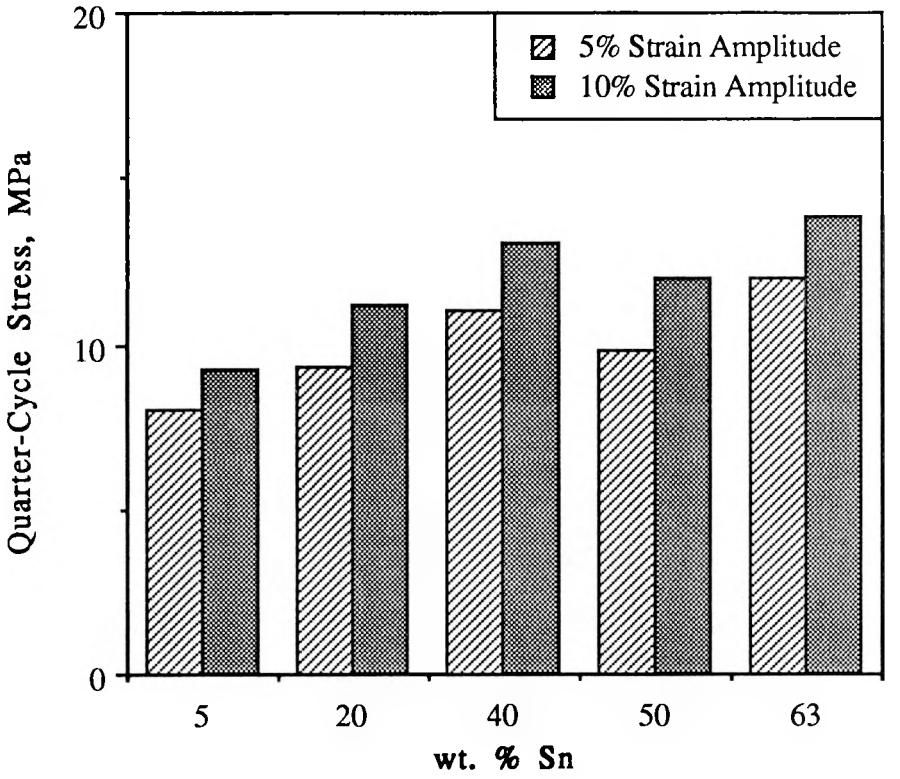

Figure 3.20. Stress reached after the first peak strain (1/4-cycle stress) as a function of composition for 5 and 10% strain ranges.

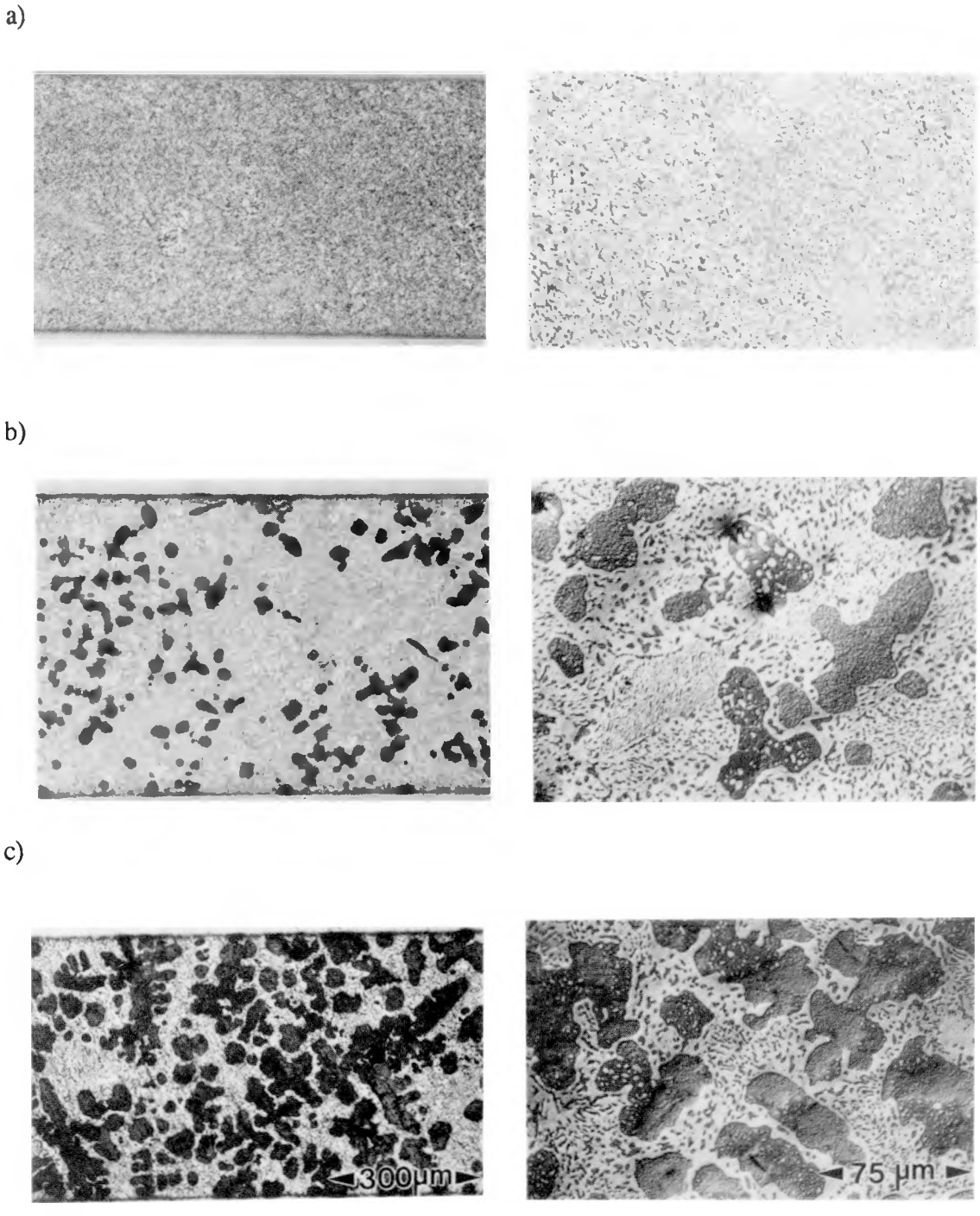

Figure 3.21. As-cast microstructures of the eutectic-rich a) 63Sn-37Pb, b) 50Sn-50Pb and c) 40Sn-60Pb alloys

XBB 898-6545C

a)

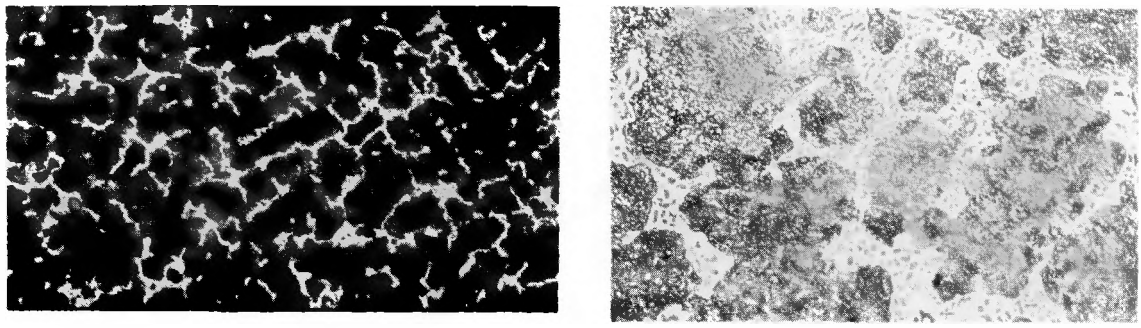

b)

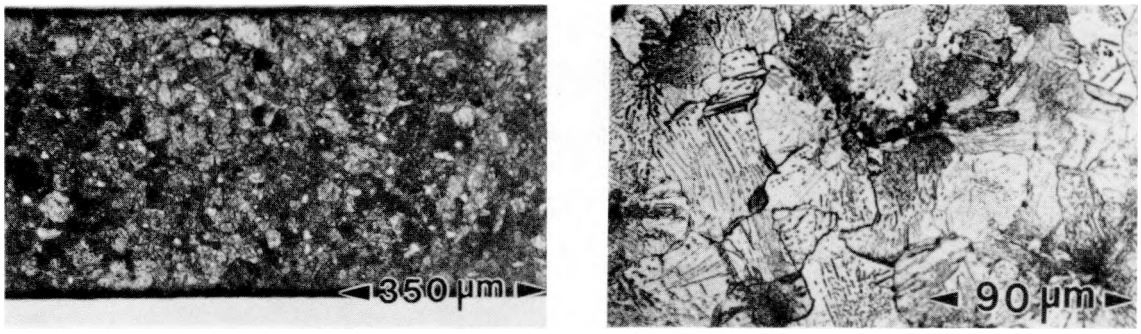

Figure 3.22. As-cast microstructures of the Pb-rich a) 20Sn-80Pb and b) 5Sn-95Pb alloys.

XBB 898-6546B

a)

b)

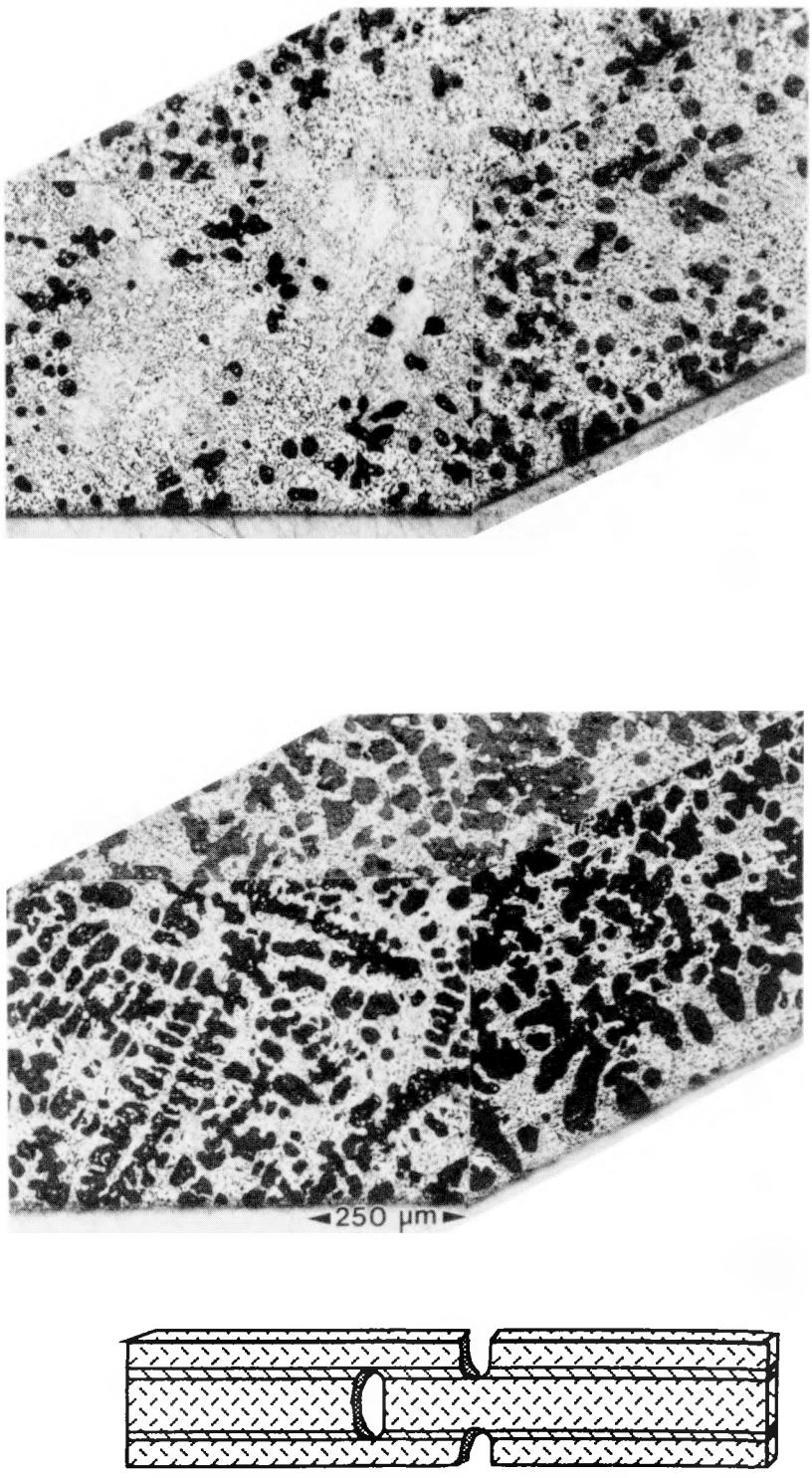

Figure 3.23. Cross sectional micrographs of the as-cast a) 50Sn-50Pb and b) 40Sn-60Pb joint microstructures. Cross sections are oriented as is the specimen schematic.

XBB 913-1894A

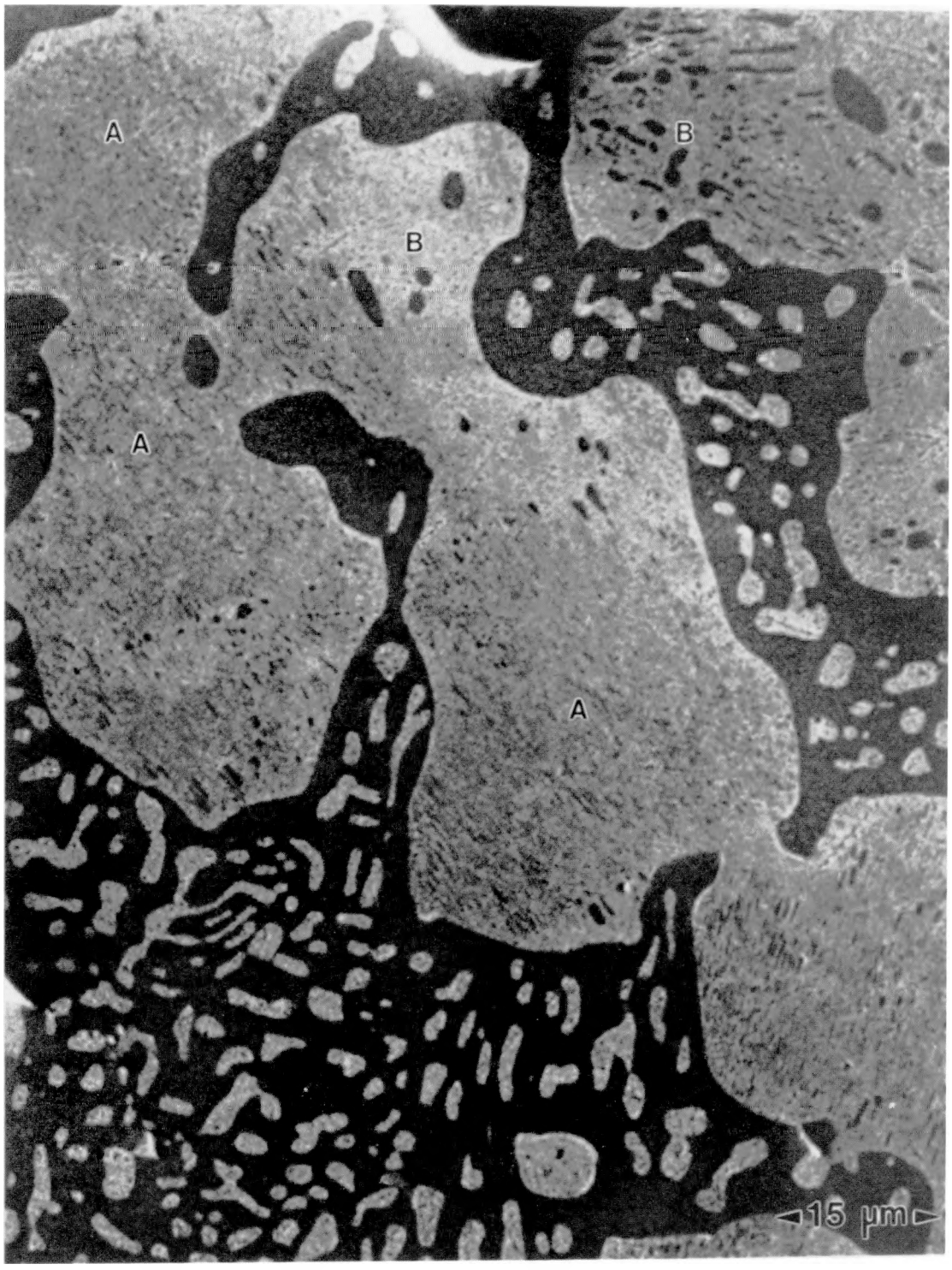

Figure 3.24. Proeutectic particles from a 40Sn-60Pb double shear solder joint. Taken in the SEM, the contrast of this micrograph is opposite to that of optical micrographs: the lighter regions are the Pb-rich phase and the darker regions correspond to the Sn-rich phase. Both very fine (A regions) and very coarse (B regions) Sn precipitate morphologies can be seen in regions of these proeutectic particles.

XBB 912-974A

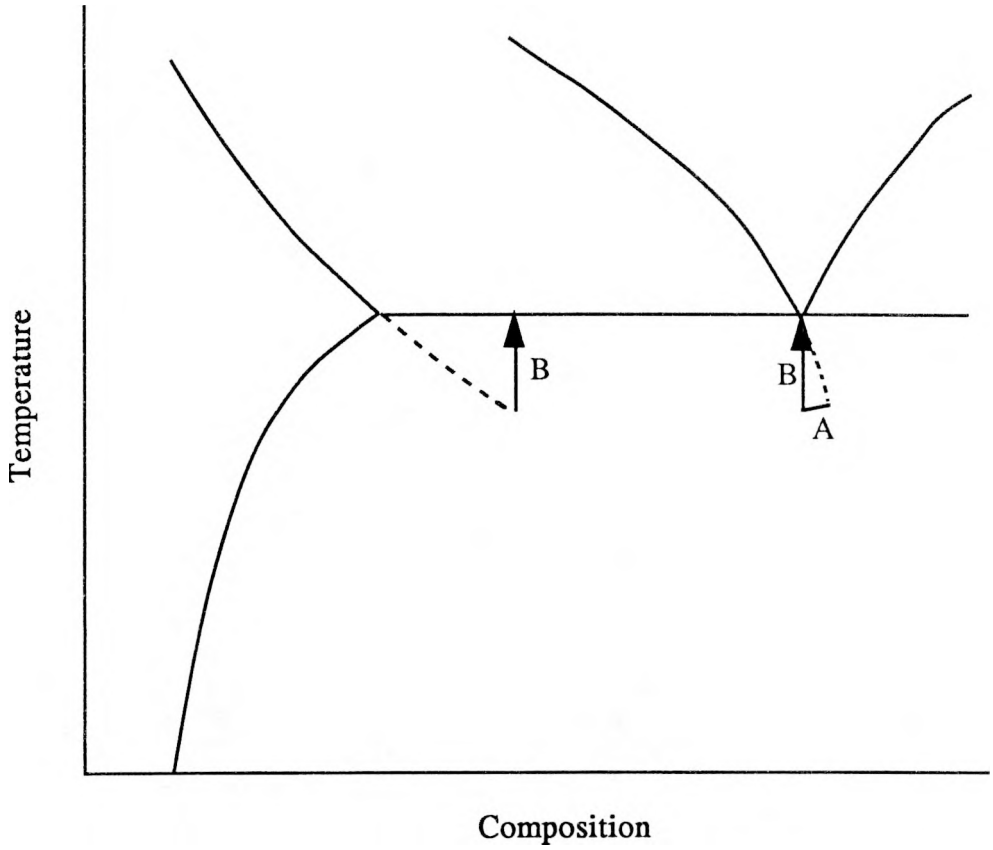

Figure 3.25. Schematic illustration of the Pb-rich region of the Sn-Pb eutectic phase diagram showing phase compositions during undercooling. The liquid and the Pb-rich solid phases will follow the dashed lines shown during undercooling of a hypoeutectic alloy. When sufficient undercooling for the nucleation of Sn is reached, Sn will nucleate in the Sn-rich regions of the liquid surrounding the primary Pb-rich particles (A). When the liquid surrounding these Sn-rich regions reaches the eutectic composition, eutectic will be nucleated with a resultant rise in temperature (B).

a)

b)

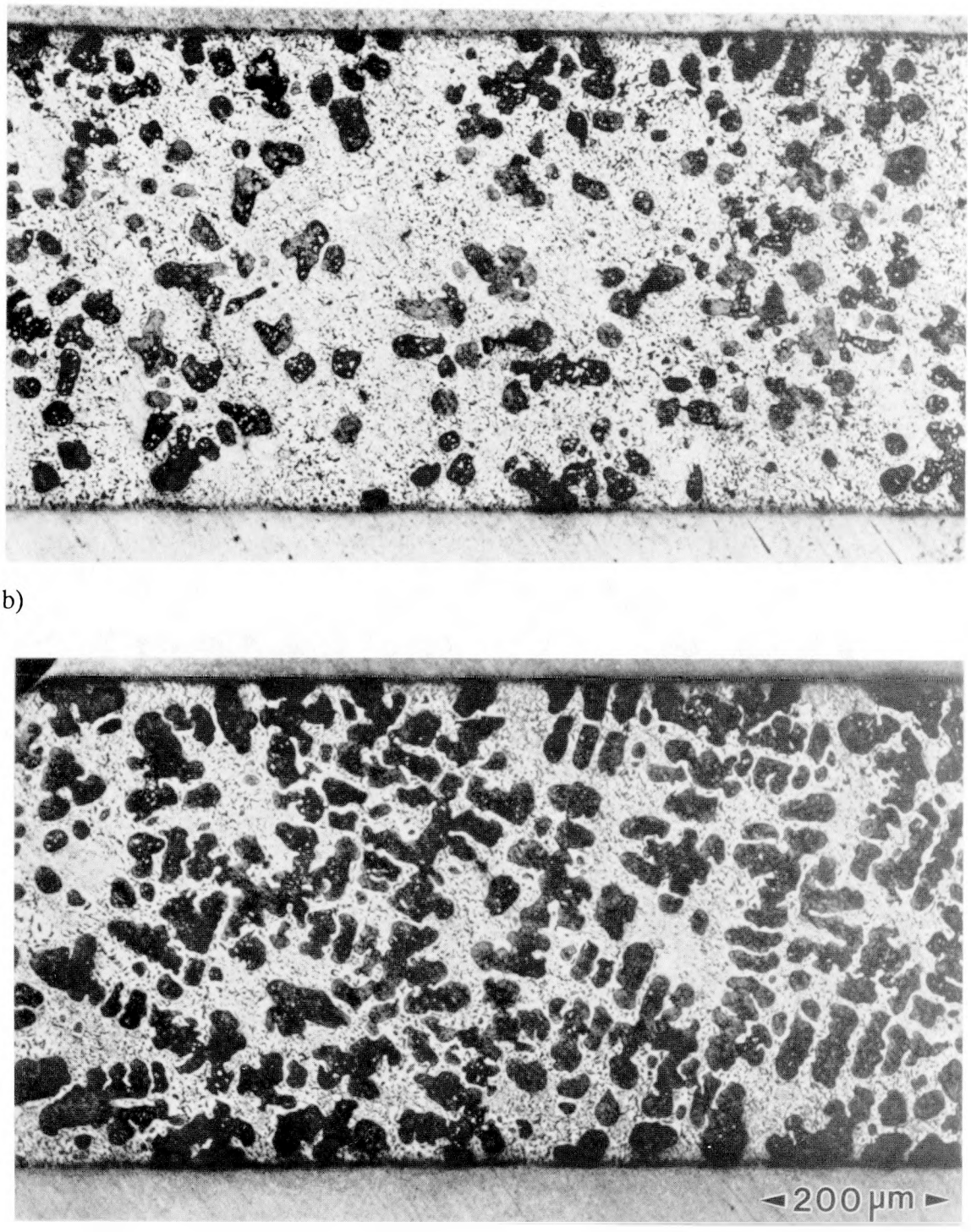

Figure 3.26. As-cast a) 50Sn-50Pb and b) 40Sn-60Pb double shear solder joint microstructures. The eutectic regions removed from the proeutectic particles in the 40Sn-60Pb alloy appear finer, more lamellar and less degenerate than those of the 50Sn-50Pb alloy.

XBB 912-969A

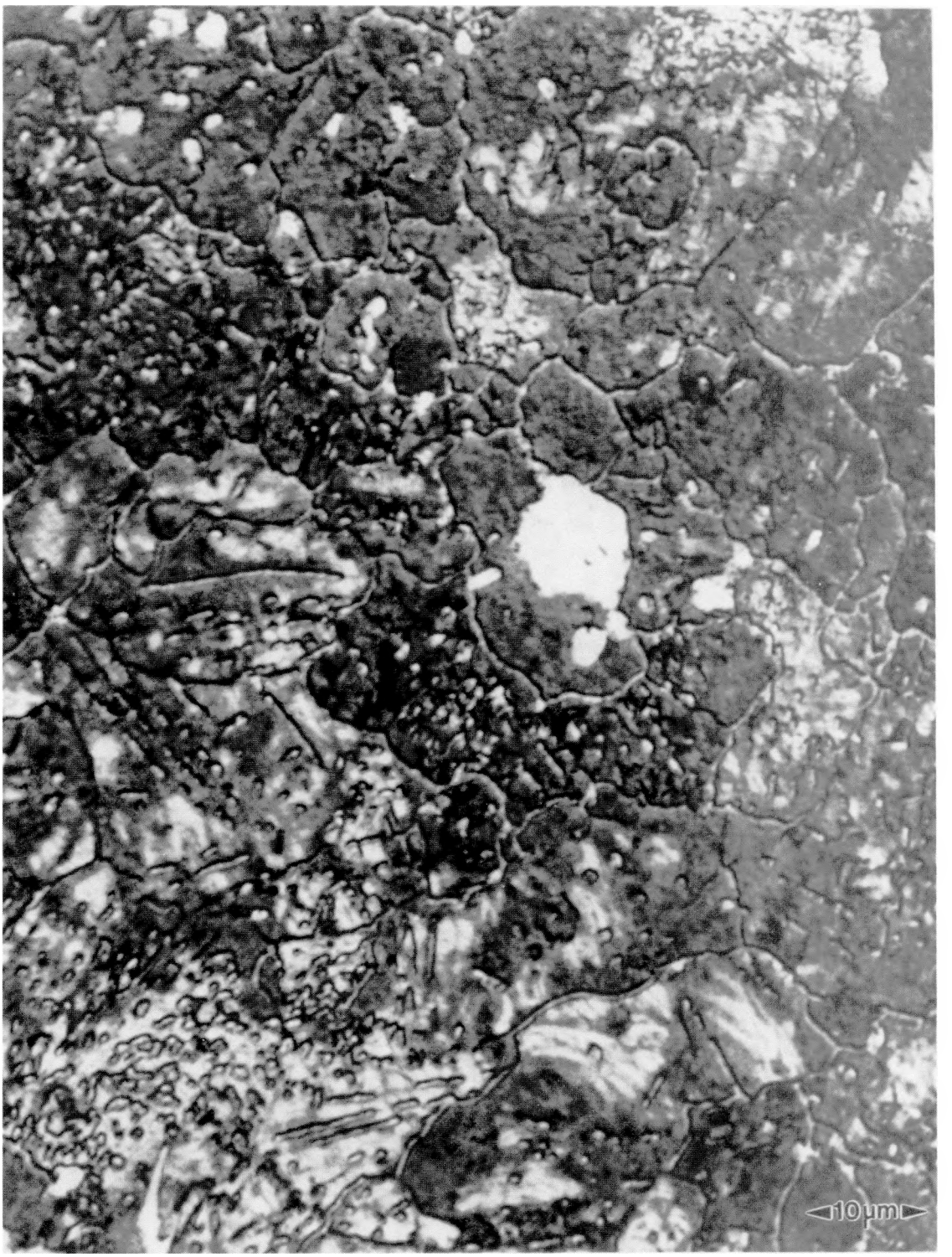

Figure 3.27. A eutectic region (white) in the as-cast 5Sn-95Pb double shear specimen solder joint. The presence of eutectic islands suggests that solidification occurred at a nonequilibrium rate.

XBB 912-965A

a)

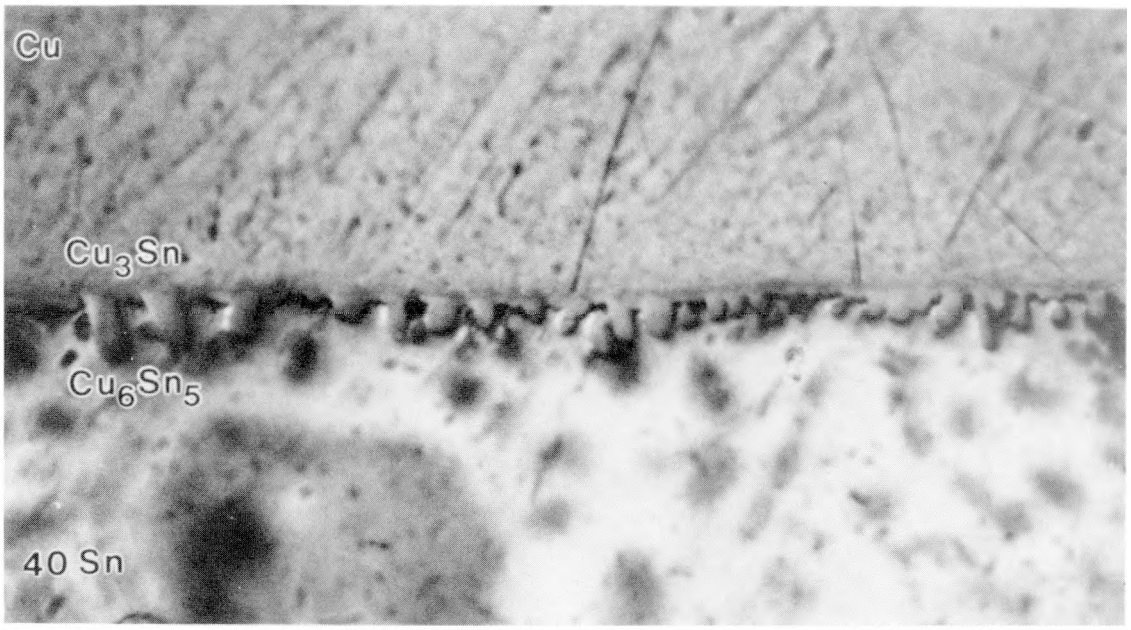

b)

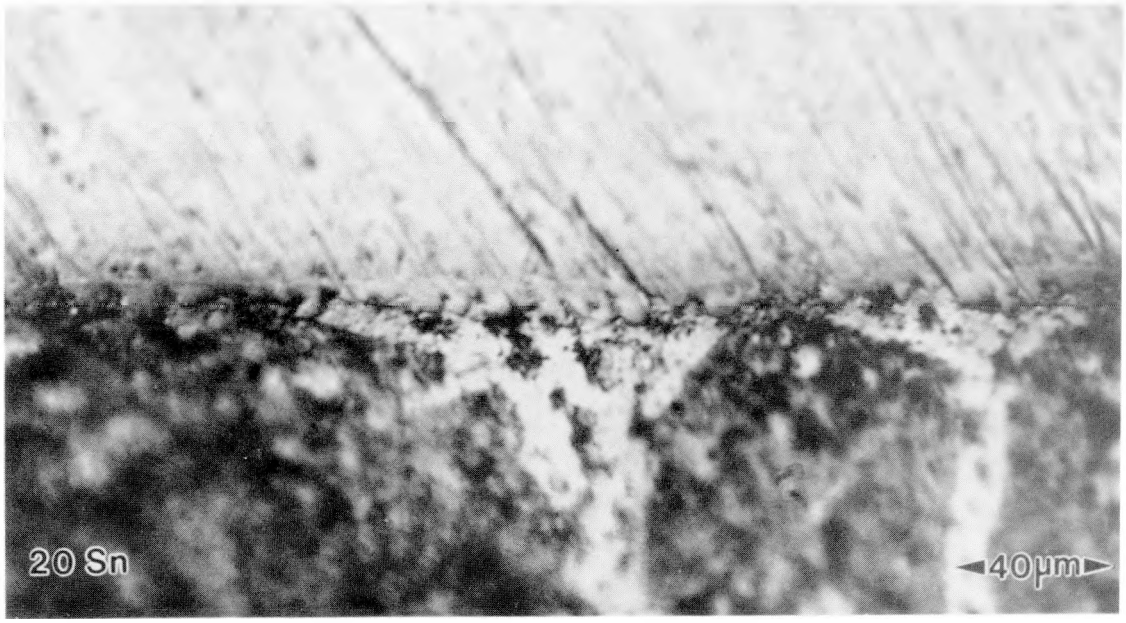

Figure 3.28. Double Cu_6Sn_5 (η) and Cu_3Sn (ε) intermetallic layers in a) 40Sn-60Pb and b) 20Sn-80Pb double shear specimen solder joint interfaces. The dark, thin layer more easily seen in (a) adjacent to the Cu is ε while the elongated whiskers growing into the solder are η.

XBB 912-973A

a)

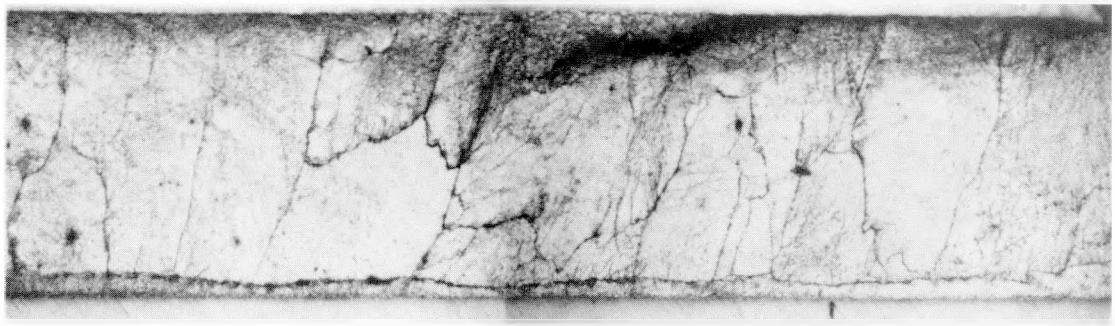

b)

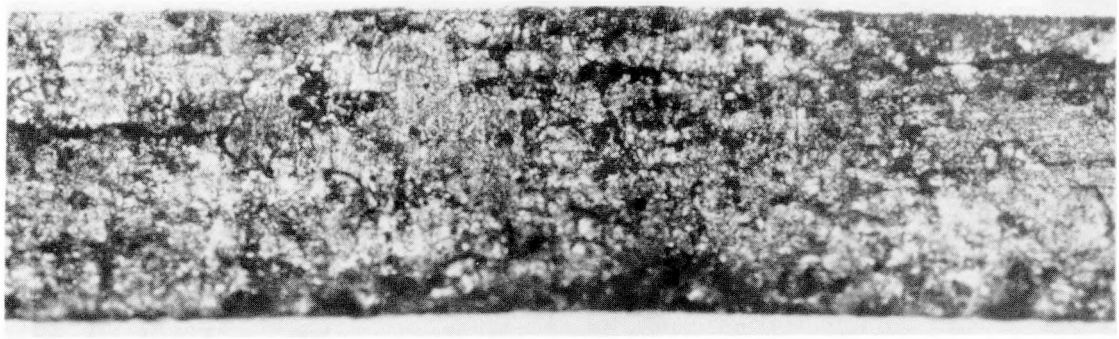

c)

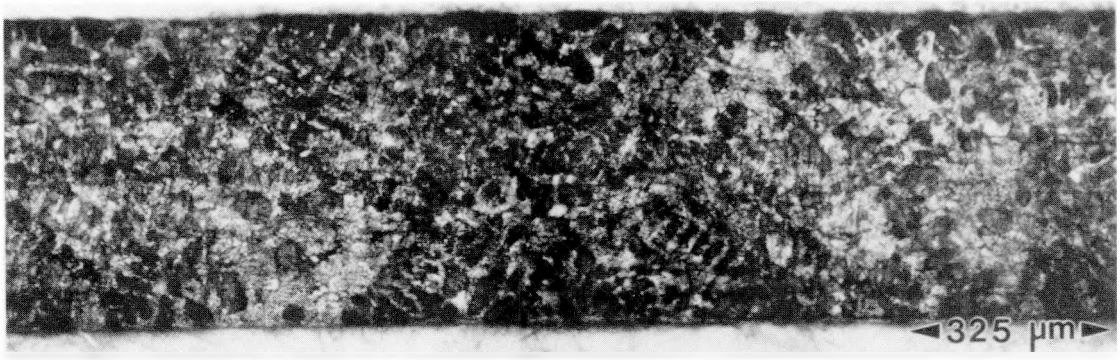

Figure 3.29. Deformation patterns formed in the eutectic-rich a) 63Sn-37Pb, b) 50Sn-50Pb and c) 40Sn-60Pb alloys. The double shear specimens were polished to 0.05µm, fatigued with approximately a 10% strain range at 75°C and observed optically with no post-fatigue surface preparation.

XBB 898-6766B

a)

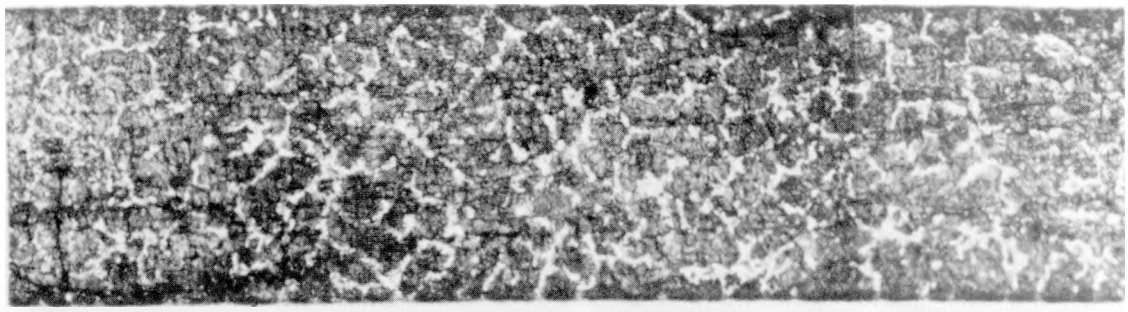

b)

Figure 3.30. Deformation patterns formed in the Pb-rich a) 20Sn-80Pb and b) 5Sn-95Pb alloys. The double shear specimens were polished to 0.05μm, fatigued with approximately a 10% strain range at 75°C and observed optically with no post-fatigue surface preparation.

XBB 898-6766A

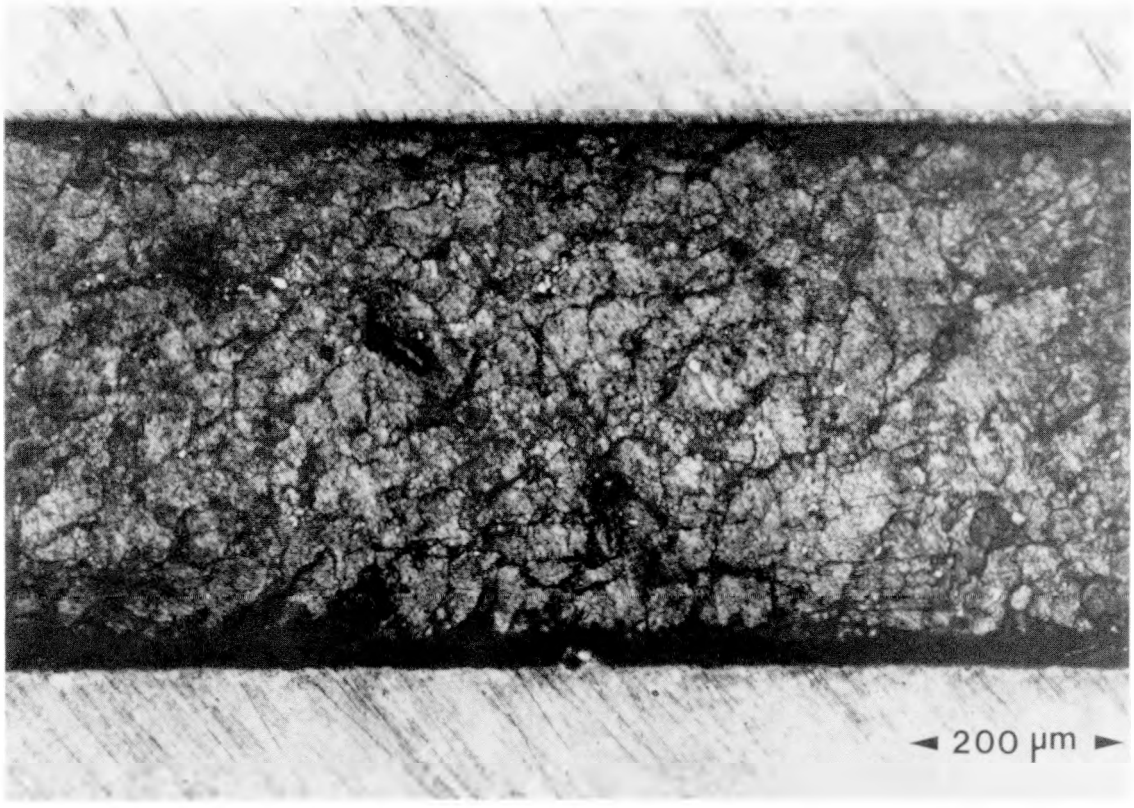

Figure 3.31. Deformation pattern formed in the Pb-rich 5Sn-95Pb alloy. The double shear specimen was polished to 0.05μm, fatigued with approximately a 5% strain range at 75°C and observed optically with no post-fatigue surface preparation.

XBB 913-1886A

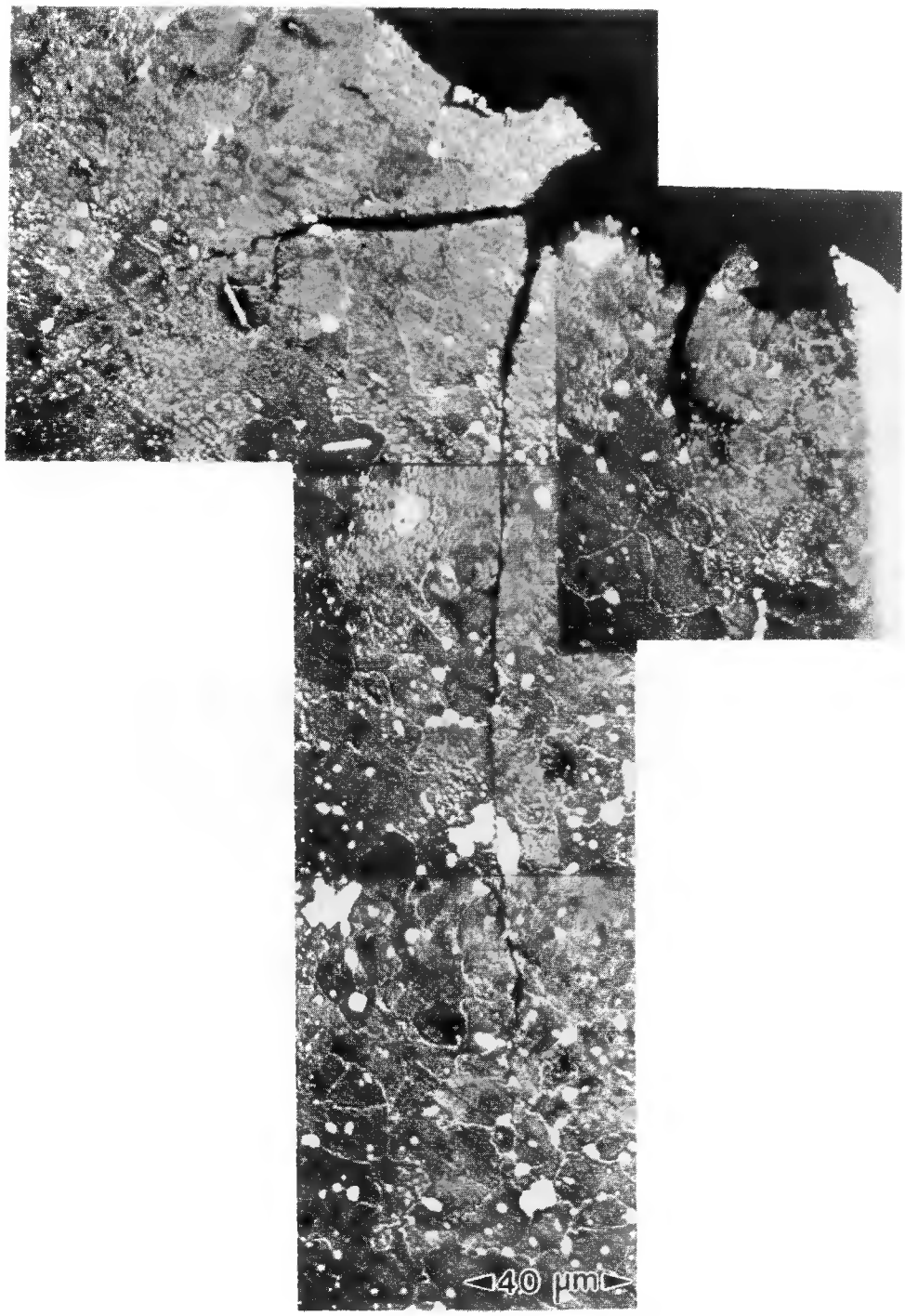

Figure 3.32. Fatigue cracks in a 5Sn-95Pb solder joint fatigued with approximately a 10% strain range at 75°C. Often, several cracks grew from each stress concentration, but usually only one crack oriented along the direction of shear continued to grow during fatigue. No cracking was seen throughout the solder joint away from the stress concentration or the principle cracks. Cracking is seen to occur along grain boundaries.

XBB 913-1896A

a)

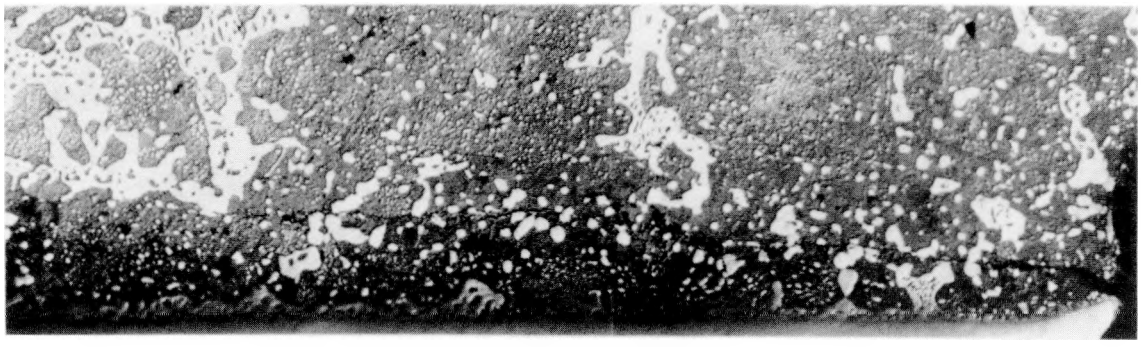

b)

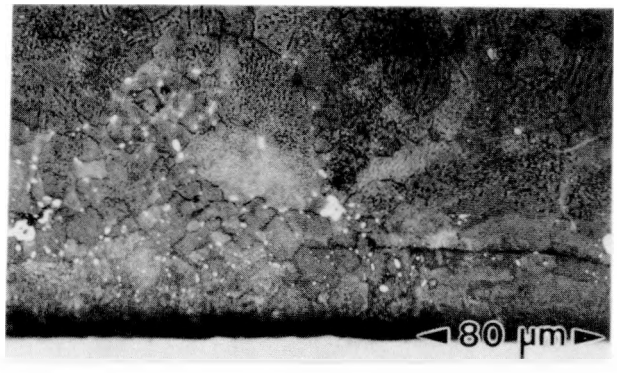

Figure 3.33. Pb-rich a) 20Sn-80Pb and b) 5Sn-95Pb solder microstructures following fatigue with between 5 and 10% strain range at 75°C.
XBB 898-6545D

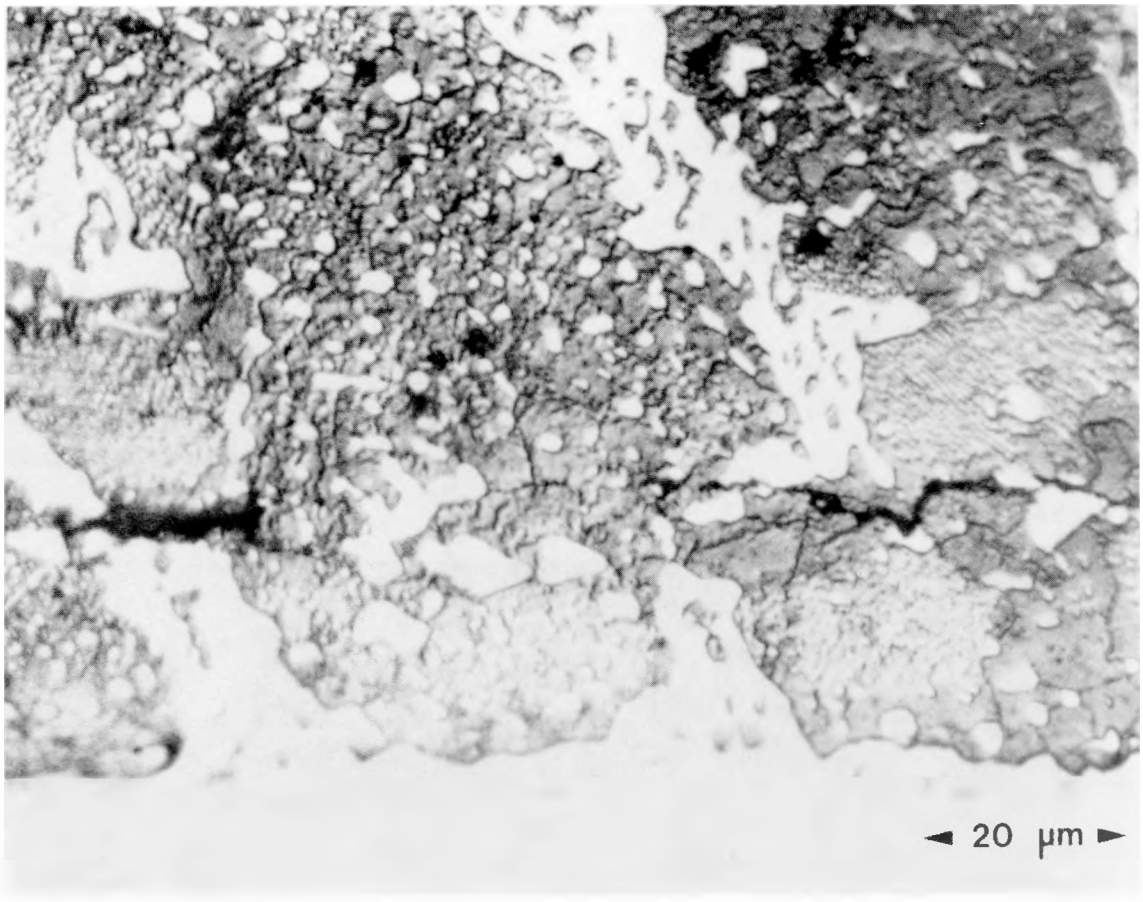

Figure 3.34. Intergranular cracking in the Pb-rich 20Sn-80Pb alloy due to fatigue at 75°C with between 5 and 10% shear strain ranges.

XBB 913-1885A

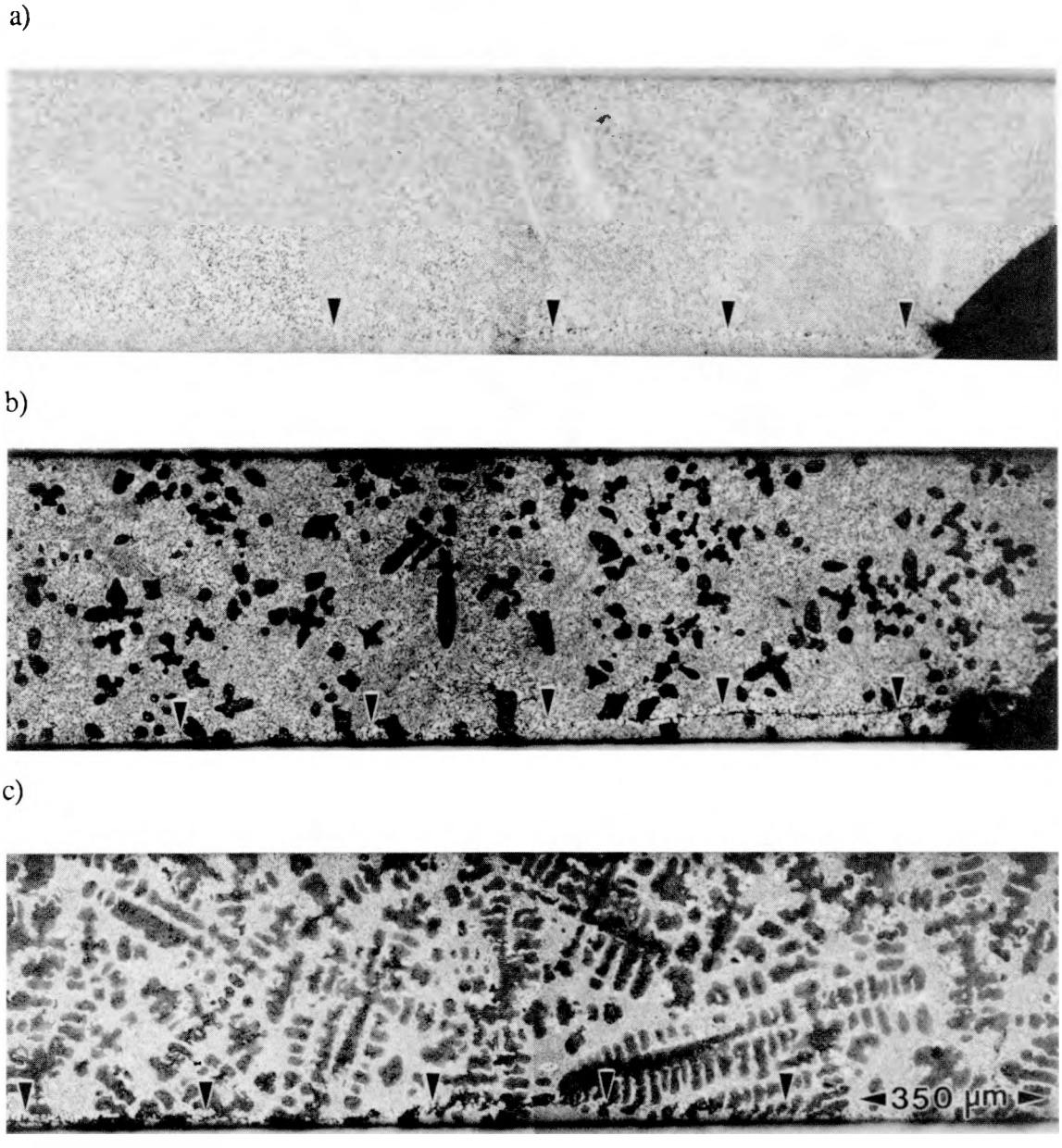

Figure 3.35. Eutectic-rich a) 63Sn-37Pb, b) 50Sn-50Pb and c) 40Sn-60Pb solder microstructures following fatigue with between 5 and 10% strain ranges at 75°C.

XBB 898-6545E

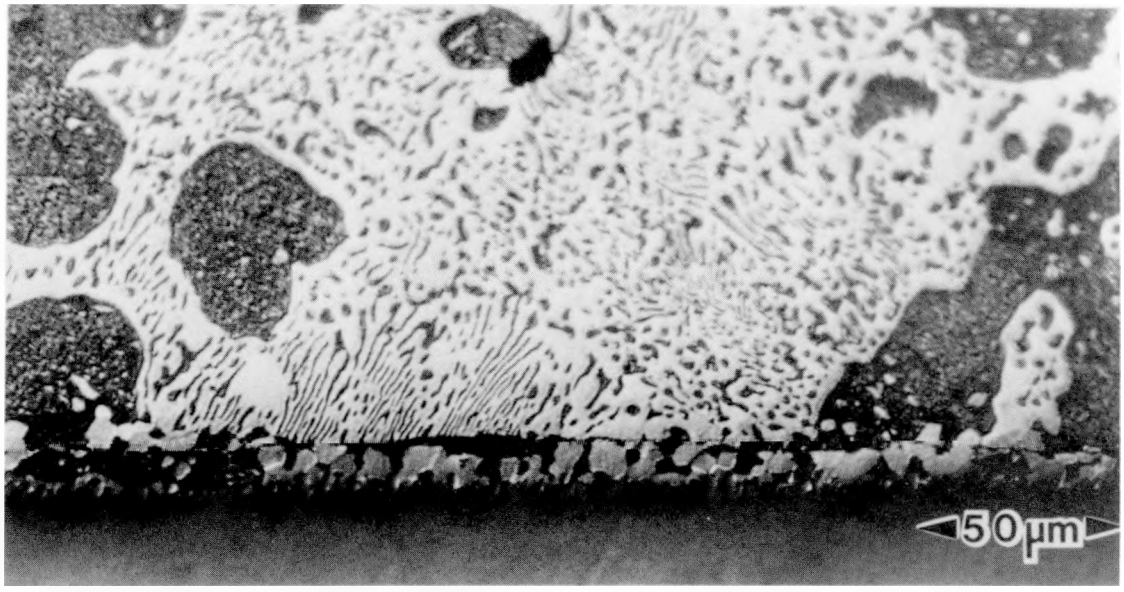

Figure 3.36. Coarsened band in a 40Sn-60Pb solder joint fatigued at 75°C with a 10% shear strain range.

XBB 898-6768A

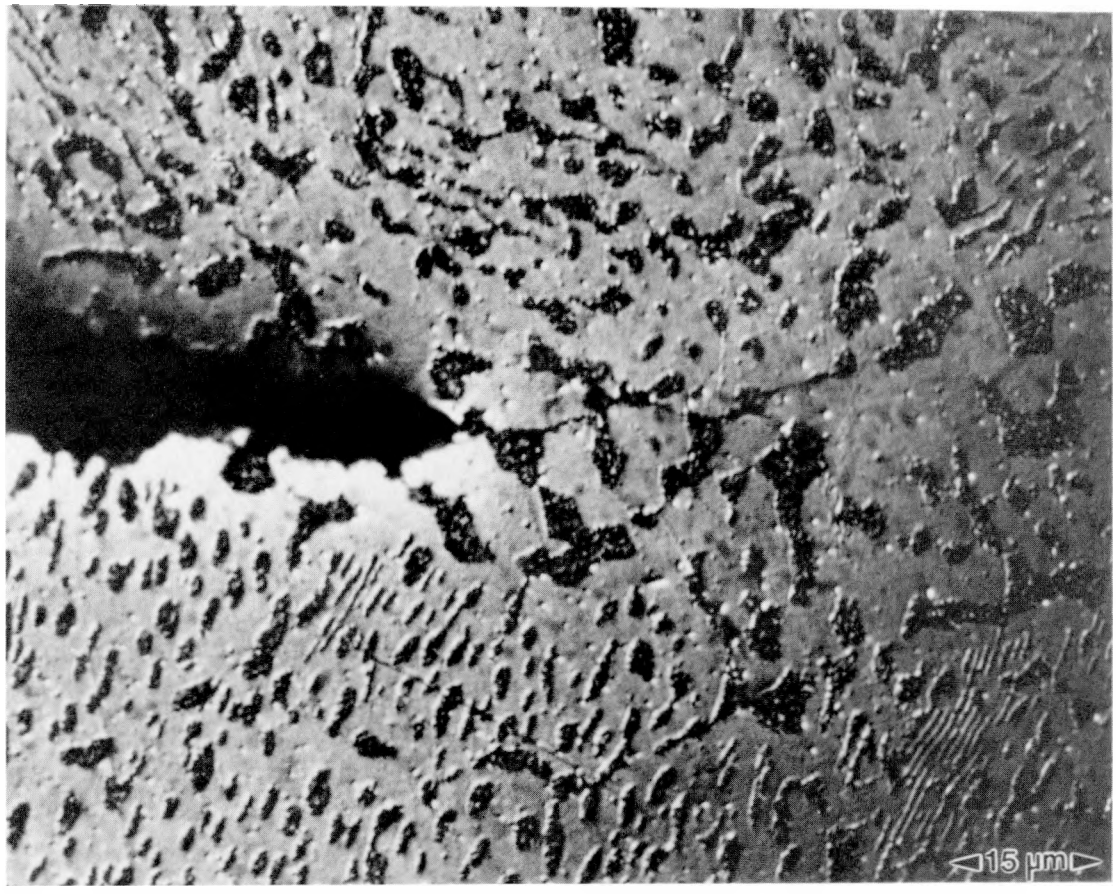

Figure 3.37. Cracking within the coarsened band of a solder joint fatigued at 75°C with a 10% strain range.

XBB 912-986A

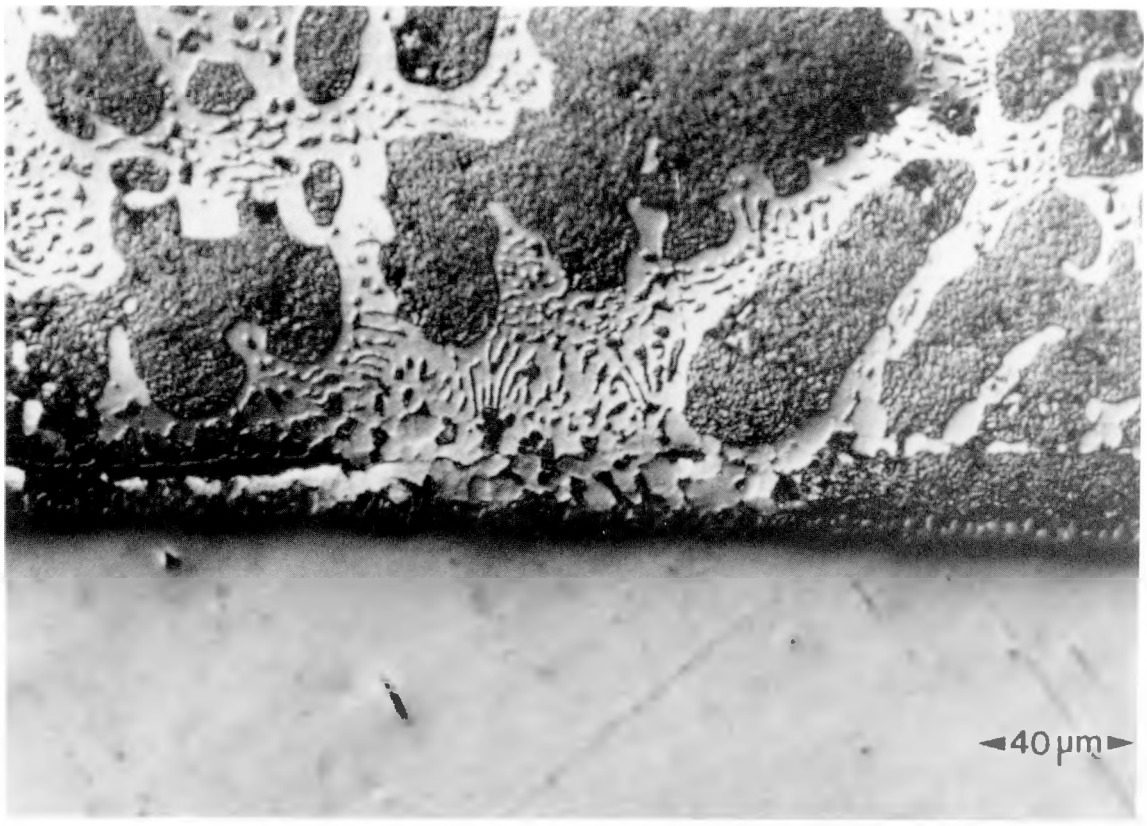

Figure 3.38. Coarsened band in a 40Sn-60Pb solder joint fatigued at 75°C with a 10% shear strain range. Coarsened bands were often observed to end at Pb-rich proeutectic particles.

XBB 913-1884A

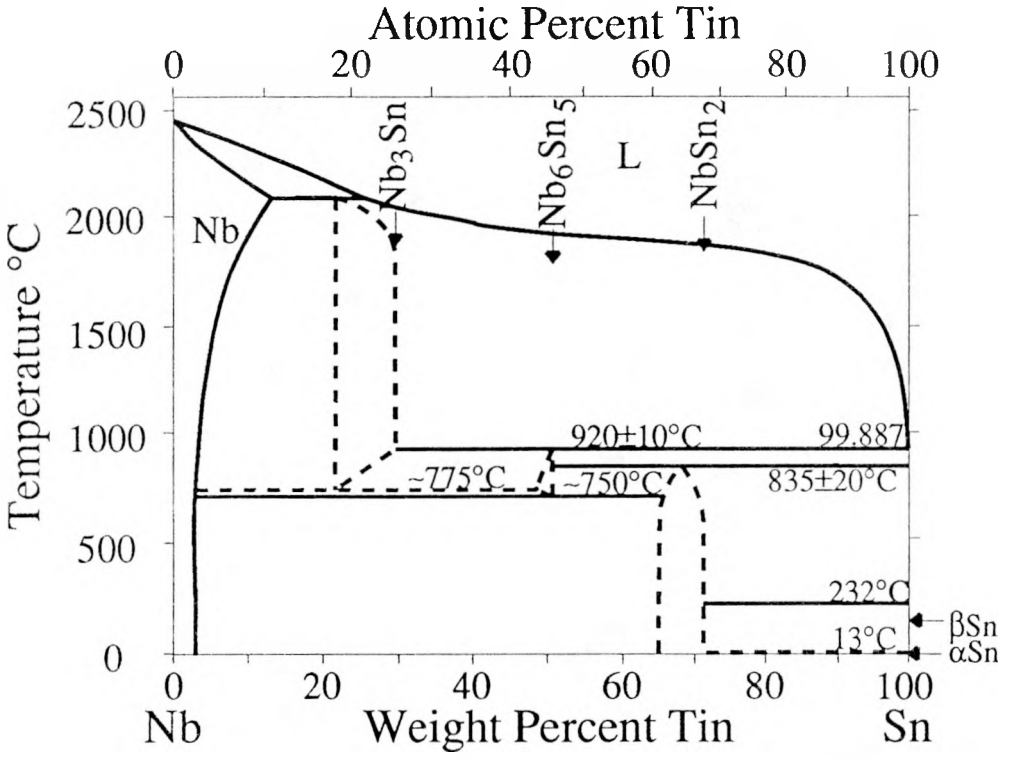

Figure 3.39. The Nb-Sn phase diagram. [Adapted from the Nb-Sn phase diagram published in Binary Alloy Phase Diagrams, Vol. 2, ed. by T.B. Massalski, ASM, Ohio (1986)]

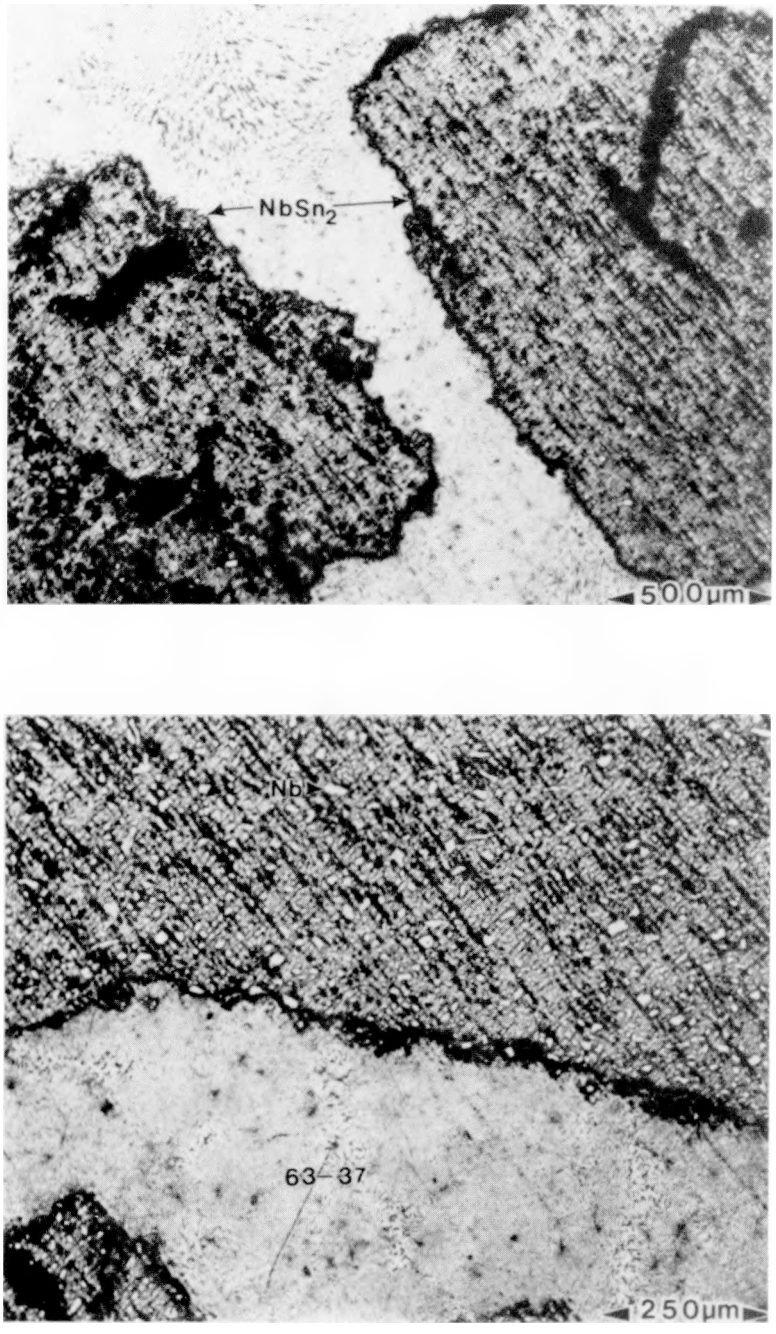

Figure 3.40. Microstructure from early attempt at adding Nb powders to eutectic Sn-Pb solder. The large particles are of $NbSn_2$ reacted between the Nb powders and the molten Sn during cooling following the pretinning operation. The residual Nb powders (white spots) are embedded within these large particles. The large $NbSn_2$ particles are surrounded by the eutectic solder to which they were later introduced.

XBB 908-7094B

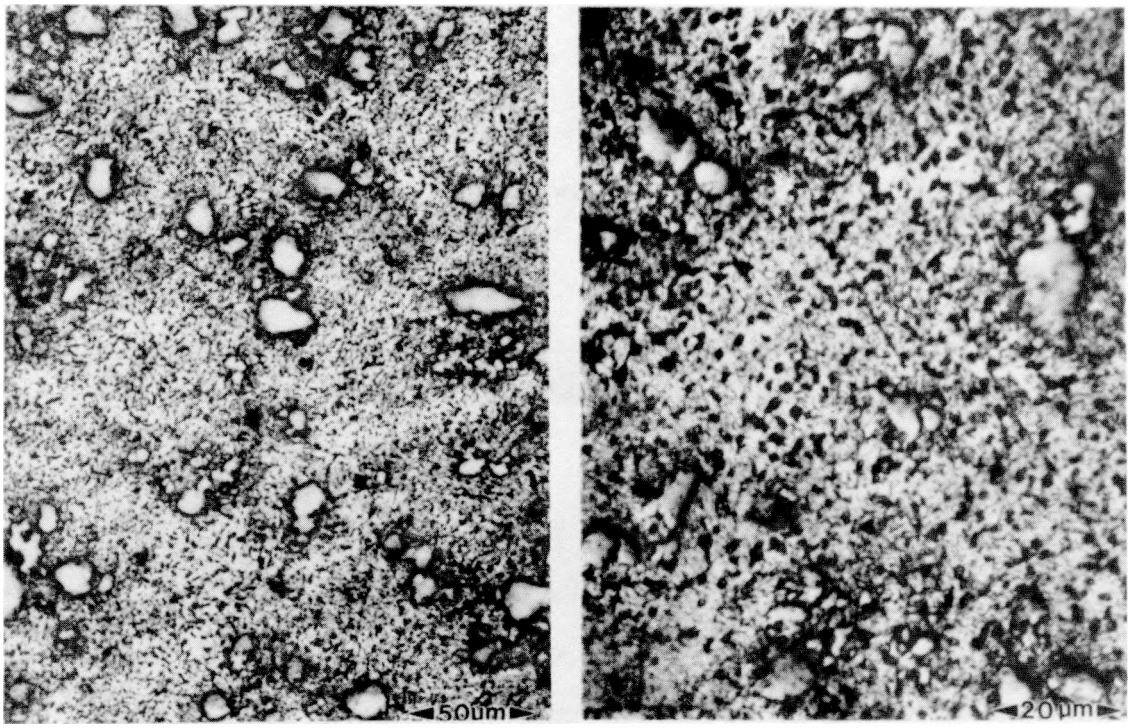

Figure 3.41. Nb powders successfully introduced to eutectic solder followed by a water quench.

XBB 909-7481A

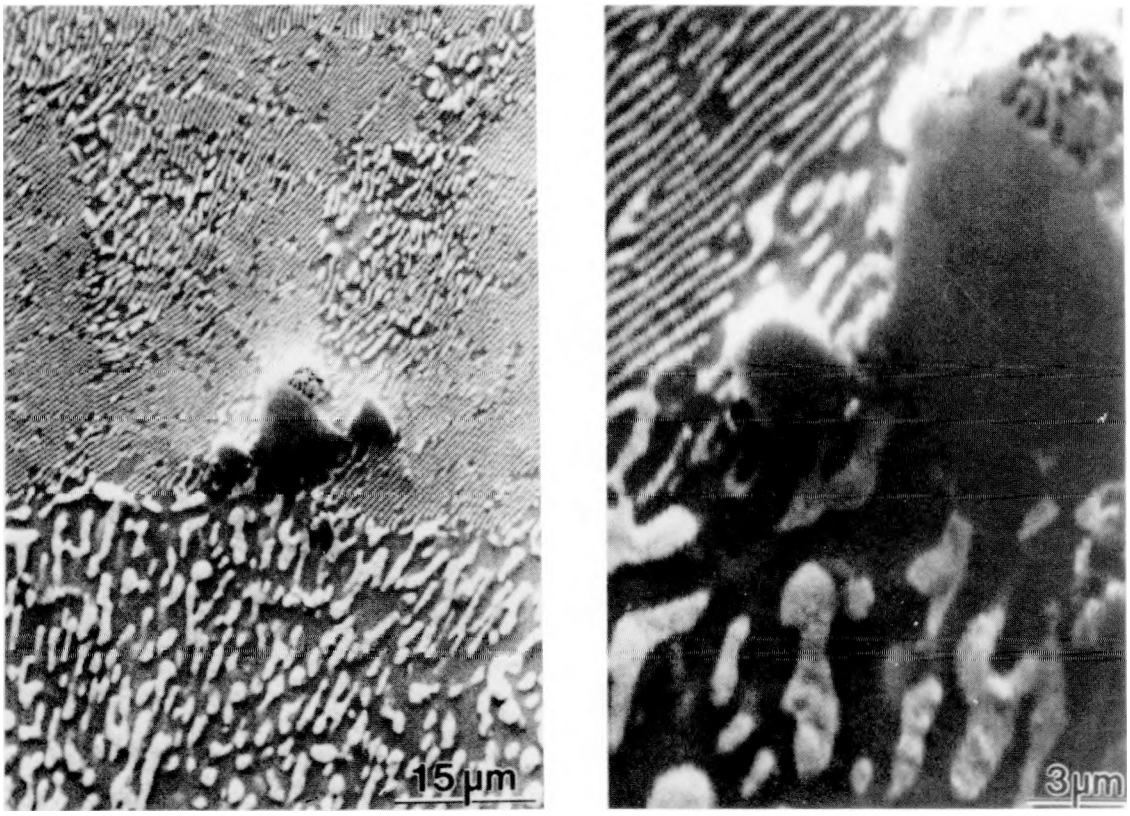

Figure 3.42. Nb powders from the same ingot as in Figure 3.41 but remelted and air cooled. The fact that lamellae grow perpendicular to the Nb powders suggests that the Nb powders nucleate the eutectic phase and are therefore wet by the solder melt.

XBB 900-8681A